**EXPLORING THE COENZYME A BIOSYNTHETIC PATHWAY
AS NOVEL ANTIBIOTIC TARGET**

by

Jiangwei Yao

A dissertation submitted in partial fulfillment
of the requirements for the degree of
Doctor of Philosophy
(Medicinal Chemistry)
in the University of Michigan
2010

Doctoral Committee:
      Assistant Professor Garry D. Dotson, Chair
      Professor Carol A. Fierke
      Professor Shaomeng Wang
      Associate Professor Bruce A. Palfey
      Research Professor Scott D. Larsen

TABLE OF CONTENTS

iii

LIST OF FIGURES

LIST OF TABLES

LIST OF APPENDICES

Appendix

Chapter 1

Coenzyme A Biosynthesis as Novel Antibacterial Target

Antibiotic Resistance

Pathogenic bacteria that are resistant to antibiotic therapy are emerging as an increasing public health threat (*1-5*). Since the 1940s, bacterial infections have been, for the most part, effectively treated with antibiotics (*1, 2*). Infections, often fatal before the advent of antibiotics, are now routinely cured with antibiotics, improving the quality of health for countless millions of people. However, increasing antibiotic resistance in prevalent pathogenic bacteria, coupled with the slow discovery of novel antibiotics, threatens to wipe out these gains and forecasts a future where bacterial infections again become difficult to treat (*2, 4, 5*). Glimpses of this future are already visible today, where highly drug resistant bacteria such as extensively drug-resistant tuberculosis (XDR-TB) often cause greater than 50% mortality rate even when patients are under intensive medical care (*6-8*).

The amount of time between introduction of antibiotics into the marketplace and observed resistance to these antibiotics widely varies, Figure 1.1 – Time Table of Introduction/Resistance (*9, 10*). So far, clinically relevant resistance has been detected for every marketed antibiotic, and high frequencies of resistance are observed for classes of commonly prescribed antibiotics (*2, 4*). Due to their broad spectrum, oral dosage, and

low side-effects, β-lactam antibiotics (composed of the four major sub-classes of penicillins, cephalosporins, carbapenems, and monobactams) tend to be the first antibiotic prescribed for most bacterial infections (*11, 12*). Earlier generations of β-lactam antibiotics lacked efficacy against Gram-negative bacteria, but newer generations, particularly third generation and later cephalosporins, have broad antibacterial spectra (*12*). Associated with β-lactam antibiotics are β-lactamase inhibitors, which have been commercialized since the 1980s. The most common resistance mechanism to β-lactams is the hydrolysis by β-lactamases (*13*). β-lactamase inhibitors have weak or no antibacterial activity by themselves, but inhibit bacterial β-lactamase, thus countering some β-lactam resistance (*14, 15*). β-lactam/β-lactamase combinations have shown good clinical efficacy against some bacteria that are not normally sensitive to β-lactam antibiotics (*16, 17*). A few other orally dosed, broad spectrum antibiotic classes, such as tetracyclines, are also prescribed, although less frequently now due to resistance or toxicity-related issues (*12*). For Gram-positive pathogenic bacteria resistant to the above mentioned antibiotics, vancomycin is historically prescribed, but Daptomycin and Linezolid, brought to market in the last decade, are also viable options (*12*). Because Gram-negative bacteria cause significantly fewer cases of contagious diseases as well as require more varied treatment, antibiotic resistance in Gram-negative bacteria (besides *Pseudomonas aeruginosa*) is less concerning (*18*). Presently, four resistant pathogens are major health concerns due to their current and developing resistance to commonly used antibiotics. They are highlighted below to justify the need for new, novel antibiotics.

Urgent Antibiotic-Resistant Pathogens

Currently, the most common antibiotic-resistant bacterium found in developed countries is methicillin resistant *Staphylococcus aureus* (MRSA) (*4, 19*). *Staph. aureus* is a Gram-positive bacterium and causes a range of diseases from minor skin infections to pneumonia, meningitis, and toxic-shock syndrome (*20*). Approximately 20% of the population carries *Staph. aureus* long-term, with the *Staph. aureus* residing in the nose and on the skin of the carriers (*20*). Additionally, a large portion of the long-term carriers tend to be hospital personnel, making *Staph. aureus* a major concern for nosocomial infections. MSRA is resistant against most β-lactam antibiotics, the first line of antibiotics prescribed against Gram-positive bacteria (*4, 21*). Approximately half of *Staph. aureus* infections observed in US hospitals are MSRA. The observed cases also exhibit high frequencies of resistance against two other common antibiotics - tetracycline and erythromycin (*4*). MRSA is difficult to treat, with vancomycin (and now Linezolid) being the typical treatment. However, cases of vancomycin (mid 1980s) and Linezolid (2003) resistant *Staph. aureus* have been found (*22, 23*). Infections of β-lactam-resistant and vancomycin-resistant *Staph. aureus* are extremely difficult to treat and result in higher mortality rates compared to antibiotic-sensitive bacterial infections (*23*). Fortunately, the current frequency of vancomycin and Linezolid resistant MRSA is very low, but it is increasing. The mechanism of acquiring vancomycin and Linezolid resistance may be gene-transfer with *Enterococci*, the next pathogen discussed (*24*).

The other commonly encountered antibiotic-resistant bacteria in hospitals are vancomycin-resistant *Enterococci* (VRE). *Enterococci* species reside within the gut of nearly all healthy adults, and the most common species are *E. faecalis* and *E. faecium*

3

(composition of these two species varies by region) (*25*). *Enterococci* cause diseases as such bacteremia and endocarditis. *Enterococci* species have remarkable intrinsic resistance to antibiotics. *E. faecalis* is intrinsically 10-100 times more resistant to penicillins when compared to the related *Streptococcus* species, and *E. faecium* is even more so (*25*). Cephalosporins do not inhibit *Enterococci* sufficiently to warrant clinical use, while *Enterococci* possess low levels of natural resistance to lincosamides and aminoglycosides (*12, 25*). In addition to intrinsic resistance, most pathogenic *Enterococci* also have acquired antibiotic resistance to tetracycline, chloramphenicol, erythromycin, aminoglycosides, and lincosamides. Because of its resistance, *Enterococci* species tend to cause opportunistic infections after the native bacterial flora has been wiped out by antibiotics, particularly cephalosporin (*25*). Previously, *Enterococci* have been treated with vancomycin, but Linezolid has since become popular. Approximately 30% of present *Enterococci* infections found in Intensive Care Units are VRE (*4*). Instances of Linezolid and Daptomycin resistant *Enterococci* have also started to occur in hospitals (*26, 27*). Since *Enterococci* tend to be opportunistic infections, the greater fear associated with *Enterococci* is the spread of vancomycin (and possibly Linezolid) resistance to other Gram-positive bacteria, such as *Staphylococcus*, *Streptococcus*, and *Bacillus* species. Particularly, *Staphylococci* and *Enterococci* share many resistance genes, presumably from horizontal transfer of these resistance genes (*28, 29*). *Staph. aureus* and *Enterococci* are also common in hospital settings and have been found in the same patient, raising concerns of about the development of vancomycin resistant MRSA, leaving few treatment options (*23*).

Mycobacterium tuberculosis is the most prevalent bacterial infection worldwide, with cases of tuberculosis (TB) mostly concentrated in developing countries and in immunocompromised individuals (*30*). One-third of the current worldwide population carries *M. tuberculosis*, although only 10% of these individuals develop full-blown TB during their lifetimes (most individuals are asymptomatic) (*31*). When left untreated, mortality rate is greater than 50%. Because the *M. tuberculosis* genome encodes for an extended-spectrum β-lactamase, most β-lactams are not effective treatments (*32*). The standard treatment for TB is a combination of ethambutol, isoniazid, pyrazinamide, rifampicin, and streptomycin for six month and with proper treatment, the mortality rate is less than 5% (*12*). However, because TB occurs primarily in poor areas of the world, patients often miss drug doses or fail to complete the course of treatment, and TB becomes resistant to one or more of the above drugs. TB that becomes resistant to isoniazid and rifampicin, the two most efficacious drugs, are classified as multidrug resistant (MDR) TB. In this situation, a second line of drugs (which are less efficacious, more toxic, or less accessible) such as quinolones or kanamycin, are deployed (*12*). TB that becomes resistant to these drugs is classified as extensively drug-resistant (XDR) TB and is extremely difficult to treat. XDR-TB often has mortality rates of greater than 50% even when under intensive treatment (*8*). Several hundred cases of transmissible XDR-TB have been characterized in South Africa (with >60% mortality rate), raising fears of further spread of this strain of difficult to treat XDR-TB (*7*).

Although it infects mostly immunocompromised individuals, *Pseudomonas aeruginosa* is another pathogenic organism of great concern due to both its inherent antibiotic resistance and genetic capacity to develop new antibiotic resistance (*6*). The *P.*

aeruginosa genome encodes a broad-spectrum β-lactamase as well as multidrug efflux pumps that give the organism a high level of inherent resistance (*13, 17, 18, 33*). While the *P. aeruginosa* β-lactamase does not have as extended a spectrum as the *M. tuberculosis* β-lactamase, it is induced to high levels of expression by certain β-lactams and β-lactamase inhibitors, including clavulanate (*34*). Furthermore, portions of *P. aeruginosa* genome exhibit high genetic polymorphism, giving highly varying profiles of antibiotic resistance between cultures and allowing *P. aeruginosa* to develop resistance mechanisms quickly (*35, 36*). Antibiotic treatments tend to be determined by bacterial culture sensitivity tests rather than empirical guidelines (*6*). After unsuccessful antibiotic treatment, *P. aeruginosa* often gain additional resistance mechanisms. *P. aeruginosa* can also form biofilms, which gives it additional antibiotic resistance (*37*). While rarer than some other common antibiotic resistance pathogens, cases of *P. aeruginosa* are among the hardest to treat.

Recent Developments in Antibiotic Research

The increasing prevalence of antibiotic resistance amongst pathogenic bacteria, particularly the ones examined above, highlights the need for new antibiotic therapy. However, the rate of antibiotic discovery has slowed significantly since the explosion of discoveries from the 1940s to the 1960s (*10*). Furthermore, many new antibiotics are derivatives of older classes, to which resistance mechanisms already exist or develop quickly. Two new antibiotic classes, Daptomycin and Linezolid, have been discovered in the last two decades. Daptomycin is a lipopeptide antibiotic, biosynthesized by strains of *Streptomyces roseosporus* (*38*). Daptomycin acts by the depolarization of cell membrane,

but only works against Gram-positive bacteria (*39*). Because Daptomycin requires intravenous dosing and has significant side effects, it is mostly used for vancomycin-resistant and methicillin-resistant Gram-positive bacteria (*12*). Linezolid is a synthetic antibacterial that inhibits protein synthesis in Gram-positive bacteria (*40*). Linezolid has long-term toxicity and is generally used, like Daptomycin, against bacteria that have acquired antibiotic resistance to other antibiotics, particularly vancomycin resistant *Enterococci (12)*. Because Linezolid is the last broad spectrum antibiotic with low frequencies of resistance, it is generally considered a "drug of last resort" – to be used only when there are no alternative treatments. Recent research has found that clavulanate, a β-lactamase inhibitor, administered with Meropenem, a β-lactam antibiotic, is effective against TB, which have been traditionally resistant against β-lactam antibiotics (*41*). This combination has been used to treat XDR-TB successfully in limited cases (*42*).

However, even with recent advances, there is still a great need for new antibiotics. Certain strains, such as *P. aeruginosa* remain difficult to treat (*6*). Resistance to new antibiotics have already appeared, and in come cases existed before commercialization of the antibiotic. The first case of linezolid resistance in *Enterococci* was reported in 1999 in a compassionate-use program, before linezolid was approved by the FDA (*43*). Linezolid resistance in *Staph. aureus* was found in 2001, one year after commercialization (*44*). Currently, multidrug resistant bacteria are pushing against the last line of antibiotic defense available. If resistance against new antibiotics such as Linezolid becomes prevalent, there will be few treatment options left.

New generations of a particular antibiotic class tend to be derived by functionalization of the core structure of older examples of that antibiotic class. As a

result, there are only about ten different antibiotic classes and thus ten distinct mechanisms of action even though many more antibiotics have been marketed (*45*). While different functional groups can affect the spectrum, toxicity, and distribution of an antibiotic, the underlying mechanism of action remains similar, so resistance develops quickly to derivatives of antibiotics that already have resistance genes in nature. Thus, the premium is in the development of a novel class of antibiotics with a novel mechanism of action on novel antibacterial targets.

There are three major criteria for a broad-spectrum antibacterial target. First, the antibiotic target should be essential to the survival of bacteria. Shutting down the target should cause bacterial death, while attenuating the target should detrimentally affect the organism. Second, the target should be essential for a large number of different bacteria in order to have a broad-spectrum effect. The actual spectrum of an antibiotic also tends to be less than the theoretical spectrum due to reasons such as an inability to penetrate cell membrane or efflux. Third, it should be possible to discriminate the bacterial target over the human target for toxicity reasons. After all, the goal of an antibiotic is to clear the bacteria without causing long-term adverse effects to the host.

One target that fulfills the above criteria is coenzyme A (CoA) biosynthesis. CoA is an indispensible cofactor for all organisms (*46, 47*). CoA functions as a biological acyl carrier, involved in essential functions such fatty acid metabolism in all organisms. Gene knockouts in the CoA biosynthetic pathway are often lethal, while reduced CoA levels lead to cell stasis, suggesting that CoA biosynthesis is essential (*48-51*). Genomic and biochemical studies have found significant differences between the bacterial CoA biosynthetic enzymes and the human CoA biosynthetic enzymes (*52-55*). Several bacteria

selective-inhibitors against pathway enzymes also have been characterized,

demonstrating that it is possible to selectively target the bacteria pathway (*56-58*).

Coenzyme A in Depth

Coenzyme A is Essential and Universal for All Organisms.

Coenzyme A, a necessary metabolite for all organisms, is required for essential

biochemical reactions such as fatty acid metabolism and the Krebs cycle (*47, 59, 60*).

CoA is involved in many different biochemical reactions, both essential and nonessential,

such that it is estimated that approximately 7-13% of all characterized enzymes require

CoA as a cofactor for activity (*47, 59*). While a few organisms, such as avian

Plasmodium falciparum, are thought to not produce CoA in certain stages of their life

cycle, all organisms require CoA for survival (*47*). Not surprisingly, CoA is a large area

of research, with focus on enzymes that use CoA, the biosynthesis of CoA, the regulation

of CoA, and how CoA is involved in diseases (*47, 61-63*).

CoA is the source of 4'-phosphopantetheine, the prosthetic group of acyl carrier

proteins (*46, 47, 62*). The thiol group on 4'-phosphopantetheine functions as a biological

acyl carrier, capable of reacting with carboxylic acid groups of various length (from two-

carbon acetyls to entire fatty acids) to form high energy thioesters. The carbon units can

then be shuttled for other uses, such as building up other metabolites (fatty acid

synthesis) or generating energy (fatty acid breakdown). The most prevalent function of

CoA is as acyl carriers, involved in pathways as diverse as polyketide/nonribosomal

peptide biosynthesis, Krebs cycle, fatty acid biosynthesis, and lipopolysaccharide

biosynthesis (*46, 47*).

CoA is also involved in some more exotic functions. For certain bacteria, CoA additionally functions as the cellular reductant. In *S. aureus* and certain *Bacillus* species, CoA and CoA metabolites, which can accumulate to millimolar levels, are believed to maintain the reducing environment of the cell, acting in place of the glutathione system which are lacking in those organisms (*64*). In *Bacillus megaterium*, protein-CoA disulfides help to maintain metabolic dormancy during spore formation (*51*). In some mammalian tissues, CoA has been found to be broken down into cysteamine, an anti-oxidant; however, the biological relevance of the reaction is unknown (*65, 66*).

Given both the essential and diverse biochemical functions involving CoA, it is unsurprising that reduced CoA levels cause either cell stasis or cell death. In bacteria such as *E. coli*, reduction of CoA levels lead to growth stasis (*50*). Knockouts of the CoA biosynthetic genes are lead to improper cell development and regulation, which can be lethal (*48, 49*). CoA biosynthesis is both essential and universal, fulfilling two criteria of a good anti-bacterial target.

The Coenzyme A Biosynthetic Pathway and Differences in Bacteria and Human

CoA is biosynthesized from the metabolic precursor, pantothenate, via five enzymatic steps, Figure 1.2 – CoA Biosynthetic Pathway (*47, 60, 67*). 4'-Phosphopantetheine, the portion of CoA that functions as cofactors to ACP, is synthesized in the first 3 enzymatic steps, while the final two enzymatic steps activate phosphopantetheine for recognition and loading onto ACP. First, pantothenate kinase (PanK; EC 2.7.1.33; *coaA*) phosphorylates pantothenate with consumption of ATP, to yield phosphopantothenate (PPA) (*68*). Second, an amide bond is formed between the

carboxyl group of PPA and the amino group of L-cysteine by

phosphopantothenoylcysteine synthetase (PPCS; EC 6.3.2.5; *coaB*), with consumption of

another NTP (*53*). Subsequent decarboxylation of the carboxylic acid moiety on the

ligated cysteine of phosphopantothenoylcysteine by phosphopantothenoylcysteine

decarboxylase (PPCDC; EC 4.1.1.36; *coaC*) gives 4'-phosphopantetheine (*69*). Next, 4'-

phosphopantetheine is adenylated by phosphopantetheine adenylyltransferase (PPAT; EC

2.7.7.3; *coaD*) to generate dephospho-coenzyme A (deCoA) (*55*). Finally, the 3'

hydroxyl group on the ribose sugar is phosphorylated to generate coenzyme A by

dephospho-CoA kinase (DPCK; EC 2.7.1.24; *coaE*) (*70*). The enzymes in the CoA

biosynthetic pathway are discussed, focusing particularly on differences between the

bacteria and human homologs as well as their potential as antibacterial targets.

Pantothenate Kinase

Pantothenate kinase, the first enzyme of the pathway, has been extensively

studied (*71-75*). Phosphorylation of pantothenate by PanK is the first committed step in

CoA biosynthesis. Pantothenate kinases from different species have been categorized into

four distinct classes by substrate affinity, pathway feedback, and structural homology.

Type I PanK, represented by the *E. coli* PanK and includes most bacterial PanK, have

high affinity for ATP and experiences feedback inhibition by CoA and CoA esters (*68,

76*). Eukaryotic PanK is similar to class I PanK biochemically, but lacks structural

homology (*75, 77*). Type II PanK, including *Staph. aureus* and several other gram

positive bacteria, has limited sequence and structural homology to eukaryotic PanK, but

is not inhibited by CoA and CoA esters (*64*). A few other unrelated bacteria such as

Pseudomonas aeruginosa, *Bacillus anthracis*, and *Helicobacter pylori* possesses type III

11

PanK, also referred to as *coaX*, that has poor ATP affinity (and potentially lacks nucleotide specificity) with no structural or sequence similarity to the other three classes (*71-73, 78*).

The structural and biochemical differences between the PanK have allowed the discovery and synthesis of bacterial-selective PanK inhibitors. Pantoyltaurine, an analogue of pantothenate where the carboxyl group is replaced with a sulfate, is the first pantothenate analogue discovered to inhibit microorganism growth (*79*). Pantothenate was found to anatagonize the antibacterial activity of pantoyltaurine, supporting the anti-PanK mechanism of pantoyltaurine. Other pantothenate analogues have shown selectivity for different organisms. For instance certain pantothenamide inhibitors show good selectivity for bacterial PanK, particularly *Staphylococcus (58)*. Some pantoyl analogues are selective for *Streptococcus* species (*57*). Interestingly, CJ-15,801, an α, β – unsaturated natural product analogue of pantothenate, was found to have μg/mL MIC against MDR *Staph. aureas* (*56*). While no pantothenate analogues have become actual antibiotics, the existence of natural products targeting the pathway as well as the ability to synthesize bacterial selective inhibitors suggests that PanK, and possibly the pathway, is a feasible target for drug development.

Phosphopantothenoylcysteine Synthetase and Phosphopantothenoylcysteine Decarboxylase

The last enzymes to be elucidated in CoA biosynthesis are phosphopantothenoylcysteine synthetase and phosphopantothenoylcysteine decarboxylase (*53, 69*). Like PanK, there are significant structural and biochemical differences between bacterial and human PPCS/PPCDC. All bacteria besides

Streptococci and *Enterococci* encode PPCS and PPCDC as a bifunctional fusion protein, with PPCS encoded in the C-terminal domain and PPCDC encoded in the N-terminal domain (*53, 69, 80, 81*). This bifunctional protein associates as a homododecamer, with the PPCS domain expressed as a homodimer and the PPCDC domain expressed as a homododecamer. In contrast, eukaryotes express PPCS and PPCDC as separate proteins, with PPCS associating as a homodimer and PPCDC associating as a homotrimer (*52*). The eukaryotic enzymes has little sequence homology with the bacterial enzymes (*82*).

Besides structural and sequence differences, preliminary studies found that bacterial and human PPCS also have different substrate specificities. In the earlier characterization of the CoA biosynthetic pathway, it was found that ATP, pantothenate, and cysteine are the only required substrates for mammalian CoA biosynthesis (*60*). However, additional CTP was required for bacterial CoA biosynthesis (*60*). Later, PPCS was identified as the bacterial enzyme requiring CTP (*53*). Preliminary studies found that human PPCS was four times faster when using ATP than when using CTP, but the question of nucleotide selectivity was not further examined (*52*). While there have been some studies on PPCS in literature, including several crystal structures as well as the characterization of the enzyme intermediate, the mechanism as well as the substrate selectivity of PPCS has not been examined in depth (*83*). However, the reported nucleotide selectivity differences coupled with the low sequence and structural homology between bacterial and human PPCS suggest that PPCS could be an interesting antibacterial target.

Like PPCS, PPCDC also has not been extensively characterized. The chemical reaction catalyzed by PPCDC – the decarboxylation of cysteine – is unusual. Only one

other enzyme identified so far, peptidyl-cysteine decarboxylase (EpiD), catalyze the

decarboxylation of another cysteine moiety (*84*). Characterizations of PPCDC have found

that flavin mononucleotide (FMN) is required for activity (*69, 85*). Based on spectral and

labeling studies, PPCDC was suggested to catalyze the decarboxylation reaction via a

thiol-carbonyl intermediate mediated by FMN, but more mechanistic data are needed

(*67*). Whether PPCDC would make an ideal antibacterial target is difficult to assess

currently. Even with low homology between human and bacteria orthologs, there is a lack

of data suggesting differences in the biochemistry of the orthologs, particularly since the

same cofactor, FMN, is involved in the reaction.

Phosphopantetheine Adenylyltransferase and Dephospho-CoA Kinase

PPAT and DPCK is also encoded and expressed differently for humans and

bacteria. In mammals, PPAT and DPCK are encoded as a bifunctional protein referred to

as CoA synthase on chromosome 17, although an unconfirmed monofunctional DPCK

was found on the same chromosome (*52, 86*). In contrast, bacteria PPAT and DPCK are

expressed monofunctionally (*87*). Bacterial PPAT is a homohexamer in solution, while

bacterial DPCK is a monomer after purification, but becomes a homotrimer at high

sulfate concentrations (*88-91*). Mammalian CoA synthase is a monomer in solution, but

is localized to the outer mitochondrial membrane via insertion of the N-terminus of the

protein into the organelle membrane (*92*). Again, bacterial and human orthologs share

little sequence homology.

PPAT is another well-studied enzyme, with purifications and characterizations for

both bacterial and mammalian species, some mechanistic data, and a few characterized

inhibitors (*55, 88, 89, 92-94*). Based on sequence homology, PPAT is a member of the

nucleotidyltransferase α/β phosphodiesterase superfamily (which many aminoacyl-tRNA synthetase belong to), with kinetic studies of the *E. coli* enzyme finding that PPAT follows a Random Bi Bi mechanism and that CoA is a feedback inhibitor of PPAT (*94*). Structure studies with substrates and products suggest that PPAT exhibits half site reactivity, as bound phosphopantetheine and dephospho-CoA only appear in one trimer of the hexamer, while ATP appears in all subunits of the hexamer, but have only partial density (*88, 89*). Based on a structure where phosphopantetheine was found in the active site of one trimer and CoA is found in the active site of the other trimer, CoA is suggested to act as an allosteric inhibitor of PPAT, although the kinetic nature of the proposed allosteric inhibition as well as whether allosteric inhibition is observed in PPAT orthologs is not explored. PPAT is believed to be an ideal antibacterial target due to the availability of structures and biochemical data as well as the poor homology and differences in expression between bacterial and human orthologs.

The adenylylation reaction to make dephospho-CoA by PPAT is reversible, requiring the phosphorylation of dephospho-CoA by DPCK to shift the equilibrium towards biosynthesis of CoA (*94*). Several structures of DPCK have been solved, but detailed mechanisms have not been published (*91*). Since relatively little is known about the biochemistry of DPCK, more studies are needed before DPCK can be examined as a potential drug target.

Objectives

Due to the reported nucleotide-selectivity difference as well as the inherent structural differences between human and bacterial orthologs, we studied PPCS as an

antibacterial target. Several bacterial PPCS along with the human PPCS were cloned, overexpressed, and purified. The mechanism and nucleotide selectivity of different PPCS was studied in depth. A high throughput screen was carried out to discover novel inhibitors of bacterial PPCS. The mechanism of inhibition of interesting compounds discovered in the screen was characterized. The effects of knocking out PPCS on the phenotype of the bacterial cells are also examined.

Furthermore, kinetic and inhibition studies were carried out on *E. faecalis* PPAT, leveraging some of the methods that we developed to study PPCS. In particular, we examined the mechanism of *E. faecalis* PPAT, the kinetic nature of the proposed allosteric CoA inhibition, as well as carry out a screen to find and characterize potential inhibitors of PPAT.

REFERENCE

1. Finch, R. G. (2004) Antibiotic resistance: a view from the prescriber. *Nat Rev Micro 2*, 989-994.
2. Fridkin, S. K., Steward, C. D., Edwards, J. R., Pryor, E. R., McGowan, J. E., Archibald, L. K., Gaynes, R. P., and Tenover, F. C. (1999) Surveillance of Antimicrobial Use and Antimicrobial Resistance in United States Hospitals: Project ICARE Phase 2. *Clin Infect Dis 29*, 245-252.
3. Ho, P.-L., Chow, K.-H., Lo, P.-Y., Lee, K.-F., and Lai, E. L. (2009) Changes in the epidemiology of methicillin-resistant Staphylococcus aureus associated with spread of the ST45 lineage in Hong Kong. *Diagnostic Microbiology and Infectious Disease 64*, 131-137.
4. Hidron, A. I., Edwards, J. R., Patel, J., Horan, T. C., Sievert, D. M., Pollock, D. A., and Fridkin, S. K. (2008) NHSN Annual Update: Antimicrobial-Resistant Pathogens Associated With Healthcare-Associated Infections: Annual Summary of Data Reported to the National Healthcare Safety Network at the Centers for Disease Control and Prevention, 2006-2007. *Infection Control and Hospital Epidemiology 29*, 996-1011.
5. Opar, A. (2007) Bad bugs need more drugs. *Nat Rev Drug Discov 6*, 943-944.
6. Livermore, D. M. (2002) Multiple Mechanisms of Antimicrobial Resistance in Pseudomonas aeruginosa: Our Worst Nightmare? *Clinical Infectious Diseases 34*, 634-640.
7. Gandhi, N. R., Moll, A., Sturm, A. W., Pawinski, R., Govender, T., Lalloo, U., Zeller, K., Andrews, J., and Friedland, G. (2006) Extensively drug-resistant tuberculosis as a cause of death in patients co-infected with tuberculosis and HIV in a rural area of South Africa. *The Lancet 368*, 1575-1580.
8. Keshavjee, S., Gelmanova, I. Y., Farmer, P. E., Mishustin, S. P., Strelis, A. K., Andreev, Y. G., Pasechnikov, A. D., Atwood, S., Mukherjee, J. S., Rich, M. L., Furin, J. J., Nardell, E. A., Kim, J. Y., and Shin., S. S. (2008) Treatment of extensively drug-resistant tuberculosis in Tomsk, Russia: a retrospective cohort study. *The Lancet 372*, 1403 - 1409.
9. Austin, D. J., Kristinsson, K. G., and Anderson, R. M. (1999) The relationship between the volume of antimicrobial consumption in human communities and the frequency of resistance. *Proceedings of the National Academy of Sciences of the United States of America 96*, 1152-1156.
10. Clatworthy, A. E., Pierson, E., and Hung, D. T. (2007) Targeting virulence: a new paradigm for antimicrobial therapy. *Nat Chem Biol 3*, 541-548.
11. Holten, K. B., and Onusko, E. M. (2000) Appropriate Prescribing of Oral Beta-Lactam Antibiotics. *Am Fam Physician 62*, 611-620.
12. Beer, M. H., Porter, R. S., and Jones, T. V. (2006) *The Merck Manual of Diagnosis and Therapy Eighteenth Edition*.
13. Jacoby, G. A. (2009) AmpC β-Lactamases. *Clin. Microbiol. Rev. 22*, 161-182.
14. Fisher, J., Charnas, R. L., and Knowles, J. R. (1978) Kinetic studies on the inactivation of Escherichia coli RTEM β-lactamase by clavulanic acid. *Biochemistry 17*, 2180-2184.

15. Charnas, R. L., and Knowles, J. R. (1981) Inactivation of radiolabeled RTEM β-lactamase from Escherichia coli by clavulanic acid and 9-deoxyclavulanic acid. *Biochemistry 20*, 3214-3219.

16. R J Wallace, J., Steele, L. C., Brooks, D. L., Luman, J. I., Wilson, R. W., and McLarty, J. W. (1985) Amoxicillin-clavulanic acid in the treatment of lower respiratory tract infections caused by beta-lactamase-positive Haemophilus influenzae and Branhamella catarrhalis. *Antimicrob Agents Chemother. 27*, 912-915.

17. Jacobs, M. R., Aronoff, S. C., Johenning, S., and Yamabe, S. (1986) Comparative activities of the β-lactamase inhibitors YTR 830, clavulanate and sulbactam combined with extended-spectrum penicillins against ticarcillin-resistant Enterobacteriaceae and pseudomonads. *J. Antimicrob. Chemother. 18*, 177-184.

18. Hancock, R. E. W. (1998) Resistance Mechanisms in Pseudomonas aeruginosa and Other Nonfermentative Gram-Negative Bacteria. *Clinical Infectious Diseases 27*, S93-S99.

19. Klevens, R. M., Edwards, J R., Tenover, F C., McDonald, L. C., Horan, T., and Gaynes, R. (2006) Changes in the Epidemiology of Methicillin Resistant Staphylococcus aureus in Intensive Care Units in US Hospitals, 1992-2003. *Clinical Infectious Diseases 42*, 389-391.

20. Kluytmans, J., van Belkum, A., and Verbrugh, H. (1997) Nasal carriage of Staphylococcus aureus: epidemiology, underlying mechanisms, and associated risks. *Clin. Microbiol. Rev. 10*, 505-520.

21. Henwood, C. J., Livermore, D. M., Johnson, A. P., James, D., Warner, M., Gardiner, A., and The Linezolid Study, G. (2000) Susceptibility of Gram-positive cocci from 25 UK hospitals to antimicrobial agents including linezolid. *J. Antimicrob. Chemother. 46*, 931-940.

22. Hiramatsu, K., Hanaki, H., Ino, T., Yabuta, K., Oguri, T., and Tenover, F. C. (1997) Methicillin-resistant Staphylococcus aureus clinical strain with reduced vancomycin susceptibility. *J. Antimicrob. Chemother. 40*, 135-136.

23. Chang, S., Sievert, D. M., Hageman, J. C., Boulton, M. L., Tenover, F. C., Downes, F. P., Shah, S., Rudrik, J. T., Pupp, G. R., Brown, W. J., Cardo, D., Fridkin, S. K., and the Vancomycin-Resistant Staphylococcus aureus Investigative, T. (2003) Infection with Vancomycin-Resistant Staphylococcus aureus Containing the vanA Resistance Gene. *N Engl J Med 348*, 1342-1347.

24. Mater, D. D. G., Langella, P., Corthier, G., and Flores, M. J. (2005) Evidence of vancomycin resistance gene transfer between enterococci of human origin in the gut of mice harbouring human microbiota. *J. Antimicrob. Chemother. 56*, 975-978.

25. Murray, B. E. (1990) The life and times of the Enterococcus. *Clin. Microbiol. Rev. 3*, 46-65.

26. Kainer, M. A., Devasia, R. A., Jones, T. F., Simmons, B. P., Melton, K., Chow, S., Broyles, J., Moore, K. L., Craig, A. S., and Schaffner, W. (2007) Response to Emerging Infection Leading to Outbreak of Linezolid-Resistant Enterococci. *Emerging Infectious Diseases 13*.

27. Hidron, A. I., Schuetz, A. N., Nolte, F. S., Gould, C. V., and Osborn, M. K. (2008) Daptomycin resistance in Enterococcus faecalis prosthetic valve endocarditis. *J. Antimicrob. Chemother.*, dkn105.

28. Clewell, D. B. (1990) Movable genetic elements and antibiotic resistance in enterococci. *European Journal of Clinical Microbiology & Infectious Diseases 9*, 90-102.

29. Noble, W. C., Rahman, M., Karadec, T., and Schwarz, S. (1996) Gentamicin resistance gene transfer from Enterococcus faecalis and E. faecium to Staphylococcus aureus, S. intermedius and S. hyicus. *Veterinary Microbiology 52*, 143-152.

30. Bloom, B. R., and Murray, C. J. L. (1992) Tuberculosis: Commentary on a Reemergent Killer. *Science 257*, 1055-1064.

31. Raviglione, M. C., Snider, D. E., Jr., and Kochi, A. (1995) Global Epidemiology of Tuberculosis: Morbidity and Mortality of a Worldwide Epidemic. *JAMA 273*, 220-226.

32. Flores, A. R., Parsons, L. M., and Pavelka, M. S., Jr. (2005) Genetic analysis of the β-lactamases of Mycobacterium tuberculosis and Mycobacterium smegmatis and susceptibility to β-lactam antibiotics. *Microbiology 151*, 521-532.

33. Poole, K. (2001) Multidrug Efflux Pumps and Antimicrobial Resistance in Pseudomonas aeruginosa and Related Organisms. *J. Mol. Microbiol. Biotechnol. 3*, 255-264.

34. Lister, P. D., Gardner, V. M., and Sander, C. C. (1999) Clavulanate induces expression of the *Pseudomonas aeruginosa* AmpC cephalosporinase at physiologically relevant concentrations and antagonizes the antibacterial activity of ticarcillin. *Antimicrob Agents Chemother. 43*, 882-889.

35. Martin, C., Ichou, M. A., Massicot, P., Goudeau, A., and Quentin, R. (1995) Genetic diversity of Pseudomonas aeruginosa strains isolated from patients with cystic fibrosis revealed by restriction fragment length polymorphism of the rRNA gene region. *J. Clin. Microbiol. 33*, 1461-1466.

36. Picard, B., Denamur, E., Barakat, A., Elion, J., and Goullet, P. (1994) Genetic heterogeneity of Pseudomonas aeruginosa clinical isolates revealed by esterase electrophoretic polymorphism and restriction fragment length polymorphism of the ribosomal RNA gene region. *J Med Microbiol 40*, 313-322.

37. Mah, T.-F., Pitts, B., Pellock, B., Walker, G. C., Stewart, P. S., and O'Toole, G. A. (2003) A genetic basis for Pseudomonas aeruginosa biofilm antibiotic resistance. *Nature 426*, 306-310.

38. Rybak, M. (2006) The efficacy and safety of daptomycin: first in a new class of antibiotics for Gram-positive bacteria. *Clin Microbiol Infect. 12*, 24-32.

39. Silverman, J. A., Perlmutter, N. G., and Shapiro, H. M. (2003) Correlation of Daptomycin Bactericidal Activity and Membrane Depolarization in Staphylococcus aureus. *Antimicrob. Agents Chemother. 47*, 2538-2544.

40. Shinabarger, D. L., Marotti, K. R., Murray, R. W., Lin, A. H., Melchior, E. P., Swaney, S. M., Dunyak, D. S., Demyan, W. F., and Buysse, J. M. (1997) Mechanism of action of oxazolidinones: effects of linezolid and eperezolid on translation reactions. *Antimicrob Agents Chemother. 41*, 2132-2136.
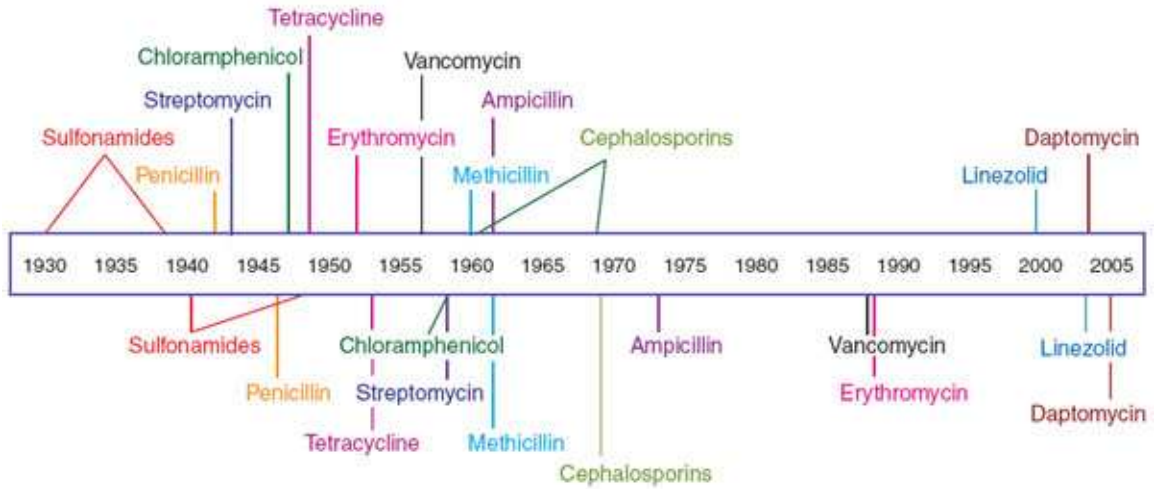
41. Hugonnet, J.-E., and Blanchard, J. S. (2007) Irreversible Inhibition of the Mycobacterium tuberculosis β-Lactamase by Clavulanate. *Biochemistry 46*, 11998-12004.

42. Hugonnet, J.-E., Tremblay, L. W., Boshoff, H. I., Barry, C. E., 3rd, and Blanchard, J. S. (2009) Meropenem-Clavulanate Is Effective Against Extensively Drug-Resistant Mycobacterium tuberculosis. *Science 323*, 1215-1218.

43. Zurenko, G. E., Todd, W. M., Hafkin, B., Kauffman, C., and Bock, J. (2000) Development of linezolid-resistant Enterococcus faecium in two compassionate use program patients treated with linezolid. *Program and abstracts of the Thirty-ninth Interscience Conference on Antimicrobial Agents and Chemotherapy*.

44. Sabol, K., Patterson, J. E., II, J. S. L., Owens, A., Cadena, J., and Jorgensen, J. H. (2005) Emergence of Daptomycin Resistance in Enterococcus faecium during Daptomycin Therapy. *Antimicrob Agents Chemother. 49*, 1664-1665.

45. Finch, R. G., Greenwood, D., Norrby, S. R., and Whitley, R. H. (2003) *Antibiotic and Chemotherapy: Anti-Infective Agents and Their Use in Therapy*.

46. Leonardi, R., Zhang, Y., Rock, C. O., and Jackowski, S. (2005) Coenzyme A: Back in action. *Prog Lip Res 44*, 125-153.

47. Spry, C., Kirk, K., and Saliba, K. J. (2008) Coenzyme A biosynthesis: an antimicrobial drug target. *FEMS Microbiol. Rev. 32*, 56-106.

48. Bosveld, F., Rana, A., van der Wouden, P. E., Lemstra, W., Ritsema, M., Kampinga, H. H., and Sibon, O. C. M. (2008) De novo CoA biosynthesis is required to maintain DNA integrity during development of the Drosophila nervous system. *Hum. Mol. Genet. 17*, 2058-2069.

49. Zhang, Y.-M., Chohnan, S., Virga, K. G., Stevens, R. D., Ilkayeva, O. R., Wenner, B. R., Bain, J. R., Newgard, C. B., Lee, R. E., Rock, C. O., and Jackowski, S. (2007) Chemical Knockout of Pantothenate Kinase Reveals the Metabolic and Genetic Program Responsible for Hepatic Coenzyme A Homeostasis. *Chemistry & Biology 14*, 291-302.

50. Jackowski, S., and Rock, C. O. (1986) Consequences of reduced intracellular coenzyme A content in Escherichia coli. *J. Bacteriol. 166*, 866-871.

51. Setlow, B., and Setlow, P. (1977) Levels of acetyl coenzyme A, reduced and oxidized coenzyme A, and coenzyme A in disulfide linkage to protein in dormant and germinated spores and growing and sporulating cells of Bacillus megaterium. *J. Bacteriol. 132*, 444-452.

52. Daugherty, M., Polanuyer, B., Farrell, M., Scholle, M., Lykidis, A., de Crecy-Lagard, V., and Osterman, A. (2002) Complete reconstitution of the human coenzyme A biosynthetic pathway via comparative genomics. *J. Biol. Chem. 277*, 21431-21439.

53. Strauss, E., Kinsland, C., Ge, Y., McLafferty, F. W., and Begley, T. P. (2001) Phosphopantothenoylcysteine synthetase from *Escherichia coli*. Identification and characterization of the last unidentified coenzyme A biosynthetic enzyme in bacteria. *J. Biol. Chem. 276*, 13513-13516.

54. Genschel, U. (2004) Coenzyme A biosynthesis: reconstruction of the pathway in archaea and an evolutionary scenario based on comparative genomics. *Mol Biol Evol 21*, 1242-1251.

55. Geerlof, A., Lewendon, A., and Shaw, W. V. (1999) Purification and Characterization of Phosphopantetheine Adenylyltransferase from Escherichia coli. *J. Biol. Chem. 274*, 27105-27111.

56. Sugie, Y., Dekker, K., Hirai, H., Ichiba, T., Ishiguro, M., Shiomi, Y., Sugiura, A., Brennan, L., Duignan, J., Huang, L. H., Sutcliffe, J., and Kojima, Y. (2001) CJ-15,801, a novel antibiotic from a fungus, *Seimatosporium* sp. *Journal of Antibiotics 54*, 1060-1065.

57. Strauss, E., and Begley, T. P. (2002) The Antibiotic Activity of N-Pentylpantothenamide Results from Its Conversion to Ethyldethia-Coenzyme A, a Coenzyme A Antimetabolite. *Journal of Biological Chemistry 277*, 48205-48209.

58. Choudhry, A. E., Mandichak, T. L., Broskey, J. P., Egolf, R. W., Kinsland, C., Begley, T. P., Seefeld, M. A., Ku, T. W., Brown, J. R., Zalacain, M., and Ratnam, K. (2003) Inhibitors of Pantothenate Kinase: Novel Antibiotics for Staphylococcal Infections. *Antimicrob. Agents Chemother. 47*, 2051-2055.

59. Leonardi, R., Zhang, Y.-M., Rock, C. O., and Jackowski, S. (2005) Coenzyme A: Back in action. *Progress in Lipid Research 44*, 125-153.

60. Brown, G. M. (1959) The metabolism of pantothenic acid. *J. Biol. Chem. 234*, 370-378.

61. Saliba, K. J., and Kirk, K. (2005) CJ-15,801, a fungal natural product, inhibits the intraerythrocytic stage of Plasmodium falciparum in vitro via an effect on pantothenic acid utilisation *Molecular and Biochemical Parasitology 141*, 129-131.

62. Rock, C. O., and Cronan, J. E. (1996) Escherichia coli as a model for the regulation of dissociable (type II) fatty acid biosynthesis. *Biochimica et Biophysica Acta (BBA) - Lipids and Lipid Metabolism 1302*, 1-16.

63. Hong, B. S., Senisterra, G., Rabeh, W. M., Vedadi, M., Leonardi, R., Zhang, Y.-M., Rock, C. O., Jackowski, S., and Park, H.-W. (2007) Crystal Structures of Human Pantothenate Kinases. *Journal of Biological Chemistry 282*, 27984-27993.

64. Leonardi, R., Chohnan, S., Zhang, Y.-M., Virga, K. G., Lee, R. E., Rock, C. O., and Jackowski, S. (2005) A Pantothenate Kinase from Staphylococcus aureus Refractory to Feedback Regulation by Coenzyme A. *Journal of Biological Chemistry 280*, 3314-3322.

65. Maras, B., Barra, D., Duprè, S., and Pitari, G. (1999) Is pantetheinase the actual identity of mouse and human vanin-1 proteins? *FEBS Letters 461*, 149-152.

66. Pitari, G., Malergue, F., Martin, F., Philippe, J. M., Massucci, M. T., Chabret, C., Maras, B., Duprè, S., Naquet, P., and Galland, F. (2000) Pantetheinase activity of membrane-bound Vanin-1: lack of free cysteamine in tissues of Vanin-1 deficient mice. *FEBS Letters 483*, 149-154.

67. Strauss, E., Zhai, H., Brand, L. A., McLafferty, F. W., and Begley, T. P. (2004) Mechanistic studies on phosphopantothenoylcysteine decarboxylase: trapping of an enethiolate intermediate with a mechanism-based inactivating agent. *Biochemistry 43*, 15520 -15533.

68. Song, W. J., and Jackowski, S. (1994) Kinetics and regulation of pantothenate kinase from Escherichia coli. *Journal of Biological Chemistry 269*, 27051-27058.

69. Kupke, T. (2001) Molecular characterization of the 4'-phosphopantothenoylcysteine decarboxylase domain of bacterial Dfp flavoproteins. *J. Biol. Chem. 276*, 27597-27604.

70. Worrall, D. M., and Tubbs, P. K. (1983) A bifunctional enzyme complex in coenzyme A biosynthesis: purification of pantetheine phosphate adenylyltransferase and dephospho-CoA kinase. *Biochem. J. 215*, 153-157.

71. Brand, L. A., and Strauss, E. (2005) Characterization of a New Pantothenate Kinase Isoform from Helicobacter pylori. *Journal of Biological Chemistry 280*, 20185-20188.

72. Hong, B. S., Yun, M. K., Zhang, Y.-M., Chohnan, S., Rock, C. O., White, S. W., Jackowski, S., Park, H.-W., and Leonardi, R. (2006) Prokaryotic Type II and Type III Pantothenate Kinases: The Same Monomer Fold Creates Dimers with Distinct Catalytic Properties. *Structure 14*, 1251-1261.

73. Nicely, N. I., Parsonage, D., Paige, C., Newton, G. L., Fahey, R. C., Leonardi, R., Jackowski, S., Mallett, T. C., and Claiborne, A. (2007) Structure of the Type III Pantothenate Kinase from Bacillus anthracis at 2.0 A Resolution: Implications for Coenzyme A-Dependent Redox Biology. *Biochemistry 46*, 3234-3245.

74. Rock, C. O., Calder, R. B., Karim, M. A., and Jackowski, S. (2000) Pantothenate Kinase Regulation of the Intracellular Concentration of Coenzyme A. *Journal of Biological Chemistry 275*, 1377-1383.

75. Rock, C. O., Karim, M. A., Zhang, Y.-M., and Jackowski, S. (2002) The murine pantothenate kinase (Pank1) gene encodes two differentially regulated pantothenate kinase isozymes. *Gene 291*, 35-43.

76. Song, W. J., and Jackowski, S. (1992) Cloning, sequencing, and expression of the pantothenate kinase (coaA) gene of Escherichia coli. *J. Bacteriol. 174*, 6411-6417.

77. Calder, R. B., Williams, R. S. B., Ramaswamy, G., Rock, C. O., Campbell, E., Unkles, S. E., Kinghorn, J. R., and Jackowski, S. (1999) Cloning and Characterization of a Eukaryotic Pantothenate Kinase Gene (panK) from Aspergillus nidulans. *Journal of Biological Chemistry 274*, 2014-2020.

78. Yang, K., Eyobo, Y., Brand, L. A., Martynowski, D., Tomchick, D., Strauss, E., and Zhang, H. (2006) Crystal Structure of a Type III Pantothenate Kinase: Insight into the Mechanism of an Essential Coenzyme A Biosynthetic Enzyme Universally Distributed in Bacteria. *J. Bacteriol. 188*, 5532-5540.

79. Pierpoint, W. S., Hughes, D. E., Baddiley, J., and Mathias, A. P. (1955) The effect of some pantothenate derivatives on growth and coenzyme-A synthesis in bacteria. *Biochem. J. 61*, 190-190.

80. Kupke, T. (2002) Molecular characterization of the 4'-phosphopantothenoylcysteine synthetase domain of bacterial Dfp flavoproteins. *J. Biol. Chem. 277*, 36137-36145.

81. Kupke, T., and Schwarz, W. (2006) 4'-Phosphopantetheine biosynthesis in archaea. *J. Biol. Rhythms 281*, 5435-5444.

82. Manoj, N., Strauss, E., Begley, T. P., and Ealick, S. E. (2003) Structure of human phosphopantothenoylcysteine synthetase at 2.3 A resolution. *Structure 11*, 927-936.

83. Stanitzek, S., Augustin, M. A., Huber, R., Kupke, T., and Steinbacher, S. (2004) Structural basis of CTP-dependent peptide bond formation in coenzyme A biosynthesis catalyzed by *Escherichia coli* PPC synthetase. *Structure 12*, 1977-1988.

84. Blaesse, M., Kupke, T., Huber, R., and Steinbacher, S. (2000) Crystal structure of the peptidyl-cysteine decarboxylase EpiD complexed with a pentapeptide substrate. *EMBO J 19*, 6299-6310.

85. Spitzer, E. D., and Weiss, B. (1985) *dfp* gene of *Escherichia coli* K-12, a locus affecting DNA synthesis, codes for a flavoprotein. *J. Bacteriol. 164*, 994-1003.

86. Aghajanian, S., and Worrall, D. M. (2002) Identification and characterization of the gene encoding the human phosphopantetheine adenylyltransferase and dephospho-CoA kinase bifunctional enzyme (CoA synthase). *Biochem. J. 365*, 13-18.

87. Martin, D. P., and Drueckhammer, D. G. (1993) Separate Enzymes Catalyze the Final Two Steps of Coenzyme A Biosynthesis in Brevibacterium ammoniagenes: Purification of Pantetheine Phosphate Adenylyltransferase. *Biochem. Biophys. Res. Commun. 192*, 1155-1161.

88. Izard, T. (2002) The crystal structures of phosphopantetheine adenylyltransferase with bound substrates reveal the enzyme's catalytic mechanism. *J. Mol. Biol. 315*, 487-495.

89. Izard, T. (2003) A Novel Adenylate Binding Site Confers Phosphopantetheine Adenylyltransferase Interactions with Coenzyme A. *J. Bacteriol. 185*, 4074-4080.

90. Mishra, P. k., Park, P. K., and Drueckhammer, D. G. (2001) Identification of yacE (coaE) as the Structural Gene for Dephosphocoenzyme A Kinase in Escherichia coli K-12. *J. Bacteriol. 183*, 2774-2778.

91. O'Toole, N., Barbosa, J. A. R. G., Li, Y., Hung, L.-W., Matte, A., and Cygler, M. (2003) Crystal structure of a trimeric form of dephosphocoenzyme A kinase from *Escherichia coli*. *Protein Sci. 12*, 237-236.

92. Zhyvoloup, A., Nemazanyy, I., Babich, A., Panasyuk, G., Pobigailo, N., Vudmaska, M., Naidenov, V., Kukharenko, O., Palchevskii, S., Savinska, L., Ovcharenko, G., Verdier, F., Valovka, T., Fenton, T., Rebholz, H., Wang, M.-L., Shepherd, P., Matsuka, G., Filonenko, V., and Gout, I. T. (2002) Molecular Cloning of CoA Synthase. *J. Biol. Chem. 277*, 22107-22110.

93. Zhao, L., Allanson, N. M., Thomson, S. P., Maclean, J. K. F., Barker, J. J., Primrose, W. U., Tyler, P. D., and Lewendon, A. (2003) Inhibitors of phosphopantetheine adenylyltransferase. *European Journal of Medicinal Chemistry 38*, 345-349.

94. Miller, J. R., Ohren, J., Sarver, R. W., Mueller, W. T., Dreu, P. d., Case, H., and Thanabal, V. (2007) Phosphopantetheine Adenylyltransferase from Escherichia coli: Investigation of the Kinetic Mechanism and Role in Regulation of Coenzyme A Biosynthesis. *J. Bacteriol. 189*, 8196-8205.

Figure 1.1: Timeline of antibiotic deployment and observed antibiotic resistance (*10*).
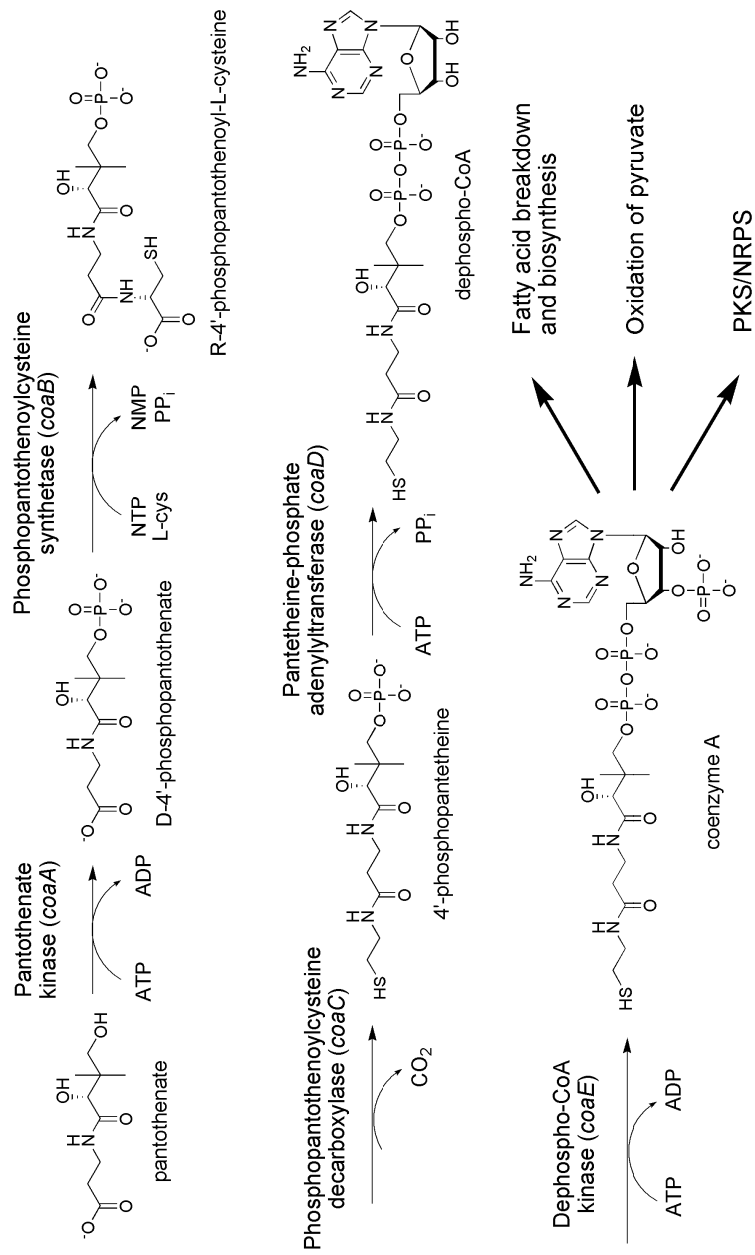
Figure 1.2: Biosynthetic pathway of coenzyme A.

Chapter 2

Characterization and Kinetics of Phosphopantothenoylcysteine Synthetase

from *Enterococcus faecalis*

BACKGROUND

Phosphopantetheine ((*R*)-3-hydroxy-4-(3-(2-mercaptoethylamino)-3-oxopropylamino)-2,2-dimethyl-4-oxobutyl dihydrogen phosphate) is an essential molecule for all living organisms (*1-3*). Phosphopantetheine is found as a part of coenzyme A (CoA), as well as a prosthetic group on acyl carrier protein (ACP) (*1*). Both CoA and ACP play essential roles in various acyl transfer reactions required for many biochemical reactions associated with intermediary metabolism and cell membrane assembly in living organisms (*4*). The essential nature of phosphopantetheine to the viability of cells makes the CoA biosynthetic pathway an intriguing target for antimicrobial development (*5, 6*).

While it has been known for decades that CoA is biosynthesized from nucleotide triphosphates (NTP), D-pantothenate, and L-cysteine, the genes involved have only been identified in recent years (*7-9*). In eukaryotic systems that have been characterized, the phosphopantetheine portion of CoA is biosynthesized from pantothenate via three chemical reactions catalyzed by three polypeptides, Figure 2.1 (*10, 11*). First,

pantothenate is phosphorylated by pantothenate kinase (PanK; EC 2.7.1.33; *coaA*), using ATP as the phosphate donor, to yield phosphopantothenate (PPA). Second, an amide bond is formed between the carboxyl group of PPA and the amino group of L-cysteine catalyzed by an ATP-dependent phosphopantothenoylcysteine synthetase (PPCS; EC 6.3.2.5; *coaB*). Subsequent decarboxylation of the carboxylic acid moiety on the ligated cysteine of phosphopantothenoylcysteine by phosphopantothenoylcysteine decarboxylase (PPCDC; EC 4.1.1.36; *coaC*) gives 4'-phosphopantetheine. In bacterial systems characterized so far, the second and third biochemical reactions – the amide bond formation between phosphopantothenate and cysteine, as well as the subsequent decarboxylation of cysteine by PPCS and PPCDC – are catalyzed by a single bifunctional polypeptide (*9, 12*). Furthermore, CTP, rather than ATP, is required by the bifunctional PPCS (*7, 9*).

PPCS from a few species have been characterized. The proposed mechanism of PPCS involves the formation a 4'-phosphopantothenoyl cytidylate intermediate in the first half reaction from the nucleophilic attack on the α-phosphate of CTP by the carboxylic acid group of phosphopantothenate, with the concomitant release of pyrophosphate. In the second half reaction, the amino group of L-cysteine attacks the cytidylate intermediate to yield phosphopantothenoylcysteine and CMP, Figure 2.2. The proposed mechanism is supported by the observation of the 4'-phosphopantothenoyl cytidylate intermediate in CTP and phosphopantothenate soaked *E. coli* N210D PPCS domain crystal structure (*13*). However, there has been no complete study on the kinetic mechanism of PPCS or attempts to examine the proposed intermediate in the course of the enzymatic reaction. Here, we overexpress, purify, and characterize PPCS from

Enterococcus faecalis, which is a monofunctional bacterial PPCS with poor homology to both human monofunctional PPCS and bacterial bifunctional PPCS/PPCDC (*5, 10*). In this study we use initial velocity, product competition, and titration experiments to elucidate the kinetic mechanism of PPCS from *E. faecalis*. Furthermore, isotope transfer studies are used to study the nature of the enzyme intermediate. Here we report for the first time the chemical mechanism and nucleotide specificity of a monofunctional bacterial PPCS.

MATERIALS AND METHODS

Materials. The chemicals used were of reagent grade or of the highest purity commercially available, and were not further purified. Source 15Q, Source 15S, and Superdex 200 were from GE Healthcare. Calcium D-pantothenate, HEPES, Tris base, ATP, CTP, Pyrophosphate Reagent, ampicillin, sodium chloride, sodium hydroxide, methanol, formic acid, sodium pyrophosphate, dithiothreitol, L-cysteine, and 97% [^{18}O] water were from Sigma-Aldrich. Lauria agar (Lennox), and Lauria broth (Lennox) were from Difco. Restriction and DNA modifying enzymes were from New England Biolabs. The *Escherichia coli* BL21 AI was obtained from Invitrogen and *E. coli* XL1 Blue was obtained from Stratagene. Polymerase Chain Reaction was performed using an Eppendorf Gradient Mastercycler and *Pfu*Turbo Hotstart DNA polymerase (Stratagene). Oligonucleotides were synthesized by Invitrogen. Qiagen minispin kits were used for DNA purification and PCR reaction cleanup. Electrospray mass spectral analysis was performed at the University of Michigan Mass Spectrometry Facility, Department of Chemistry. DNA sequencing was performed by the University of Michigan, Biomedical Research Resources Core Facility.

Cloning, Overexpression, and Purification of E. faecalis PPCS. The *coaB* gene

was amplified from *E. faecalis* genomic DNA (strain ATCC 700802), via PCR, using the

forward primer GCGCCATATGGATGTTTTAGTTACTGCTGGCGG and the reverse

primer GCGCCTCGAGTCATTGTTGTTCTCTCCATTTCTTTTC to introduce an *Nde*I

site (shown underlined) upstream of the gene and an *Xho*I site downstream of the gene.

The resulting PCR product, encoding the entire *coaB* gene, was digested with *Nde*I and

*Xho*I, and ligated into pET23a(+) (Novagen) which had also been restricted with *Nde*I

and *Xho*I. The desired plasmid was designated pUMGD1 and the insert was confirmed by

DNA sequencing. *E. coli* strain BL21 AI harboring the plasmid pUMGD1 was incubated

in four 1 L flasks containing 250 ml each of LB-ampicillin media (5 g of NaCl, 5 g of

yeast extract, 10 g tryptone, and 100 mg of ampicillin per L) at 37ºC with vigorous

shaking (250 rpm) until the optical density at 600 nm reached 0.6 - 0.8. The culture was

cooled to 17ºC and induced with a final concentration of 0.065% w/v L-arabinose.

Incubation (17ºC, 250 rpm) was continued overnight. Cells from the 1 L of culture were

harvested by centrifugation at 10,000 x g, washed with 20 mM HEPES pH 8.0, and

suspended in 80 ml of 20 mM HEPES pH 8.0. The cells were disrupted by French Press,

and the resulting suspension was centrifuged at 20,000 x g for 30 minutes to separate the

crude cytosol (supernatant) from cellular debris (pellet). The cytosol was

chromatographed on a Source 15Q column (8 mL of resin per 250 mL of cell culture)

equilibrated with 20 mM HEPES pH 8.0, washed with three column volumes of

equilibration buffer, and eluted over a 10 column volume linear gradient of 0 - 0.5 M

NaCl in 20 mM HEPES pH 8.0. Fractions were analyzed by SDS-PAGE and fractions

containing PPCS were pooled, and passed through a 320 mL Superdex 200 prep grade

column equilibrated in 20 mM HEPES pH 8.0 containing 150 mM NaCl. The purified fractions were dialyzed against 20 mM HEPES pH 8.0, and stored at -80°C.

Cloning, Overexpression, and Purification of the pyrophosphate dependent fructose-6-phosphate kinase (PPi-FPK). The *E. coli* codon optimized PPi-PFK gene (DNA 2.0) of *Propionibacterium freudenreichii*, containing a *Nde*I site upstream and a *Xho*I site downstream of the gene, was digested with *Nde*I and *Xho*I and ligated into pET23a(+) via the same sites. The resulting vector was designated pUMJY901. Growth, expression, and purification protocols used were the same as for PPCS (above).

Cloning, Overexpression, and Purification E. faecalis pantothenate kinase. The *coaA* gene was amplified from *E. faecalis* genomic DNA (strain ATCC 700802), via PCR, using the forward primer CGTA<u>CATATG</u>GACGATAAAATGAATTAC and the reverse primer CGTA<u>CTCGAG</u>TTAATATTTACGTAGATAG to introduce an *Nde*I site (shown underlined) upstream of the gene and an *Xho*I site downstream of the gene. The resulting PCR product, encoding the entire *coaA* gene, was digested with *Nde*I and *Xho*I, and ligated into *Nde*I and *Xho*I digested pET23a(+) (Novagen). The resulting vector was designated pUMJY010 and verified via DNA sequencing. Growth, expression, and purification protocols used were the same as for PPCS (above).

High Resolution Mass Spectrometry. The purified *E. faecalis* PPCS was dialyzed against H_2O, and brought to 50/50 methanol/water containing 1% formic acid. The sample (final protein concentration of 0.2 mg/mL) was submitted for positive-ion ESI-MS.

Synthesis of 4'-phosphopantothenate. 4'-Phosphopantothenate was synthesized via previously published procedures (*9*).

Synthesis of [carboxyl-^{18}O]Phosphopantothenate. Methyl D-pantothenate (18.6 mg, 80 µmole) was treated with 0.4 M Na^{18}OH in 200 µL final volume (8 µL of 10 M NaOH and 192 µL of 97% H$_2$^{18}O for a final concentration of 93.2% ^{18}O) for 2 hours at room temperature. The reaction was then neutralized by applying to an AG MP-50 resin spin column (H$^+$ form; 1 mL) and centrifuged at 1000 x *g* for 2 minutes to yield [*carboxyl*-^{18}O] D-pantothenate. The labeled pantothenate was then converted, biochemically, into [*carboxyl*-^{18}O] D-phosphopantothenate by incubating at 30°C overnight in the presence of 1.1 equivalent ATP and 10 µM *E. faecalis* pantothenate kinase in 50 mM HEPES, pH 8.0 (5 mL final volume). The reaction was separated on a Source 15Q column (8 mL) via a linear gradient elution of 0 - 0.4 M NaCl in water. Fractions containing labeled phosphopantothenate, detected enzymatically using the PPCS assay (described below), were combined and lyophilized. The lyophilized fractions were subjected to gel filtration on a BioGel P-2 column (240 mL) in water to remove NaCl. The relevant fractions were lyophilized and characterized. ^{1}H NMR (500 MHz, D$_2$O): δ 0.82 (s, 3H), 0.99 (s, 3H), 2.41 (t, 2H), 3.39 (dd, 1H), 3.42 (dt, 2H), 3.75 (dd, 1H), 4.1 (s, 1H). ^{13}C NMR (125 MHz, D$_2$O): δ 17.96 (s), 21.42 (s), 36.12 (s), 36.72 (s), 38.35 (d), 70.69 (d), 74.77 (s), 174.76 (s), 180.268 (s, caboxylate ^{18}O), 180.295 (s, caboxylate ^{16}O), ratio of carboxylate species 92 to 10 (^{18}O to ^{16}O; Figure 2.5).

^{18}O Transfer Reaction. Reaction mixture of 10 mM CTP, 10 mM MgCl$_2$, 12 mM [*carboxyl*-^{18}O] D-phosphopantothenate, 10 mM L-cysteine, 10 mM DTT, and 2.4 µM *E. faecalis* PPCS in 500 µL of 100 mM Tris HCl pH 7.6 was incubated for 1 hour at 37°C. The reaction was then filtered through a Microcon YM-10 membrane (Amicon) at 13,000 x *g* and 15°C for 30 minutes to remove the enzyme. To the filtrate was added 120 µL

^2H_2O, and the solution was analyzed via ^{31}P NMR. Analogous control experiments with unlabeled D-phosphopantothenate or without enzyme were also performed.

NMR spectroscopy. Proton-decoupled ^{31}P NMR spectra were recorded on a Bruker DRX500 spectrometer (11.75 T) at a probe temperature of 298 K, tuned to 202.4 MHz, using 5-mm high resolution NMR tubes. Spectra were obtained with a spectral width of 80000 Hz, 1.0 s relaxation delay, and 32,768 complex points in the time domain using simultaneous detection of real and imaginary components. The time domain data were apodized with an exponential (0.5 Hz) prior to zero-filling followed by Fourier transformation. Chemical shifts are reported relative to an external sample of 10 mM inorganic phosphate (0.0 ppm) in 100 mM Tris-HCl (pH 7.6) and 10% ^2H_2O.

Proton-decoupled ^{13}C NMR spectra were recorded on a Bruker DRX500 spectrometer (11.75 T) at a probe temperature of 298 K, tuned to 125.7 MHz, using 5-mm high resolution NMR tubes. Spectra were obtained with a spectral width of 25000 Hz, 1.0 s relaxation delay, and 32,768 complex points in the time domain using simultaneous detection of real and imaginary components. The time domain data were apodized with an exponential (0.5 Hz) prior to zero-filling followed by Fourier transformation. Chemical shifts are reported relative to tetramethylsilane (0.0 ppm).

Enzyme Assay. The PPCS reaction was observed in the forward reaction via an enzyme linked assay, where the production of pyrophosphate from PPCS activity was coupled to the oxidation of NADH, which could be monitored as a disappearance of absorption at 340 nm. All of the components of the pyrophosphate detection system are available commercially as the Pyrophosphate Reagent (PR) from Sigma-Aldrich. It was necessary that additional units of PPi-PFK be added to the commercial preparation in

order to use it as a continuous assay. With this modification, PPCS activity could be observed in real time under our experimental conditions. The assays were performed on a SpectraMax M5 (Molecular Devices) microplate reader using 96-well half-area plates (Costar UV), where each assay has 100 μL final volume. Each vial of the PR was resuspended in 4.5 mL of 100 mM HEPES pH 7.6. The assay mix consisted of 30 μL PR, 1U of additional PPi-PFK, 10 mM DTT, and varying concentrations of the substrates (CTP, L-cysteine, and PPA) in a volume of 70 μL buffered in 50 mM Tris-HCl and pH 7.6. All assay mixes contained $MgCl_2$ in 1:1 molar stoichiometry with nucleotide triphosphate in addition to the 2 mM $MgCl_2$ already present from the PR. The assay mix and the enzyme solution (275 nM PPCS in 50 mM Tris-HCl pH 7.6) were incubated at 37˚C for 15 min before the assay. Reactions were initiated by adding 30 μL of enzyme solution to the assay mix. The oxidation of NADH, monitored by a decreasing UV absorbance at 340 nm ($\varepsilon = 6.22$ mM^{-1}cm^{-1}), was measured over the course of the assay and the activity of the enzyme was calculated by adjusting for pathlength (0.5 cm) and taking into account that each mole of pyrophosphate produced leads to the oxidation of 2 moles of NADH. Assays were run in duplicates, with the average velocities reported.

Initial Velocity Studies. Pairwise analysis, where initial velocities were measured with varying concentrations of one substrate at different fixed concentrations of a second substrate while holding the third substrate at saturation, were conducted. For instance, initial velocities as a function [CTP] were measured at several fixed levels of [PPA] (0.6, 0.3, 0.15, 0.075, and 0.0375 mM) with constant level of [cysteine] (1 mM). Pairwise analyses were performed for all three substrates sets.

Product Inhibition Studies. Initial velocities were measured against different concentrations of one substrate with fixed concentrations of the other two substrates and different fixed concentrations of the product inhibitor. For example, initial velocities versus [CTP] were measured at 0.15 mM PPA, 1 mM cysteine, and several fixed levels of [CMP] (0, 250, 500, and 1000 µM).

Data Analysis. Initial velocity was first graphically analyzed as Lineweaver-Burke double reciprocal plots. Velocity versus the varying [substrate] data was fit to equation 1 to determine the K_m^{app} and k_{cat}^{app}, which was in turn used to derive the fitting lines in the Lineweaver-Burke plots. The different patterns in the Lineweaver-Burke plots arising from the pairwise or inhibition analysis was used to determine which terreactant kinetic mechanism describes PPCS. The initial velocity data from the three sets of pairwise analysis was fit to the initial velocity equation (equation 2) describing the appropriate mechanism (Bi Uni Uni Bi Ping Pong) to determine the relevant kinetic parameters. Likewise, product inhibition data was fitted to the appropriate product inhibition equations (equation 3-5) to determine the relevant kinetic parameters.

$$v = \frac{V_{max}^{app}[A]}{K_m^{app} + [A]} \quad (1)$$

$$v = \frac{V_{max}[A][B][C]}{K_{ia}K_{mB}[C] + K_{mC}[A][B] + K_{mB}[A][C] + K_{mA}[B][C] + [A][B][C]} \quad (2)$$

$$v = \frac{V_{max}[A]}{K_{mA}\left(1 + \frac{K_{ia}K_{mB}}{K_{mA}[B]} + \frac{K_{ia}K_{mB}[R]}{K_{mA}K_{ir}[B]} + \frac{[R]}{K_{ir}}\right) + [A]\left(1 + \frac{K_{mB}}{[B]} + \frac{K_{mC}}{[C]}\right)} \quad (3)$$

$$v = \frac{V_{max}[B]}{K_{mB}\left(1 + \dfrac{K_{ia}}{[A]} + \dfrac{K_{ia}[R]}{K_{ir}[A]}\right) + [B]\left(1 + \dfrac{K_{mA}}{[A]} + \dfrac{K_{mC}}{[C]} + \dfrac{K_{mA}[R]}{K_{ir}[A]}\right)} \quad (4)$$

$$v = \frac{V_{max}[C]}{K_{mC} + [C]\left(1 + \dfrac{K_{mA}}{[A]} + \dfrac{K_{mB}}{[B]} + \dfrac{K_{ia}K_{mB}}{[A][B]} + \dfrac{K_{ia}K_{mB}[R]}{K_{ir}[A][B]} + \dfrac{K_{mA}[R]}{K_{ir}[A]}\right)} \quad (5)$$

In these equations, v is initial velocity and V_{max} is maximum velocity. K_{mA}, K_{mB}, and K_{mC} are the Michaelis constants for substrates A, B, and C, respectively. K_{iA} is the dissociation constant of substrate A and K_{ir} is the inhibition constant of the product R.

Isothermal Titration Calorimetry. Isothermal titration calorimetry (ITC) was performed to determine the dissociation constant, K_d, of CTP to the *E. faecalis* PPCS enzyme. The experiment was conducted on a VP-ITC instrument from MicroCal. The titration experiment was run at 30°C with 50 µM *E. faecalis* PPCS enzyme and 15 mM Mg-CTP, both in 50 mM sodium phosphate buffer, pH 7.6. The solvation energy of injecting Mg-CTP was determined by performing the same above experiment, except substituting the dialysis buffer for enzyme in the sample cell. The solvation energy was subtracted from the corresponding titration energy to get the energy of binding. The collected result is analyzed via the Origin software (OriginLab Corp), using the one site model with the stoichiometry of binding, n, held at 1, equation 6.

$$Q = \frac{(n[M]_t \, \Delta H \, V_0)}{2}\left\{1 + \frac{[L]_t}{n[M]_t} + \frac{1}{nK_a[M]_t} - \sqrt{\left(1 + \frac{[L]_t}{n[M]_t} + \frac{1}{(nK_a[M]_t)}\right)^2 - \frac{4[L]_t}{n[M]_t}}\right\} \quad (6)$$

RESULTS

Expression and Purification of recombinant E. faecalis PPCS. From the Source 15Q anion exchange column, PPCS eluted at 200 mM NaCl. Fractions containing PPCS

from the anion exchange column were further purified via gel filtration chromatography, and PPCS was >98% pure as determined by SDS-PAGE (Figure 2.3) after gel filtration chromotography. Approximately 30 mg of soluble PPCS was obtained per liter of cell culture from our purification procedure. The native oligomerization state of PPCS was determined via gel filtration, where the elution volume of PPCS on a Superdex 200 HR column was compared to the elution volumes of known protein standards (Bio-Rad gel filtration standard). Compared to the known standards, PPCS eluted as an approximately 60 kDa molecule, which is suggestive of a homodimer (monomer weight of 28.5 kDa for a theoretical mass 57 kDa).

The molecular weight of PPCS was determined by positive-ion ESI-MS, Figure 2.4. The purified PPCS has a molecular mass of 28415.0 Da, corresponding to the calculated mass of the recombinant protein (28525.2 Da) associating with one molecule of sodium (23 Da) and without the amino terminal methionine (133.2 Da). The mass determination shows that *E. faecalis* PPCS has no additional mass from the likes of attached prosthetic group, in agreement with previously characterized *E. coli* PPCS (*9*).

ATP/CTP Specificity of E. faecalis PPCS. Because the sequence homology of *E. faecalis* PPCS is similarly divergent from both human and *E. coli* PPCS, the nucleotide specificity of *E. faecalis* PPCS was determined. The *E. faecalis* enzyme was assayed in the presence of either 10 mM ATP or CTP, 0.6 mM PPA, and 1 mM cysteine (saturating conditions for all substrates). The PPCS reaction with ATP showed only 8% of the activity compared to the PPCS reaction using CTP, suggesting that the *E. faecalis* enzyme is highly selective for CTP like other bacterial PPCS.

Oxygen Transfer during PPCS Catalysis. From the ^{13}C NMR spectrum of

[*carboxyl-*^{18}O] phosphopantothenate, two NMR resonances separated by 0.027 ppm,

corresponding to [*carboxyl-*^{16}O] phosphopantothenate and [*carboxyl-*^{18}O]

phosphopantothenate are observed. These two resonances integrate to a ratio of 1 to 9.2,

signifying that the labeled phosphopantothenate contains 90% [18]O distributed between

the two carboxylate oxygens, consistent with the percentage of [18]O (93%) contained in

the saponification reaction. [*carboxyl-*^{18}O] Phosphopantothenate was used as a substrate

for the *E. faecalis* PPCS enzymatic reaction to observe the formation of the

phosphopantothenoyl cytidylate intermediate. At the end of the reaction, the PPCS

protein was filtered out of solution and ^{31}P NMR spectra was taken on the remaining

solution. Two NMR resonances, 0.025 ppm apart, were observed corresponding to CMP

labeled with one or zero [18]O atom, Figure 2.5. The upfield shifted CMP resonance,

corresponding to [18]O labeled CMP, represents approximately 45% of the total CMP

resonances, consistent with the transfer of one of the two equivalent carboxylate oxygens

of PPA. A single resonance corresponding to unlabeled CMP was observed in the [31]P

NMR spectra of the control reaction, where unlabelled phosphantothenate was used as

substrate. The incorporation of [18]O from [*carboxyl-*^{18}O] phosphopantothenate into CMP

over the course of the PPCS enzymatic reaction is consistent with the formation of the

proposed phosphopantothenoyl cytidylate intermediate.

Enzyme Mechanism. Initial velocity was measured against varying concentrations

of one substrate at fixed, changing levels of a second substrate. The resulting data was

plotted as a double reciprocal plot and the resulting patterns were used to diagnose the

enzyme mechanism. In the double reciprocal plot of initial velocity against [CTP] at

various [PPA] with saturating [cysteine], the fitted lines intersect to the left of the y-axis, consistent with CTP and PPA having a sequential relationship to each other, Figure 2.6. Thus, in the overall mechanism, both CTP and PPA must bind to the enzyme before potential product release steps. In the double reciprocal plot of initial velocity against [cysteine] at various [PPA], the fitted lines are parallel, consistent with a mechanism where PPA and cysteine are Ping-Pong with respect to each other, Figure 2.7. In the overall mechanism, the binding of PPA and the binding of cysteine are interrupted by a product release step. Likewise, the double reciprocal plot of initial velocity against [cysteine] at various [CTP] also exhibits a parallel pattern, consistent with a mechanism where PPA and CTP are Ping-Pong with respect to each other, Figure 2.8. Given that CTP and PPA must both bind to the enzyme before any product can release, the only terreactant mechanism consistent with the observed pairwise relationships between the substrates is the Bi Uni Uni Bi Ping Pong mechanism.

To determine the order of CTP and PPA binding, the product inhibition patterns of CMP with respect to the three substrates are examined. In the double reciprocal plot of initial velocity against [CTP] at various [CMP], the fitted lines intersect on the y-axis, consistent with CMP as a competitive inhibitor with respect to CTP, Figure 2.9. In the double reciprocal plot of initial velocity against [PPA] at various [CMP], the fitted lines intersect in the second quadrant, suggesting that CMP is a noncompetitive inhibitor with respect to PPA, Figure 2.10. Finally, in the double reciprocal plot of initial velocity against [cysteine] at various [CMP], the fitted lines are parallel, suggesting that CMP is an uncompetitive inhibitor with respect to cysteine, Figure 2.11. Together, the three sets of inhibition patterns are consistent with a Bi Uni Uni Bi Ping Pong mechanism where

CTP binds first to the free enzyme and CMP is released last to give the free enzyme (Figure 2.12).

The steady state kinetic parameters are determined by fitting the collected data to the initial velocity equation of a Bi Uni Uni Bi Ping Pong mechanism, equation 2, and are collected in Table 2.1. The inhibition patterns of CMP with respect to the three substrates, as well as the calculated K_i of CMP from each set of inhibition data are collected in Table 2.2.

Isothermal Titration Colorimetry. The dissociation constant, K_d, for Mg-CTP binding to *E. faecalis* PPCS was determined via isothermal titration calorimetry. The heat of binding from injecting Mg-CTP was integrated to give the binding isotherm, Figure 2.13. The binding isotherm was fit to a one site model, and the association constant, K_a, was calculated to equal $1.55 \times 10^3 \pm 1.4 \times 10^2$ M^{-1}. The dissociation constant, K_d, of Mg-CTP was determined to be 645 µM by taking the inverse of K_a. This K_d is extremely close to the dissociation constant of CTP calculated from the kinetic studies (defined as K_{ia}), 650 µM, despite minor differences in experimental conditions. The matching dissociation constants from two independent experiments strongly support a mechanism where CTP binds first to the enzyme, as the calculated K_{ia} variable of a similar random ordered binding mechanism would consist of a combination of different rate constants and thus be expected to have a different value than the K_d of CTP calculated from the ITC.

DISCUSSION

Phosphopantothenoylcysteine synthetase catalyzes the amide bond formation between 4'-phosphopantothenate and L-cysteine in the second enzymatic step of CoA

biosynthesis (*7, 9*). Because of the essential function of CoA in the growth and survival of all living organisms, selective inhibitors of bacterial PPCS activity could be broad spectrum antibiotics (*5, 6*). PPCS from *E. faecalis* represents a previously uncharacterized class of bacterial PPCS, found in several clinically and bioterrorism relevant bacteria, such as *Streptococcus pneumoniae* and *Bacillus anthracis* (*5, 10*). This class of PPCS is expressed monofunctionally, in contrast to other bacterial PPCS, which are expressed as a fusion protein with phosphopantothenoylcysteine decarboxylase, the next enzyme in the pathway. In order to better understand the biochemistry of PPCS to facilitate inhibitor design, *E. faecalis* PPCS has been cloned, overexpressed, and purified. The purified protein underwent kinetic and isotopic labeling studies to better understand the mechanism of this novel class of monofunctional bacterial PPCS.

Even though *E. faecalis* PPCS has similarly distant homology to both the bifunctional bacterial PPCS and the monofunctional human PPCS, our kinetic studies found that *E. faecalis* PPCS is CTP specific like all other bacterial PPCS characterized to date (*5*). Thus, it's likely that all bacterial PPCS, whether expressed as a bifunctional polypeptide with PPCDC or as a monofunctional protein, are CTP-specific. In contrast, the monofunctional human PPCS has been reported to be ATP selective(*5-7*). The observed difference in nucleotide specificity between the bacterial and mammalian PPCS likely have implications regarding the evolution and regulation of the CoA biosynthetic pathway, and could also offer the biochemical differences required to develop selective bacterial PPCS inhibitors (*14*).

To establish the formation of the proposed phosphopantothenoyl cytidylate intermediate in the PPCS enzymatic reaction, ^{18}O transfer studies were conducted on the

PPCS enzymatic reaction. Because ^{18}O has a significant one-bond nuclear shielding effect upon carbon and phosphorus atoms, the transfer of the ^{18}O atom can be observed via NMR in terms of the resulting upfield shift of these nuclei (*15-19*). When [*carboxyl-*^{18}O]-labeled phosphopantothenate was used for the PPCS enzymatic reaction, approximately half of the ^{18}O were incorporated into the phosphate group of the reaction product CMP. This is consistent with a kinetic mechanism where the phosphopantothenoyl cytidylate intermediate is formed from the attack of the carboxylate of PPA on the α-phosphate of CTP with release of pyrophosphate. In the second half reaction, attack from L-cysteine on the intermediate produces phosphopantothenoylcysteine and CMP, with one of the oxygen in the carboxyl group of PPA transferred into the product CMP. The phosphopantothenoyl cytidylate intermediate has been observed in the crystal structure of the N210D mutant *E. coli* PPCS which cannot complete the enzymatic reaction, but here we show that the phosphopantothenoyl cytidylate intermediate is formed over the course of the PPCS enzymatic reaction (*13*).

Our kinetic and ITC studies found that *E. faecalis* PPCS follows a Bi Uni Uni Bi Ping Pong kinetic mechanism where CTP bindings first and CMP releases last. The observed structural changes of the previously crystallized N210D mutant *E. coli* PPCS is consistent with our proposed mechanism (*13*). In the structure of the apo-form of the *E. coli* PPCS, residues 284-299 and residues 354-363 are unresolved and presumed to be disordered. Since several of these disordered residues form contacts with the substrate PPA, the cleft where PPA eventually binds is not well formed and solvent exposed as a result. In contrast, the CTP binding pocket is mostly formed, and CTP presumably can bind. In the CTP bound structure, residues 284-289, 298, and 299 become ordered and

interact with the binding site on the other dimer to help fully form the PPA binding cleft. From the crystal structure, the binding of CTP is requisite for the binding of PPA, consistent with the ordered binding mechanism we propose.

The Ping-Pong portion of the proposed kinetic mechanism refers to the release of PP_i prior to the binding and attack of cysteine. This was observed in the crystal structures as well. When both PPA and CTP were soaked with the protein crystal, 4'-phosphopantothenoyl cytidylate was resolved in the binding site, with pyrophosphate no longer present, consistent with the release of PP_i before the nucleophilic attack from cysteine (*13*). In the same structure, residues 354-363 became ordered so most of the phosphopantothenoyl cytidylate intermediate was no longer solvent exposed, except for the activated acid group which the cysteine would attack in the second half reaction. When all three substrates were soaked with the crystals, only CMP is observed in the active site, suggesting that phosphopantothenoylcysteine was released first, same as the order proposed in our kinetic mechanism.

From our kinetic, chemical, and ITC studies, we determined that *E. faecalis* PPCS follows a Bi Uni Uni Bi Ping Pong mechanism with CTP binding first and CMP releasing last. Our proposed mechanism is consistent with data from literature, including a series of crystal structures of the N210D mutant *E. coli* PPCS. In our proposed mechanism, CTP and PPA bind sequentially to the PPCS enzyme to react and form the proposed 4'-phosphopantothenoyl cytidylate intermediate with released of pyrophosphate. Next, L-cysteine attacks the carbonyl group of the mixed anhydride to form the reaction products phosphopantothenoylcysteine and CMP, with phosphopantothenoylcysteine released before CMP.

REFERENCE

1. Majerus, P. W., Alberts, A. W., and Vagelos, P. R. (1965) Acyl Carrier Protein. Iv. the Identification of 4'-Phosphopantetheine as the Prosthetic Group of the Acyl Carrier Protein. *Proc Natl Acad Sci U S A 53*, 410-417.
2. Anderson, M. S., Bulawa, C. E., and Raetz, C. R. (1985) The biosynthesis of gram-negative endotoxin. Formation of lipid A precursors from UDP-GlcNAc in extracts of Escherichia coli. *J Biol Chem 260*, 15536-15541.
3. Brozek, K. A., and Raetz, C. R. (1990) Biosynthesis of lipid A in Escherichia coli. Acyl carrier protein-dependent incorporation of laurate and myristate. *J Biol Chem 265*, 15410-15417.
4. Magnuson, K., Jackowski, S., Rock, C. O., and Cronan, J. E., Jr. (1993) Regulation of fatty acid biosynthesis in Escherichia coli. *Microbiol Rev 57*, 522-542.
5. Gerdes, S. Y., Scholle, M. D., D'Souza, M., Bernal, A., Baev, M. V., Farrell, M., Kurnasov, O. V., Daugherty, M. D., Mseeh, F., Polanuyer, B. M., Campbell, J. W., Anantha, S., Shatalin, K. Y., Chowdhury, S. A., Fonstein, M. Y., and Osterman, A. L. (2002) From genetic footprinting to antimicrobial drug targets: examples in cofactor biosynthetic pathways. *J Bacteriol 184*, 4555-4572.
6. Zhang, Y. M., White, S. W., and Rock, C. O. (2006) Inhibiting bacterial fatty acid synthesis. *J Biol Chem 281*, 17541-17544.
7. Brown, G. M. (1959) The metabolism of pantothenic acid. *J Biol Chem 234*, 370-378.
8. Kupke, T., Uebele, M., Schmid, D., Jung, G., Blaesse, M., and Steinbacher, S. (2000) Molecular characterization of lantibiotic-synthesizing enzyme EpiD reveals a function for bacterial Dfp proteins in coenzyme A biosynthesis. *J Biol Chem 275*, 31838-31846.
9. Strauss, E., Kinsland, C., Ge, Y., McLafferty, F. W., and Begley, T. P. (2001) Phosphopantothenoylcysteine synthetase from Escherichia coli. Identification and characterization of the last unidentified coenzyme A biosynthetic enzyme in bacteria. *J Biol Chem 276*, 13513-13516.
10. Genschel, U. (2004) Coenzyme A biosynthesis: reconstruction of the pathway in archaea and an evolutionary scenario based on comparative genomics. *Mol Biol Evol 21*, 1242-1251.
11. Daugherty, M., Polanuyer, B., Farrell, M., Scholle, M., Lykidis, A., de Crecy-Lagard, V., and Osterman, A. (2002) Complete reconstitution of the human coenzyme A biosynthetic pathway via comparative genomics. *J. Biol. Chem. 277*, 21431-21439.
12. Kupke, T., Hernandez-Acosta, P., Steinbacher, S., and Culianez-Macia, F. A. (2001) Arabidopsis thaliana flavoprotein AtHAL3a catalyzes the decarboxylation of 4'-Phosphopantothenoylcysteine to 4'-phosphopantetheine, a key step in coenzyme A biosynthesis. *J Biol Chem 276*, 19190-19196.
13. Stanitzek, S., Augustin, M. A., Huber, R., Kupke, T., and Steinbacher, S. (2004) Structural basis of CTP-dependent peptide bond formation in coenzyme A

biosynthesis catalyzed by Escherichia coli PPC synthetase. *Structure 12*, 1977-1988.

14.   Ostrander, D. B., O'Brien, D. J., Gorman, J. A., and Carman, G. M. (1998) Effect of CTP synthetase regulation by CTP on phospholipid synthesis in Saccharomyces cerevisiae. *J Biol Chem 273*, 18992-19001.

15.   Hansen, D. E., and Knowles, J. R. (1981) The stereochemical course of the reaction catalyzed by creatine kinase. *J Biol Chem 256*, 5967-5969.

16.   Hansen, D. E., and Knowles, J. R. (1982) The stereochemical course at phosphorus of the reaction catalyzed by phosphoenolpyruvate carboxylase. *J Biol Chem 257*, 14795-14798.

17.   Kohlbrenner, W. E., Nuss, M. M., and Fesik, S. W. (1987) 31P and 13C NMR studies of oxygen transfer during catalysis by 3-deoxy-D-manno-octulosonate cytidylyltransferase from Escherichia coli. *J Biol Chem 262*, 4534-4537.

18.   Dotson, G. D., Dua, R. K., Clemens, J. C., Wooten, E. W., and Woodard, R. W. (1995) Overproduction and one-step purification of Escherichia coli 3-deoxy-D-manno-octulosonic acid 8-phosphate synthase and oxygen transfer studies during catalysis using isotopic-shifted heteronuclear NMR. *J Biol Chem 270*, 13698-13705.

19.   Zheng, R., and Blanchard, J. S. (2001) Steady-state and pre-steady-state kinetic analysis of Mycobacterium tuberculosis pantothenate synthetase. *Biochemistry 40*, 12904-12912.
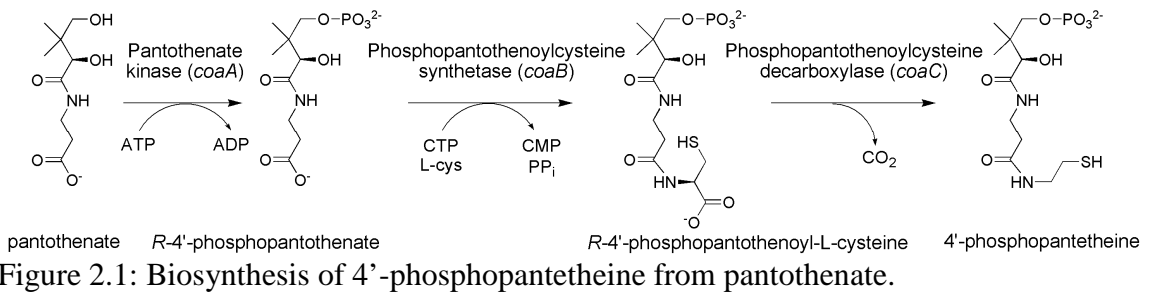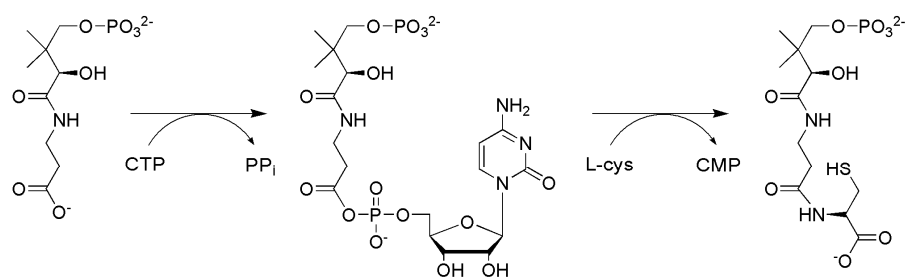
Figure 2.1: Biosynthesis of 4'-phosphopantetheine from pantothenate.

D-4'-phosphopantothenate   phosphopantothenoyl cytidylate   R-4'-phosphopantothenoyl-L-cysteine

Figure 2.2: The proposed chemical mechanism of the PPCS enzymatic reaction.
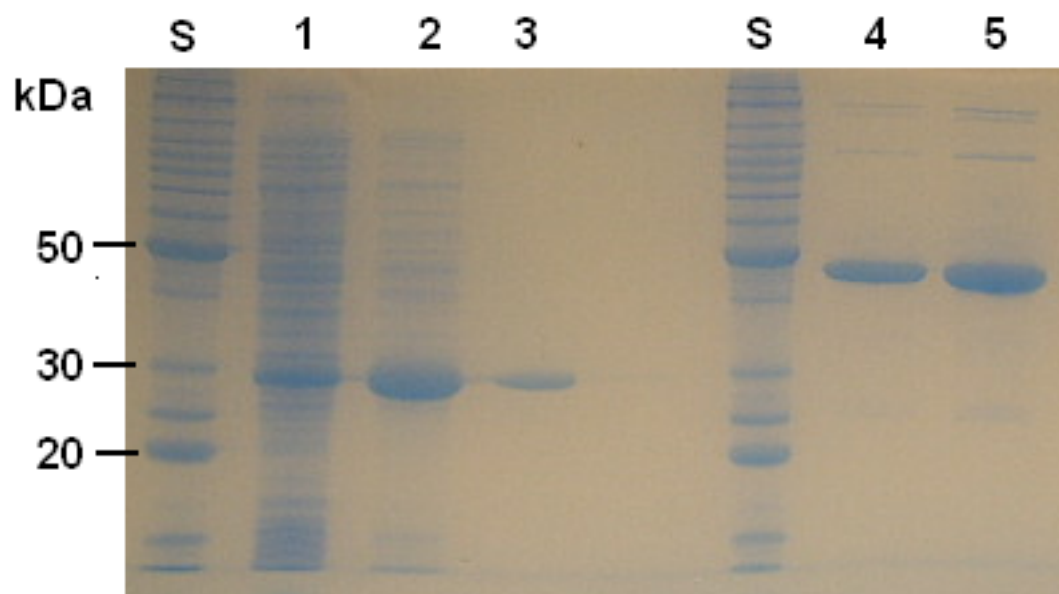
Figure 2.3: *E. faecalis* PPCS SDS-PAGE. *Lanes S*: Protein weight standards. *Lane 1*: *E. coli* BL21 AI/pUMGD1 crude extract expressing recombinant *E. faecalis* PPCS. *Lane 2*: *E. faecalis* PPCS extract after purification through source 15Q anion exchange *Lane 3*: *E. faecalis* PPCS extract after both source 15Q and Superdex 200 gel filtration. *Lanes 4 and 5*: Purified recombinant *P. freudenreichii* PPi-FPK.
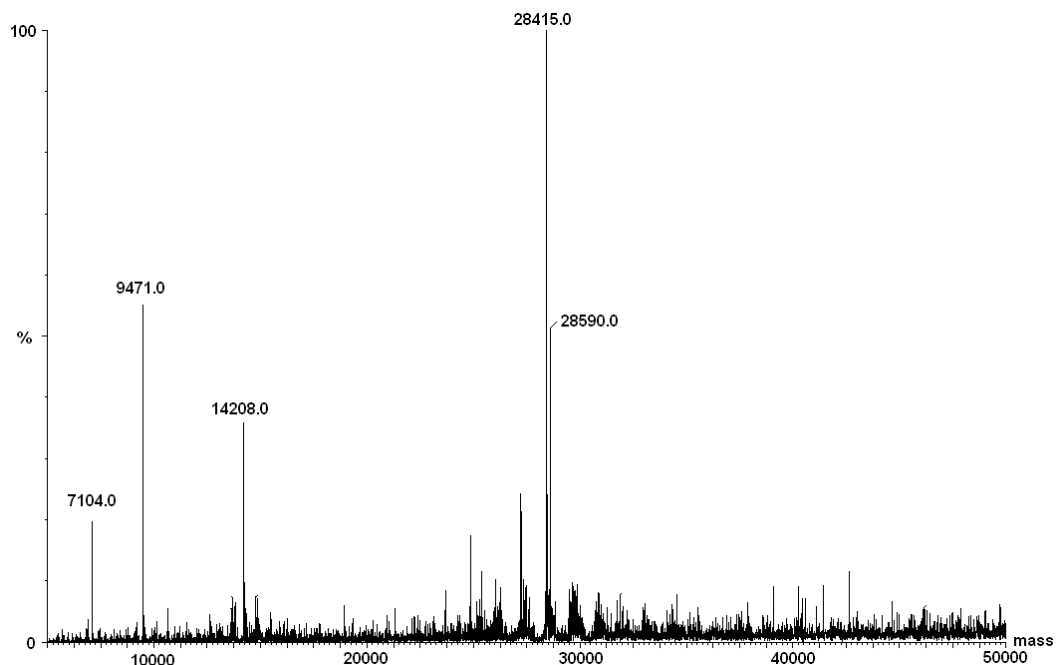
Figure 2.4: Positive-ion ESI-MS of purified *E. faecalis* PPCS. The observed mass (28415.0 Da) correspondes to the calculated mass of the recombination PPCS (28522.2 Da) without the N-terminal methionine (133.2 Da) and associating with one molecule of sodium (23 Da).
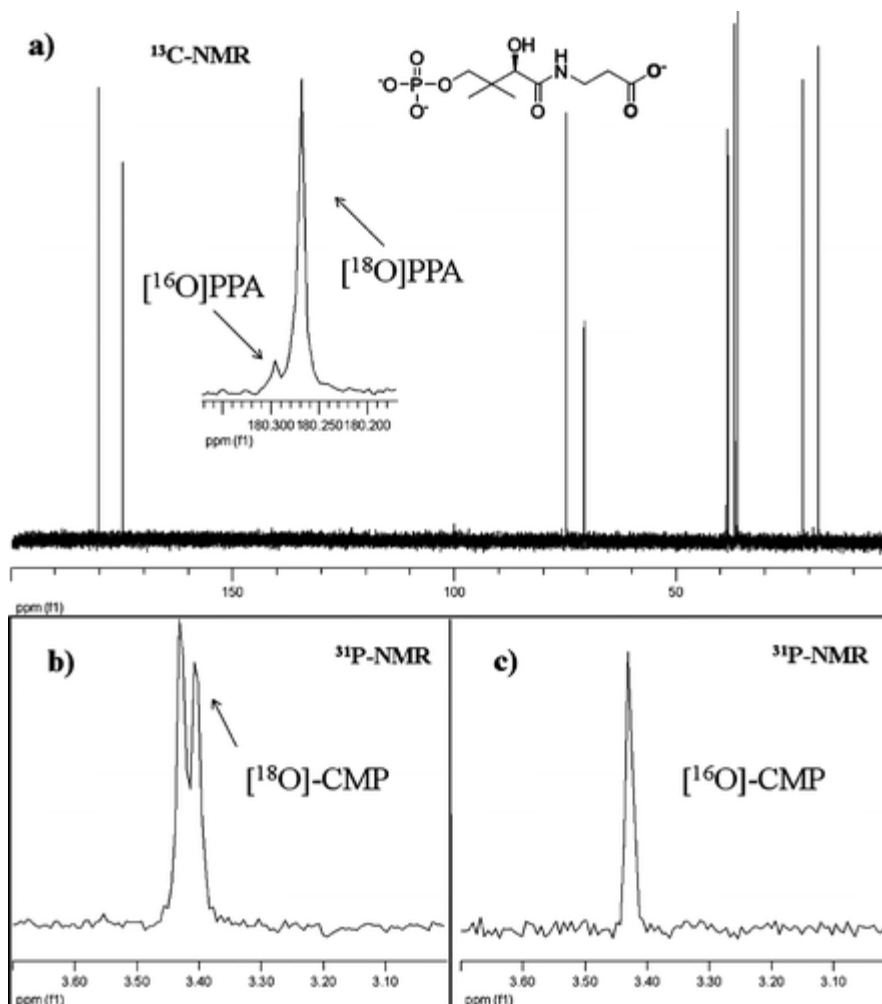
Figure 2.5: ^{13}C and ^{31}P NMR spectra of ^{18}O transfer experiment. (a) ^{13}C NMR (proton-decoupled) spectrum of [*carboxyl*-^{18}O]phosphopantothenate. (b) ^{31}P NMR (proton-decoupled) spectrum of CMP produce during PPCS catalysis using [*carboxyl*-^{18}O]phosphopantothenate. (c) ^{31}P NMR (proton-decoupled) spectrum of CMP produce during PPCS catalysis using unlabeled phosphopantothenate.
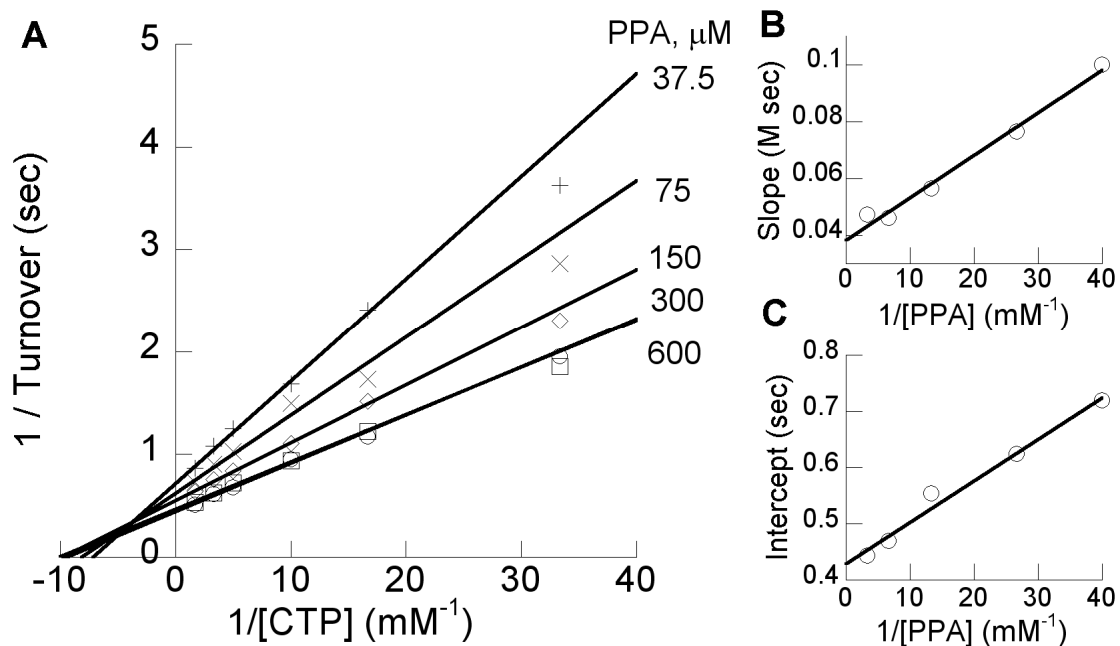
Figure 2.6: Pairwise analysis of CTP and PPA. Initial velocity analysis of PPCS with varying [CTP] and [PPA] at 1 mM cysteine. **A.** Double-reciprocal plot of velocity data. **B.** Secondary plot of slope versus reciprocal [PPA]. **C.** Secondary plot of intercepts versus reciprocal [PPA].
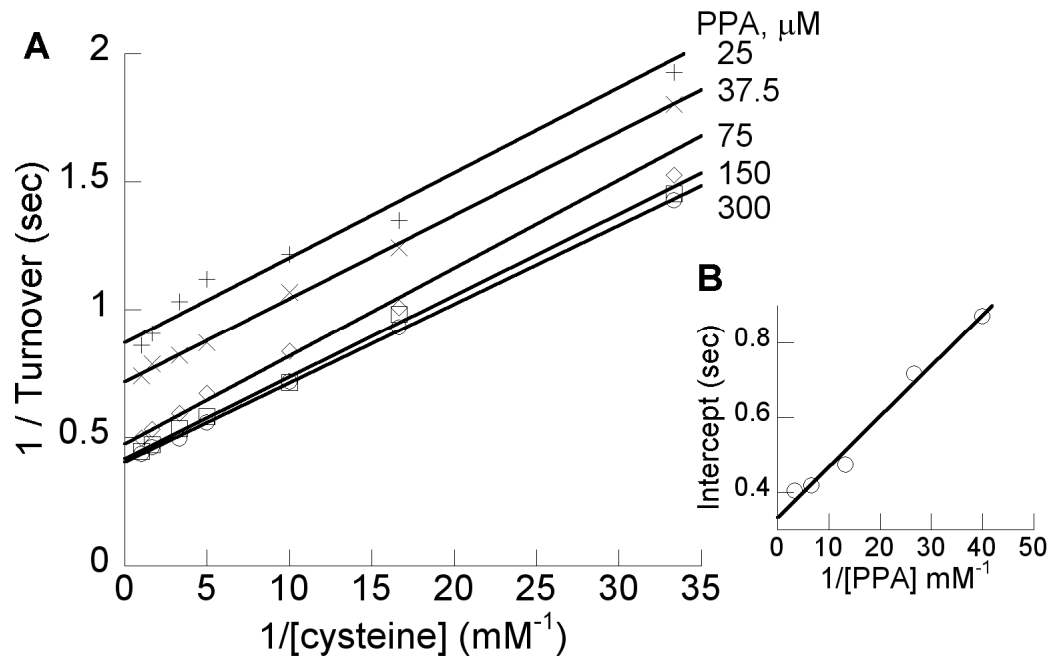
Figure 2.7: Pairwise analysis of cysteine and PPA. Initial velocity analysis of PPCS with varying [cysteine] and [PPA] at 0.6 mM CTP. **A.** Double-reciprocal plot of velocity data. **B.** Secondary plot of intercepts versus reciprocal [PPA].
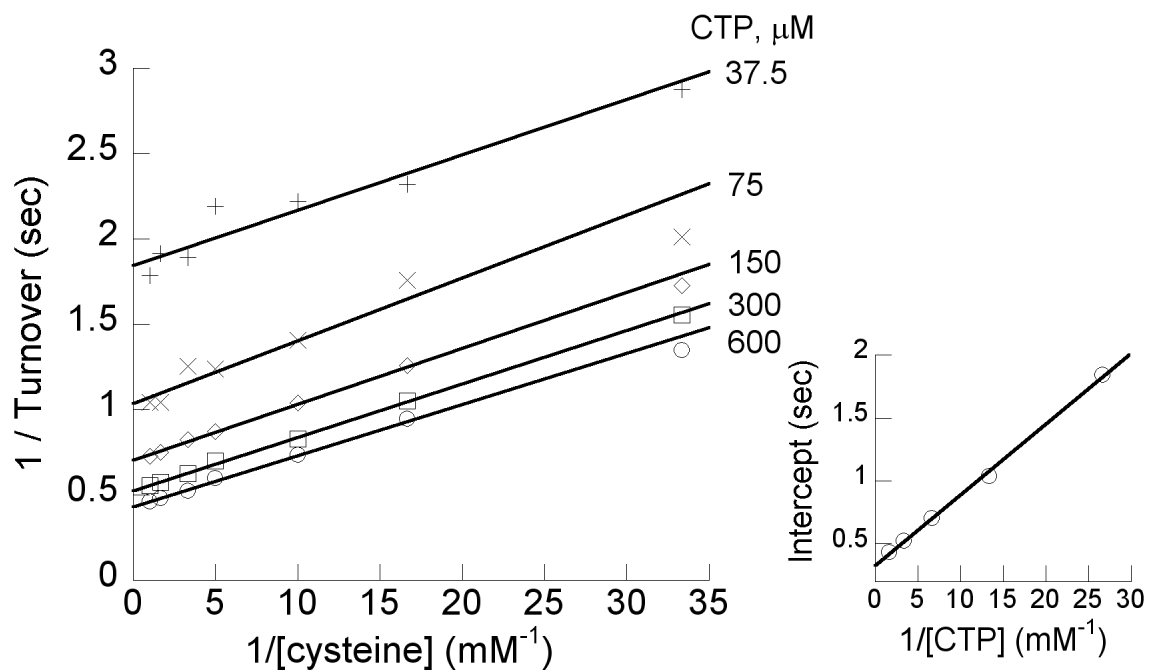
Figure 2.8: Pairwise analysis of cysteine and CTP. Initial velocity analysis of PPCS with varying [cysteine] and [CTP] at 0.6 mM PPA. **A.** Double-reciprocal plot of velocity data. **B.** Secondary plot of intercepts versus reciprocal [CTP].
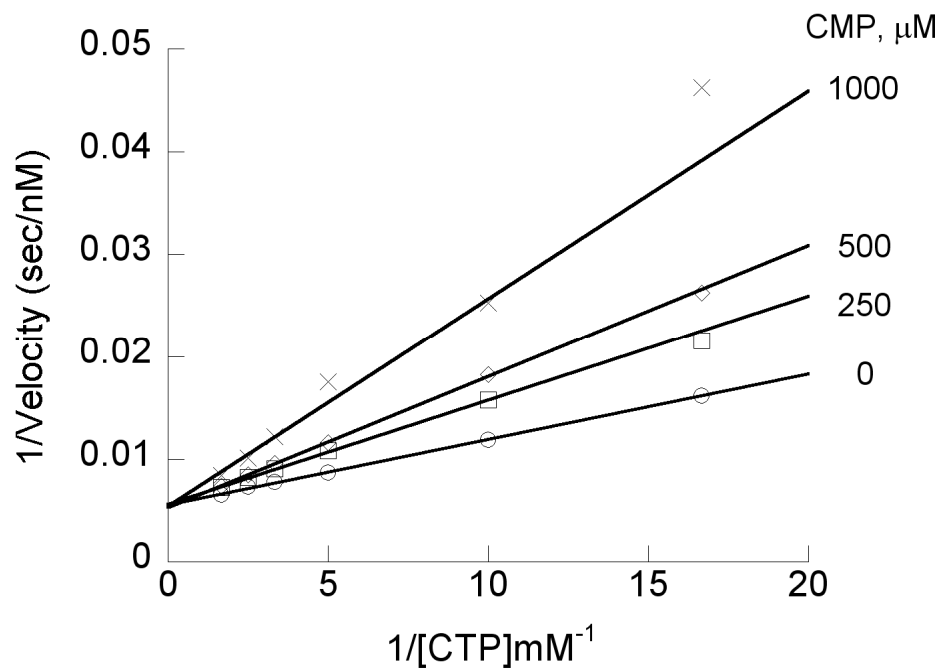
Figure 2.9: Product inhibition analysis of CMP versus CTP. Initial velocity analysis of PPCS versus varying [CTP] at different fixed [CMP] with 0.15 mM PPA and 1 mM cysteine. Double-reciprocal plot of velocity data.
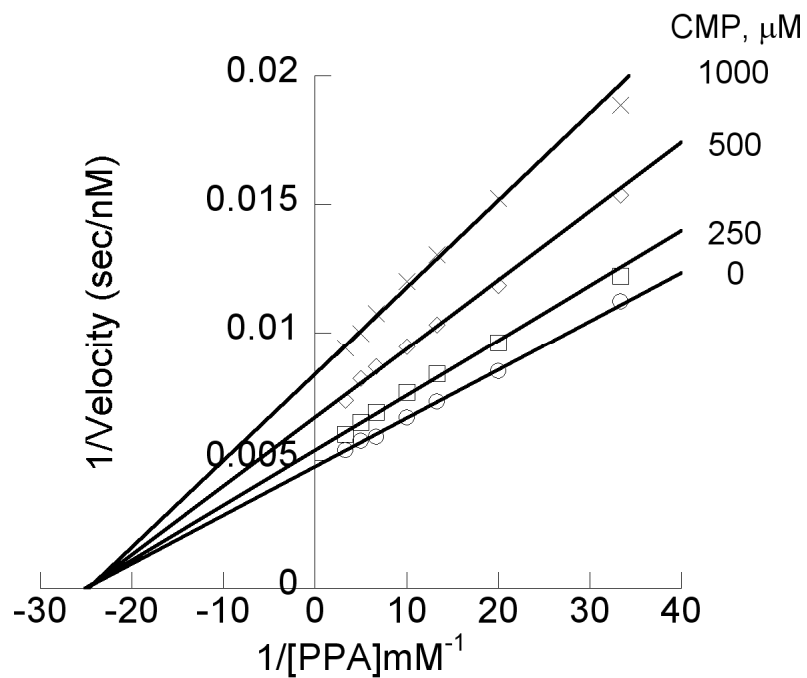
Figure 2.10: Product inhibition analysis of CMP versus PPA. Initial velocity analysis of PPCS versus varying [PPA] at different fixed [CMP] with 0.3 mM CTP and 1 mM cysteine. Double-reciprocal plot of velocity data.
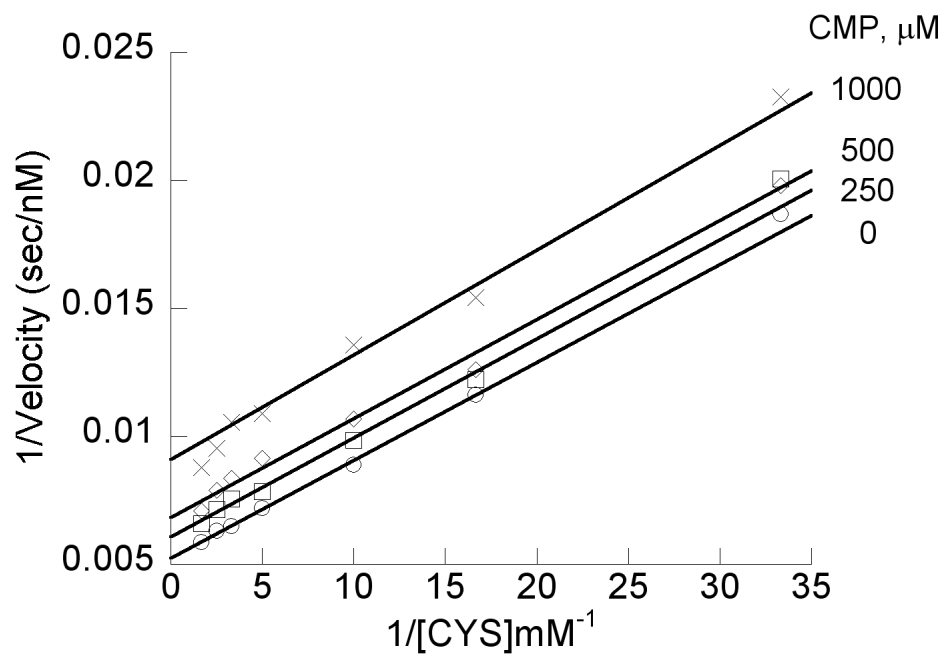
Figure 2.11: Product inhibition analysis of CMP versus cysteine. Initial velocity analysis of PPCS versus varying [cysteine] at different fixed [CMP] with 0.3 mM CTP and 0.3 mM PPA. Double-reciprocal plot of velocity data.

CTP   PPA   PP$_i$ Cys   PPA-Cys   CMP

PPCS   PPCS:CTP   ⎛ PPCS:CTP:PPA   ⎞ PPCS:CMP-PPA ⎛PPCS:CMP-PPA:Cys⎞ PPCS:CMP PPCS
                  ⎝ PPCS:CMP-PPA:PP$_i$⎠   ⎝PPCS:CMP:PPA-Cys⎠
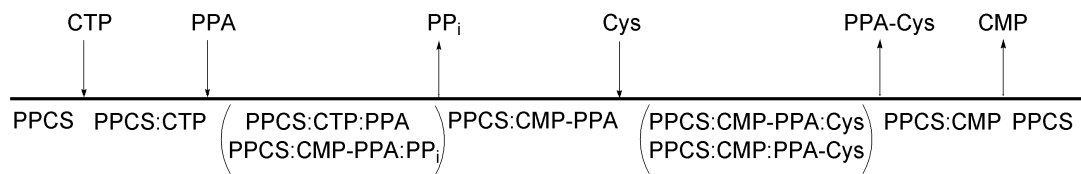
Figure 2.12: The proposed kinetic mechanism of the PPCS enzymatic reaction.
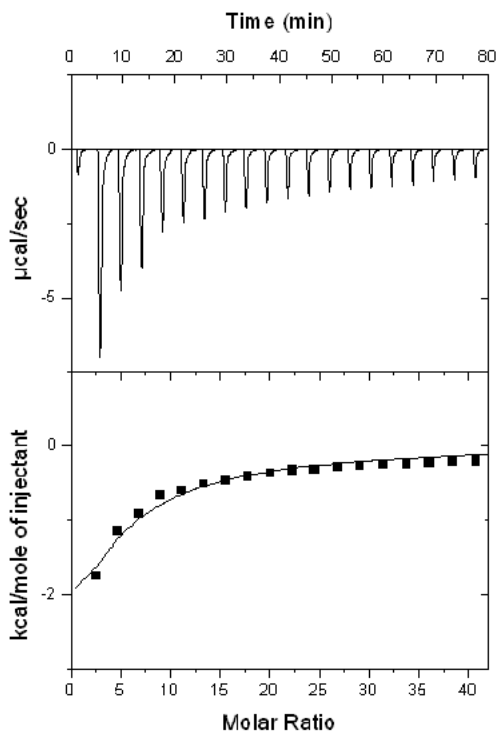
Figure 2.13: Isothermal titration calorimetry of *E. faecalis* PPCS with Mg-CTP. Top: Heat exchange as CTP is injected (corrected for enthalpy of injection). Bottom: Integrated heats (■) and curve fit using a one site binding model.

Table 2.1: Kinetic Parameters of *E. faecalis* PPCS at pH 7.6 and 37ºC

K_{iCTP}	$650 \pm 350 \ \mu M$
K_{mCTP}	$160 \pm 20 \ \mu M$
K_{mPPA}	$17 \pm 6 \ \mu M$
K_{mcys}	$86 \pm 7 \ \mu M$
k_{cat}	$2.9 \pm 0.1 \ sec^{-1}$

Table 2.2: Product Inhibition Patterns for *E. facaelis* PPCS

inhibitor	variable substrate	fixed substrates	pattern	calc K_{iCMP}
CMP	CTP	PPA, cysteine	comp	760 ± 90 μM
CMP	PPA	CTP, cysteine	mixed	520 ± 20 μM
CMP	cysteine	CTP, PPA	uncomp	730 ± 100 μM

Chapter 3

Characterization of Human Phosphopantothenoylcysteine Synthetase

BACKGROUND

Phosphopantothenoylcysteine synthetase (PPCS; EC 6.3.2.5; *coaB*) is the second enzyme in the biosynthetic pathway of coenzyme A, an essential biological molecule (*1-3*). CoA functions as a biological acyl carrier, used in functions both essential, such as fatty acid metabolism and pyruvate oxidation, and nonessential, such as polyketide and non-ribosomal peptide biosynthesis (*1-4*). CoA is synthesized from pantothenate (vitamin B_5) via five enzymatic steps (*1, 2, 5-7*). The first three enzymatic steps result in the synthesis of phosphopantetheine, which contains a primary thiol group that is responsible for the chemical reactivity and biological activity of CoA and acyl carrier proteins (ACP) (*5, 6*). The final two enzymatic steps result, overall, in the ligation of phosphopantetheine to an adenosine-3,5-diphosphate group, which functions primarily for substrate recognition by CoA-utilizing enzymes and as a leaving group for phosphopantetheine loading onto carrier proteins (*2, 6*). Because molecules containing the phosphopantetheine group are vital to life, the CoA biosynthetic pathway presents an interesting antimicrobial target (*1, 2, 8, 9*).

Preliminary studies on the human PPCS found that while the human enzyme can use both ATP and CTP, under saturating substrate conditions, the observed enzyme

turnover is four times faster under ATP conditions than under CTP conditions (*6*). In contrast, bacterial PPCS, whether monofunctionally expressed, like in *Enterococcus* and *Streptococcus* species, or bifunctionally expressed with phosphopantothenoylcysteine decarboxylase (PPCDC), like in the majority of other bacterial species, are CTP specific (*5, 10-13*). This difference in nucleotide specificity between human and bacterial PPCS raises the possibility of designing selective inhibitors of bacterial PPCS.

Recent studies carried out on the *Enterococcus faecalis* PPCS showed that the monofunctional bacterial PPCS catalysis proceeds via a Bi Uni Uni Bi Ping Pong kinetic mechanism, which involves the formation of a phosphopantothenoyl cytidylate intermediate, Figure 3.1 (*13*). However, detailed kinetic and chemical characterizations of PPCS from human have not been reported. In this study, thorough steady-state and inhibition kinetic studies are performed on the purified human PPCS to determine its overall kinetic mechanism. Also, isotopic oxygen transfer studies are carried out to establish the chemical mechanism, as well as the evaluation of divalent metals to determine those that support enzymatic catalysis. Finally, the nucleotide specificity of the human PPCS relative to the *E. faecalis* PPCS is assessed to determine the feasibility of designing bacterial selective PPCS inhibitors based on nucleotide selectivity differences.

MATERIALS AND METHODS

Materials

The chemicals used were of reagent grade or better, and used without further purification. The Mono Q 5/50 GL column was purchased from GE Healthcare. Ni-NTA resin was from Qiagen. Calcium pantothenate, ATP, CTP, Pyrophosphate Reagent, ampicillin, isopropyl β-D-1-thiogalactopyranoside, sodium chloride, magnesium

chloride, imidazole, sodium hydroxide, methanol, formic acid, dithiothreitol, L-cysteine, HEPES, Tris HCl, and 97% [^{18}O] water were purchased from Sigma-Aldrich. Luria-Bertani agar and broth were from Difco. UTP, GTP, and BL21(DE3) *Escherichia coli* cells were purchased from Invitrogen. DNA restriction and ligation enzymes were from New England Biolabs, while XL-1 Blue *E. coli* cells were from Stratagene. Qiagen minispin kits were used for DNA purification and cleanup, while DNA sequencing was performed by the University of Michigan DNA Sequencing Core facility.

Cloning, Overexpression, and Purification of human PPCS

The *E. coli* codon optimized human PPCS (*coaB*) gene, engineered with a *Nde*I restriction site upstream and a *Xho*I restriction site downstream of the gene (no stop codon), was obtained from DNA 2.0, Inc. (Menlo Park, CA, USA). The synthesized gene was restricted with *Nde*I/*Xho*I and ligated into pET23a(+) (Novagen) restricted with *Nde*I/*Xho*I. The resulting construct was sequenced and designated pUMJY120ho. *E. coli* strain BL21(DE3) carrying plasmid pUMJY120ho was grown in four 1 L flasks each containing 250 mL of LB broth with 100 mg/L of ampicillin. The cultures were incubated at 37°C with shaking (250 rpm) to an optical density at 600 nm of 0.6. The cultures were then cooled to 25°C, induced with a final concentration of 0.5 mM IPTG, and allowed to grow overnight at 25°C and 250 rpm. Cells from the cultures were harvested by centrifugation at 5,000 x g, washed with 50 mL of 20 mM HEPES pH 8.0, and finally resuspended in 15 mL of 20 mM HEPES pH 8.0 for each liter of culture. The cells were mechanically lysed via French Press, and the resulting suspension separated at 20,000 x g for 30 min. The crude cytosol was rocked gently with Ni-NTA resin (4 mL per 1 L culture) in a solution of 10 mM imidazole and 20 mM HEPES pH 8.0 for 15 minutes.

The resin mix was placed in an empty 20 mL chromatography column and the flow through volume collected. The column was washed with 5 column volumes (CV) of 50 mM imidazole, 20 mM HEPES pH 8.0, followed by 5 CV of 50 mM imidazole, 500 mM NaCl, 20 mM HEPES pH 8.0, and 2 CV of 20 mM HEPES pH 8.0. Finally, the column was eluted with 250 mM imidazole, 20 mM HEPES pH 8.0. The eluted fractions were diluted 4-fold, and loaded onto a Mono Q 5/50 GL column pre-equilibrated with 3 CV of 20 mM HEPES pH 8.0 buffer. The column was washed with 3 CV of equilibration buffer and eluted over a 10 CV linear gradient of 0 – 0.5 M NaCl in 20 mM HEPES pH 8.

Electrospray Mass Spectrometry (ES-MS).

Protein mass spectrum was acquired by the University of Michigan Protein Structure Facility. Purified human PPCS-his$_6$ (45 µM) was analyzed by LC-MS on a nanoAcquity/Qtof premier instrument. The sample was diluted 1:10 with 0.1% formic acid and a 10 µl aliquot was chromatographed on a C8 column. The PPCS peak was analyzed by ES-MS in positive ion mode.

Synthesis of 4'-phosphopantothenate.

4'-Phosphopantothenate (PPA) and [*carboxyl*-^{18}O] phosphopantothenate were synthesized as previously described(*13*). The ^{18}O-labeled PPA contains 93% ^{18}O in the carboxylate group as measured by ^{13}C-NMR analysis (*5, 13*).

^{18}*O Transfer Reactions.*

Reactions, consisting of 7.1 µM human PPCS, 10 mM MgCl$_2$, 12 mM [*carboxyl*-^{18}O] phosphopantothenate, 10 mM L-cysteine, 10 mM DTT, and either 10 mM ATP or CTP in 500 µL of 100 mM Tris HCl pH 7.6, were incubated for 60 min at 37°C. Reactions were then filtered via centrifugation through a Microcon YM-10 membrane

(Amicon) at 13,000 x g and 15°C for 30 minutes. ^2H_2O, 120 µL, was added to the filtrate, and the mixture analyzed by ^{31}P NMR. Control reactions were performed containing either no enzyme or unlabeled phosphopantothenate.

Proton-decoupled ^{31}P NMR spectra were recorded on a Bruker DRX500 spectrometer (11.75 T) at a probe temperature of 298 K, tuned to 202.4 MHz, using 5-mm high resolution NMR tubes. Spectra were obtained with a spectral width of 80000 Hz, 1.0 s relaxation delay, and 32,768 complex points in the time domain using simultaneous detection of real and imaginary components. The time domain data were apodized with an exponential (0.5 Hz) prior to zero-filling followed by Fourier transformation. Chemical shifts are reported relative to an external sample of 10 mM inorganic phosphate (0.0 ppm) in 100 mM Tris-HCl (pH 7.6) and 10% ^2H_2O.

Enzyme Kinetics

The previously optimized enzyme linked assay, where the production of pyrophosphate in the PPCS reaction is linked to the oxidation of two molecules of NADH, was used for kinetic studies (*13*). Assays were performed in 96 well format in a final volume of 100 µL, using the SpectraMax M5 microplate reader from Molecular Devices. Enzyme solutions, (1.16 µM PPCS for ATP containing experiments and 1.55 µM PPCS for CTP containing experiments and inhibition experiments) buffered in 100 mM Tris HCl pH 7.6, and assay mix, consisting of the pyrophosphate linked assay components, 10 mM DTT, and various concentrations of substrates and inhibitor, were incubated at 37ºC for 15 minutes before the reaction. The reactions were started by adding 30 µL of the enzyme solution to 70 µL of assay mix. The oxidation of NADH, as monitored by the decreasing absorbance at 340 nm, was measured over the course of the

reaction. The activity of the enzyme was calculated by taking into account that each mole of pyrophosphate causes the oxidation of 2 moles of NADH, with $\varepsilon_{340} = 6.22$ mM^{-1}cm^{-1} for NADH. The average activity of duplicate assay runs is reported.

Pairwise and inhibition kinetic studies were conducted to determine the mechanism of the enzyme. In pairwise kinetic studies, initial velocities were measured as a function of a first substrate, with changing concentrations of a second substrate and fixed concentrations of a third substrate. For instance, initial velocity versus [ATP] were measured at several different [PPA] (50, 75, 100, and 300 µM) at 1 mM cysteine. Pairwise analyses were performed for the three possible substrate combinations under both ATP and CTP substrate conditions. For inhibition studies, initial velocities as a function of one substrate is measured at fixed concentrations of the other two substrates and various concentrations of the desired inhibitor. For example, initial velocity against [CTP] was measured at several different concentrations of [CMP] (0, 1.5, 3, 5 mM), 0.1 mM PPA, and 0.1 mM cysteine. Inhibition kinetics of CMP and AMP with respect to ATP and CTP are examined. Inhibition of UTP and GTP against CTP was also studied. Initial velocities from pairwise and product inhibition experiments were plotted as double-reciprocal Lineweaver-Burk plots. Nonlinear fit to equation 1 was used to determine K_m^{app} and k_{cat}^{app} for each set of initial velocity data, with the calculated parameters used for fit in the Lineweaver-Burk plots. The patterns of the Lineweaver-Burk plots were used to diagnose the inhibition or kinetic mechanism, and the initial velocity data was fit to the relevant kinetic equations of the determined mechanism, equations 2 and 3. In cases where cooperativity was observed, the data was fit to the analogous equations modified for cooperativity via a simple Hill model where the Hill

constant, n, was used to measure cooperativity, equations 4 and 5. Lineweaver-Burk plots of cooperative substrates were modified by making the x-axis a function of $1/[S]^n$ rather than $1/[S]$. In some cases, the data was plotted as Hill Plots to compare the degrees of cooperativity, and fits in the Hill plot was determined using the calculated n, K_m^{app} and k_{cat}^{app}. The inhibition equation of inhibitors competitive to the first substrate was derived via the same logic and method used to derive for competitive inhibitors of bisubstrate enzyme reaction (*14*). The resulting equation is the same as the inhibition equation for the last product to release, equation 3. This was expected as under steady state initial velocity conditions, the last product to release only interacts with the free enzyme as a competitive inhibitor to the first substrate that binds. Thus, the inhibition constant of competitive inhibitors to ATP/CTP was calculated via fitting to equation 3.

$$v = \frac{V_{max}^{app}[A]}{K_m^{app} + [A]} \quad (1)$$

$$v = \frac{V_{max}[A][B][C]}{K_{ia}K_{mB}[C] + K_{mC}[A][B] + K_{mB}[A][C] + K_{mA}[B][C] + [A][B][C]} \quad (2)$$

$$v = \frac{V_{max}[A]}{K_{mA}\left(1 + \dfrac{K_{ia}K_{mB}}{K_{mA}[B]} + \dfrac{K_{ia}K_{mB}[R]}{K_{mA}K_{ir}[B]} + \dfrac{[R]}{K_{ir}}\right) + [A]\left(1 + \dfrac{K_{mB}}{[B]} + \dfrac{K_{mC}}{[C]}\right)} \quad (3)$$

$$v = \frac{V_{max}^{app}[A]^n}{\left(K_m^{app}\right)^n + [A]^n} \quad (4)$$

$$v = \frac{V_{max}[A]^n[B][C]}{K_{ia}{}^n K_{mB}[C] + K_{mC}[A]^n[B] + K_{mB}[A]^n[C] + K_{mA}{}^n[B][C] + [A]^n[B][C]} \quad (5)$$

Eikonogen Assay. The Eikonogen assay, which allows for direct quantification of pyrophosphate, was used to study the effects of divalent metals on PPCS (*15, 16*). Eikonogen assay components were made as described in literature. The assay was

performed by quenching the volume of interest with 50 µL of 2.5% w/v ammonium molybdate in 5 N sulfuric acid. Next 50 µL of 0.5 M β-mercaptoethanol and 20 µL of Eikonogen solution were added sequentially to the mixture. The mixture was incubated at 37°C for 10 minutes, and then absorbance at 580 nm was read to quantify the amount of pyrophosphate ($\varepsilon_{580} = 25{,}000$ M^{-1} cm^{-1}).

PPCS Metal Dependence. The activity of human and *E. faecalis* PPCS in the presence of 100 µM to 1.25 mM of Mg^{2+}, Mn^{2+}, Zn^{2+}, Fe^{2+}, and Cd^{2+} as well as no divalent metal was measured via the previously described Eikonogen assay. A 40 µL enzymatic reaction containing 100 nM of *E. faecalis* PPCS or 600 nM of human PPCS, 300 µM L-cysteine, 300 µM phosphopantothenate, 1 mM DTT, 500 µM CTP, 5 mM DTT, and one of the above divalent metals over a concentration of 100 µM to 1.25 mM in 100 mM HEPES, pH 8.0 was run at room temperature. The reaction was quenched with the Eikonogen assay after 25 min at room temperature, and the activity was determined. The results were compared to a control with no divalent metals and a control with no enzyme. The enzyme turnover was calculated using $\varepsilon_{580} = 25{,}000$ M^{-1} cm^{-1} for the detection of pyrophosphate by the Eikonogen assay, and that adding 120 µL of the various Eikonogen components to the 40 µL aliquot of reaction dilutes the original reaction volume by 4 fold. Assays were performed in duplicates with the averages reported.

Metal Inhibition Experiment. Pairwise competition experiments, where initial velocity against [Mg^{2+}] is measured at fixed, changing concentrations of [Ca^{2+}] and 1.25 mM CTP, 0.6 mM PPA, and 0.6 mM L-cysteine with 100 nM *E. faecalis* PPCS (or 400

nM human PPCS), was conducted using the Eikonogen assay. Assays were performed in duplicates with the averages reported.

Inductively Coupled Plasma Mass Spectrometry of PPCS. Inductively coupled plasma mass spectrometry (ICP-MS) were performed on purified human and *E. faecalis* PPCS to determine the amount of various divalent metals associated with the enzymes. ICP-MS was performed by the W. M. Keck Elemental Geochemistry Laboratory at the University of Michigan. Samples containing approximately 100 µM of enzyme, along with the blank purification buffer, were submitted. The concentration of the metals and mole equivalent of metals reported are adjusted for the basal amount of metals present in the purification buffer.

RESULTS

Purification of Recombinant Human PPCS

A T7-RNA polymerase promoter based expression plasmid (pET23a) was used to overexpress human PPCS in *E. coli* BL21(DE3). The *E. coli* codon optimized open reading frame expressed very well upon induction with IPTG at 25°C, yielding 10 mg of soluble purified PPCS per liter of cell culture. The C-terminal his_6-tagged protein was purified by metal affinity chromatography (Ni-NTA) followed by an anion exchange column to remove imidazole and trace protein impurities. The protein was >95% pure as determined by SDS-PAGE gel, with a specific activity of 0.9 µmol/min/mg.

Electrospray mass spectrum of the purified PPCS-his_6 gave a molecular mass of $34,939.5 \pm 3.5$ Da, and is consistent with the molecular mass of the engineered protein predicted from the DNA sequence, minus the N-terminal methionine, Figure 3.2.

Nucleotide Selectivity and ATP Cooperativity

In the presence of the same amount of PPCS, the measured maximal velocities utilizing either ATP or CTP as a substrate were within 30% of each other, suggesting that the human PPCS enzyme does not have a significant preference for ATP or CTP, and can use either nucleotide with similar efficiencies. However, neither GTP nor UTP supported enzyme activity with the human enzyme, as was also the case for the *E. faecalis* PPCS (data not shown). Pairwise and inhibition kinetic experiments were then conducted to determine the steady state kinetic constants of the human PPCS enzyme under both ATP and CTP substrate conditions.

While the velocity versus [CTP] curve is a standard hyperbolic curve that fits to the form of a standard Michaelis-Menten equation, the velocity versus [ATP] curve is more sigmoidal, indicative of cooperativity in ATP binding. This apparent cooperativity was observed consistently at different concentrations of PPA and cysteine. Fitting the velocity versus [ATP] curve to a Michaelis-Menten equation modified for cooperativity via the Hill model, equation 4, we found that the Hill constant, n, is equal to approximately 1.7 for ATP at varying concentrations of cysteine and PPA. In comparison, the theoretical maximum Hill constant for positive cooperativity is equal to the oligomeric state of the enzyme, which would be 2 for the dimeric human PPCS. Thus, the human PPCS has strong positive cooperativity for ATP, but is not cooperative for CTP. Additional kinetic experiments found that cysteine and PPA do not exhibit cooperative behavior under ATP or CTP conditions.

Enzyme Mechanism

In the double reciprocal plot of initial velocity against [CTP] with changing [PPA], the initial velocity patterns intersect to the left of the y-axis, Figure 3.3. This pattern supports a mechanism where CTP and PPA are bound to the enzyme sequentially, prior to chemical reaction and product release. In the double reciprocal plot of initial velocity against [CTP] with changing [cysteine], the initial velocity patterns at different [cysteine] are parallel, Figure 3.4, which is suggestive of a Ping Pong relationship where there is a product release between CTP and cysteine binding. Likewise, the double reciprocal plot of initial velocity against [PPA] with changing [cysteine] also has parallel patterns, so PPA and cysteine also have a Ping Pong relationship with respect to each other, Figure 3.5. Overall, the pairwise kinetic analysis of human PPCS gives patterns expected for a Bi Uni Uni Bi Ping Pong kinetic mechanism.

Since human PPCS exhibits apparent cooperativity, n = 1.7, for ATP, the double reciprocal plots of velocity vs. ATP was plotted with $1/[ATP]^{1.7}$ on the x-axis rather than $1/[ATP]$ as usual. With this modification, the expected patterns from the pairwise kinetic analysis was observed (Figure 3.6-3.8). Thus, both under ATP and CTP conditions, the enzyme follows a Bi Uni Uni Bi Ping Pong mechanism, except that ATP binds with an apparent positive cooperativity of n = 1.7.

The steady state kinetic constants under ATP or CTP conditions were calculated via nonlinear fit to the velocity equations of the Bi Uni Uni Bi Ping Pong mechanism (modified for cooperativity for ATP), and collected in Table 3.1. The calculated steady state constants for the *E. faecalis* PPCS are included in Table 3.1 for comparison.

70

Inhibition kinetics of the last product released, either CMP or AMP, against the first substrate expected to bind, ATP or CTP, were examined. To further investigate the ability of the enzyme to use ATP and CTP with seemingly equal proficiency, the inhibition of CMP on ATP as well as the inhibition of AMP on CTP was studied. Starting with CTP, the double-reciprocal inhibition plots of velocity vs. [CTP] with varying [AMP] or [CMP] have the fitted lines intersect on the y-axis, demonstrating the competitive inhibition of AMP or CMP on CTP (Figure 3.9A-B). Under ATP conditions, the fitted lines of the double-reciprocal inhibition plot of velocity vs. [ATP] at various [CMP] also intersect on the y-axis, consistent with CMP as a competitive inhibitor of ATP, Figure 8C. The observed inhibition patterns of AMP on ATP were more complicated than the other inhibition patterns. Nonlinear fitting to equation 4 of initial velocity vs. [ATP] at different concentrations of AMP found that in addition to increasing the apparent K_m of ATP, increasing concentrations of AMP also weakly decreased the apparent Hill constant n, from n = 1.68 at no AMP to n = 1.38 at 5 mM of AMP. However, at up to even 5 mM of AMP, there seems to be minimal effect on the calculated apparent V_{max}, so AMP was classified as a competitive inhibitor that also decreases the apparent cooperativity. This data is presented as a Hill plot to show the change in cooperativity (Figure 3.10).

Oxygen Transfer during PPCS Catalysis

[*carboxyl-*^{18}O] PPA (93% ^{18}O) was used as a substrate for the human PPCS reactions, under both CTP and ATP conditions. ^{18}O labeling experiments were conducted in a way to help corroborate the calculated k_{cat} values, specifically that the reaction rates under ATP and CTP are similar. Enough PPCS enzyme was used so that if the reaction

with CTP were 4 times slower than with ATP, as suggested in literature, then the CTP

reaction would not have reached completion. As both sets of reactions reached

completion as detected via ^{31}P NMR (data not shown), PPCS turnovers with either ATP

or CTP as substrate are similar in rate. Figure 3.11A shows the ^{31}P NMR spectrum of the

product CMP formed during the PPCS reaction with CTP and labeled PPA. Two NMR

resonance peaks 0.025 ppm apart corresponding to the CMP labeled with and without ^{18}O

atom in the phosphate group. The upfield resonance corresponds to CMP labeled with

one ^{18}O atom and integrates to approximately 46% of the total CMP peaks, consistent

with the transfer of one of the two carboxylate oxygens of PPA to CMP. The control

reaction, ran with unlabeled PPA, Figure 3.11B, only has a single resonance peak for the

CMP produced from the reaction. Likewise, for PPCS reactions under ATP conditions

with [*carboxyl*-^{18}O] PPA, an analogous set of spectra were observed (Figure 3.11C-D).

These experiments support the formation of a phosphopantothenoyl adenylate or

cytidylate intermediate in the human PPCS reaction mechanism. Thus, both ATP and

CTP undergo similar chemical mechanisms.

UTP and GTP Inhibition

In addition to determining whether UTP or GTP supported PPCS activity, the

ability of UTP or GTP to inhibit human PPCS activity was also examined. In the double

reciprocal plot of initial velocity against [CTP] at varying concentrations of either UTP or

GTP, the fitted lines intersect on the y-axis, indicating that UTP and GTP are competitive

inhibitors with respect to CTP (Figure 3.12). The inhibition constants of UTP and GTP,

as well as the product inhibition constants of CMP and AMP, were determined via

nonlinear fit to equation 3. Table 3.2 shows the aforementioned inhibition constants along

with the calculated dissociation constants, K_{ia}, of CTP and ATP. These dissociation/inhibition constants present the affinity of the particular nucleotide to the free enzyme.

ICP-MS of Purified PPCS.

Samples of purified *E. faecalis* and human PPCS were submitted for ICP-MS analysis for detection of associated divalent metals, Table 3.3. No divalent metals were found to be associated with the purified enzymes, except for calcium. Approximately 0.25 mole equivalents Ca^{2+} were detected with the purified *E. faecalis* PPCS. In comparison, only 0.05 mole equivalents of Ca^{2+} were detected with the purified human PPCS. Due to the observed binding of Ca^{2+} to PPCS, inhibition of Ca^{2+} on the *E. faecalis* PPCS was examined.

PPCS Metal Dependence.

The activity of the *E. faecalis* and human PPCS in presence of a concentration range of various biologically relevant divalent metals was determined, Figure 3.13. For both species of PPCS, minimal pyrophosphate producing activities were observed under no divalent metal or any concentration of Zn^{2+} or Cd^{2+} that we tested. Activities were supported by Mg^{2+}, Mn^{2+}, and Fe^{2+} for both PPCS homologues. Increasing concentrations of Mg^{2+} and Mn^{2+} is correlated with increased activity, although Mn^{2+} reached saturating activity at lower concentrations compared to Mg^{2+}. Although increasing Fe^{2+} levels increased activity at low concentrations, at above 0.3-0.6 mM, increasing Fe^{2+} started to cause a decrease in observed activity. Also, the maximum level of activity supported by Fe^{2+} is lower than the maximum level of activity supported by Mg^{2+} or Mn^{2+}. For the *E. faecalis* PPCS, the highest activity observed with Fe^{2+} is approximately 60% of the

highest activity observed for Mg^{2+} or Mn^{2+}. For the human PPCS, the highest activity observed with Fe^{2+} is less than 50%

Calcium Inhibition.

Because calcium was found to bind to *E. faecalis* PPCS, but not human PPCS, whether calcium inhibited the PPCS reaction was examined. We found Ca^{2+} to be an inhibitor of the *E. faecalis* PPCS, but no inhibition of the human PPCS was observed at up to 0.5 mM of Ca^{2+}. From the Mg^{2+} - Ca^{2+} competition experiments, increasing concentrations of Ca^{2+} increased the apparent K_m of Mg^{2+} but did not affect the V_{max}, while the fitted lines interested at the y-axis on the double reciprocal plot of the initial velocity data. The observed data is consistent with Ca^{2+} as a competitive inhibitor of Mg^{2+}, Figure 3.14. Since both Ca^{2+} and Mg^{2+} have binding affinities for CTP, the actual underlying mechanism of Ca^{2+} inhibition is complicated, with Ca^{2+} possibly binding to either the PPCS enzyme or CTP. Furthermore, CTP are at high concentrations due to the sensitivity limitation of the Eikonogen assay, making it impossible to determine the binding affinities from the experiment.

DISCUSSION

Previous studies have found that bacterial PPCS, both monofunctional and bifunctional, are CTP specific, while preliminary studies with the human PPCS suggests that the human PPCS prefer ATP (*5, 6, 10, 13*). This potential difference in substrate selectivity suggests that PPCS could be a novel antibacterial target, so studies were carried out to examine the substrate selectivity as well as the kinetic and chemical mechanisms of the human PPCS.

Different classes of aminoacyl-tRNA synthetases (aaRS), which also proceed via an acyl adenylate intermediate, have been shown to undergo varied kinetic mechanisms. Most show a Bi Uni Uni Bi ping pong mechanism analogous to that determined for *E. faecalis* PPCS (*17, 18*). However, a number of aaRSs display a sequential mechanism where all three substrates bind prior to the formation of the acyl adenylate intermediate (*19*). From our steady state kinetic studies, the kinetic data suggests that the human PPCS follows an ordered Bi Uni Uni Bi Ping Pong mechanism under both ATP and CTP conditions, similar to the kinetic mechanism determined for *E. faecalis* PPCS previously reported, Figure 3.1 (*13*). The steady state constants under the two conditions (ATP/CTP) were calculated for human PPCS (Table 3.1). In contrast to previous studies, the human PPCS seems to be equally proficient with either nucleotide. Overall, the k_{cat} values are similar under both conditions (0.56 ± 0.01 sec^{-1} for ATP vs. 0.53 ± 0.02 sec^{-1} for CTP), and the K_m for CTP (269 ± 14 μM) and ATP (265 ± 20 μM) are also comparable. The K_m for PPA is somewhat lower under ATP conditions (13 ± 1 μM) than CTP conditions (57 ± 5 μM), although the relevance of this difference under physiological conditions may be indistinct.

^{18}O transfer studies were conducted to establish the formation of a phosphopantothenoyl cytidylate or a phosphopantothenoyl adenylate intermediate during human PPCS catalysis under CTP or ATP conditions, respectively. Under the proposed kinetic mechanism, the carboxylate of PPA attacks the α-phosphate on ATP/CTP to form an adenylate/cytidylate intermediate. Since the PPA is labeled with ^{18}O on the carboxylate group, upon the formation of a nucleotide-activated intermediate the ^{18}O atom would reside in the bridging oxygen of the mixed anhydride intermediate. Upon

reaction with cysteine in the second half reaction the bridging oxygen would be incorporated into the product AMP/CMP. Since ^{18}O has significant one bond nuclear shielding effect on phosphorus atoms that it is bonded to, the incorporation of ^{18}O into the phosphate of AMP/CMP causes a measurable upfield shift in the NMR resonance of the phosphorus atom to which it is directly bound (*20, 21*). As only about 50% of the nucleotide monophosphates would be incorporated with ^{18}O, two adjacent resonance peaks for the phosphorus atom of the product CMP/AMP would be expected. When the PPCS enzymatic reaction, under both CTP and ATP conditions, were conducted with labeled PPA, two resonance signals of similar magnitude for the phosphate group of the product CMP/AMP were indeed observed, supporting the formation of a phosphopantothenoyl cytidylate or a phosphopantothenoyl adenylate intermediate in the human PPCS reaction mechanism. From the collected kinetic and chemical data, it seems that PPCS catalysis using either CTP or ATP proceeds via the same chemical mechanism. There is, however, one major difference between ATP and CTP conditions. In the kinetic experiments, ATP demonstrates positive cooperative binding, with a Hill constant of 1.7, while CTP shows no cooperativity. Since the difference between ATP and CTP is the nucleobase, adenosine must somehow be responsible for the cooperativity. This idea is somewhat supported by the inhibition study of AMP on ATP. As expected, AMP is a competitive inhibitor of ATP. However, increasing concentrations of AMP also weakly decreases the apparent cooperativity of ATP, which is consistent with the adenosine moiety being responsible for the observed cooperativity.

For the human PPCS, the calculated K_{ia} values for CTP and ATP, as well as the calculated K_i for GTP, UTP, CMP, and AMP, are comparable because they each measure

the affinity of that nucleotide to the free enzyme. Furthermore, GTP, UTP, CMP, and AMP are competitive with respect to CTP and/or ATP, so they likely bind similarly to the free enzyme as ATP and CTP, with the caveat that the triphosphate group of GTP and UTP must bind differently enough to not support enzyme turnover. When comparing the K_{ia} values of CTP and ATP to the K_i values of GTP and UTP, it becomes apparent that the human enzyme has little nucleotide binding specificity. The K_{ia} of ATP (465 ± 89 µM) is similar in magnitude to the K_i of GTP (372 ± 11 µM) and the K_i of UTP (662 ± 47 µM). While the K_{ia} of CTP (74 ± 30 µM) is somewhat smaller, the corresponding K_i of CMP (4.69 ± 0.55 mM) is actually larger than the K_i of AMP (3.70 ± 0.43 mM) suggesting that cytidine does not bind tighter to the free enzyme than any other nucleotide. This lack of nucleotide discrimination is consistent with structural data for the human PPCS. While only the structure of the human apo-enzyme (PDBID 1P9O) is available, from structural comparisons to the phosphopantothenoyl cytidylate bound *E. coli* structure (PDBID 1U7Z) it has been noted that the nucleotide binding pocket of the human PPCS is bigger than that of the *E. coli* PPCS, and thus capable of accommodating both purines and pyrimidines (*22, 23*). Furthermore, the amino acid residues forming the nucleotide binding pocket of the human PPCS was observed to have significantly higher temperature factor compared to the rest of the protein, suggesting flexibility for those amino acids residues. Our finding that all four nucleotides can bind to the human PPCS is consistent with a flexible nucleotide binding pocket.

When comparing the affinities of the human PPCS for CTP and CMP to the affinities of the bacterial PPCS (represented by the *E. faecalis* PPCS as it has calculated affinity values) for CTP and CMP, the K_{ia} of CTP for the human PPCS is 74 µM which is

tighter than the K_{ia} of CTP for the *E. faecalis* PPCS at 650 μM. However, the human

PPCS binds to CMP much more weakly, with K_i of CMP for the human PPCS at 4.7

mM. In contrast, the K_i of CMP for *E. faecalis* PPCS is approximately 670 μM (*13*). *E.*

faecalis PPCS binds CMP approximately 7 times as tightly as the human PPCS,

suggesting that the CMP has selectivity towards the bacterial enzyme. Furthermore, the

larger pool of ATP (1-10 mM) in mammalian cells, compared to the smaller pool of CTP

(~100 μM) in bacterial cells, would reduce the inhibitory effects of a competitive

inhibitor directed against the nucleotide binding site of human PPCS (*24, 25*). This along

with the weaker binding of CMP to the human PPCS (as compared to the *E. faecalis*

PPCS) suggests that it may be feasible to develop bacterial selective inhibitors by

mimicking the cytosine or CMP group.

From the metal studies, we found that both *E. faecalis* and human PPCS require

either Mg^{2+} or Mn^{2+} for enzymatic activity. The metal profile is consistent with other

pyrophosphate producing enzymes, in particular pantothenate synthetase, also involved in

the biosynthesis of CoA (*21, 26*). Fe^{2+} supported some activity, but only at low

concentrations. ICP-MS did not detect Mg^{2+}, Mn^{2+}, or Fe^{2+} associated with PPCS at

above baseline levels, suggesting that these divalent meals did not associate tightly with

PPCS. Interestingly, *E. faecalis* PPCS was associated with approximately 0.25 mole

equivalents of Ca^{2+}, while the human PPCS did not. Competition experiments found that

Ca^{2+} was a competitive inhibitor with respect to Mg^{2+} for the *E. faecalis* PPCS, but did

not inhibit human PPCS to an observable extent at 0.5 mM. In the x-ray crystal structure

of the *E. coli* Asn210Asp PPCS mutant in complex with CTP, a divalent metal assigned

as Ca^{2+} was observed in the active site binding to the α- and β-phosphates of CTP and

Asp279 of the enzyme (*23*), which is consistent with our findings that calcium is associated with *E. faecalis* PPCS. However, the lack of calcium association and inhibition for the human PPCS is surprising, since bacterial and human PPCS catalyze the same reaction via a similar mechanism.

Kinetic and labeling studies support that the human PPCS follows an ordered Bi Uni Uni Bi Ping Pong mechanism like its bacterial counterpart. However, in contrast to bacterial PPCS which are essentially CTP specific, the human enzyme uses ATP and CTP with similar affinity and chemical mechanisms, highlighting the differences in the nucleotide binding between the respective enzymes. More interesting is that the human enzyme has an apparent positive cooperativity for ATP, but no cooperativity for CTP. These findings raise interesting questions about which nucleotide triphosphate is used predominantly in vivo as well as the evolutionary reasons for the human PPCS to become less nucleotide specific.

REFERENCES

1. Brown, G. M. (1959) The metabolism of pantothenic acid. *J. Biol. Chem. 234*, 370-378.
2. Spry, C., Kirk, K., and Saliba, K. J. (2008) Coenzyme A biosynthesis: an antimicrobial drug target. *FEMS Microbiol. Rev. 32*, 56-106.
3. Magnuson, K., Jackowski, S., Rock, C. O., and Cronan, J. E., Jr. (1993) Regulation of fatty acid biosynthesis in Escherichia coli. *Microbiol. Mol. Biol. Rev. 57*, 522-542.
4. Majerus, P. W., Alberts, A. W., and Vagelos, P. R. (1965) Acyl carrier protein, IV. The identification of 4′-phosphopantetheine as the prosthetic group of the acyl carrier protein. *Proc. Natl. Acad. Sci. USA 53*, 410-417.
5. Strauss, E., Kinsland, C., Ge, Y., McLafferty, F. W., and Begley, T. P. (2001) Phosphopantothenoylcysteine synthetase from *Escherichia coli*. Identification and characterization of the last unidentified coenzyme A biosynthetic enzyme in bacteria. *J. Biol. Chem. 276*, 13513-13516.
6. Daugherty, M., Polanuyer, B., Farrell, M., Scholle, M., Lykidis, A., de Crecy-Lagard, V., and Osterman, A. (2002) Complete reconstitution of the human coenzyme A biosynthetic pathway via comparative genomics. *J. Biol. Chem. 277*, 21431-21439.
7. Genschel, U. (2004) Coenzyme A biosynthesis: reconstruction of the pathway in archaea and an evolutionary scenario based on comparative genomics. *Mol Biol Evol 21*, 1242-1251.
8. Gerdes, S. Y., Scholle, M. D., D'Souza, M., Bernal, A., Baev, M. V., Farrell, M., Kurnasov, O. V., Daugherty, M. D., Mseeh, F., Polanuyer, B. M., Campbell, J. W., Anantha, S., Shatalin, K. Y., Chowdhury, S. A. K., Fonstein, M. Y., and Osterman, A. L. (2002) From genetic footprinting to antimicrobial drug targets: examples in cofactor biosynthetic pathways. *J. Bacteriol. 184*, 4555-4572.
9. Zhang, Y.-M., White, S. W., and Rock, C. O. (2006) Inhibiting bacterial fatty acid synthesis. *J. Biol. Chem.*, R600004200.
10. Kupke, T., and Schwarz, W. (2006) 4'-Phosphopantetheine biosynthesis in archaea. *J. Biol. Rhythms 281*, 5435-5444.
11. Kupke, T. (2002) Molecular characterization of the 4'-phosphopantothenoylcysteine synthetase domain of bacterial Dfp flavoproteins. *J. Biol. Chem. 277*, 36137-36145.
12. Kupke, T. (2001) Molecular characterization of the 4'-phosphopantothenoylcysteine decarboxylase domain of bacterial Dfp flavoproteins. *J. Biol. Chem. 276*, 27597-27604.
13. Yao, J., Patrone, J. D., and Dotson, G. D. (2009) Characterization and kinetics of phosphopantothenoylcysteine synthetase from *Enterococcus faecalis*. *Biochemistry 48*, 2799-2806.
14. Yu, M., Magalhaes, M. L. B., Cook, P. F., and Blanchard, J. S. (2006) Bisubstrate inhibition: theory and application to N-acetyltransferases. *Biochemistry 45*, 14788-14794.
15. Kuang, Y., Salem, N., Wang, F., Schomisch, S. J., Chandramouli, V., and Lee, Z. (2007) A colorimetric assay method to measure acetyl-CoA synthetase activity:

Application to woodchuck model of hepatitis virus-induced hepatocellular carcinoma. *J. Biochem. Biophys. Methods 70*, 649-655.

16. Putnins, R. F., and Yamada, E. W. (1975) Colorimetric determination of inorganic pyrophosphate by a manual or automated method. *Anal. Biochem. 68*, 185-195.

17. Allende, C. C., Chaimovich, H., Gatica, M., and Allende, J. E. (1970) The aminoacyl transfer ribonucleic acid synthetases. II. Properties of an adenosine triphosphate-threonyl transfer ribonucleic acid synthetase complex. *J. Biol. Chem. 245*, 93-101.

18. Papas, T. S., and Mehler, A. H. (1971) Kinetic studies of the prolyl transfer ribonucleic acid synthetase of Escherichia coli. Order of addition of substrates and release of products. *J. Biol. Chem. 246*, 5924-5928.

19. Freist, W., Sternbach, H., and Cramer, F. (1981) Arginyl-tRNA synthetase from Baker's Yeast. *Eur. J. Biochem. 119*, 477-482.

20. Dotson, G. D., Dua, R. K., Clemens, J. C., Wooten, E. W., and Woodard, R. W. (1995) Overproduction and one-step purification of *Escherichia coli* 3-deoxy-D-manno-octulosonic acid 8-phosphate synthase and oxygen transfer studies during catalysis using isotopic-shifted heteronuclear NMR. *J. Biol. Chem. 270*, 13698-13705.

21. Zheng, R., and Blanchard, J. S. (2001) Steady-state and pre-steady-state kinetic analysis of *Mycobacterium tuberculosis* pantothenate synthetase. *Biochemistry 40*, 12904-12912.

22. Manoj, N., Strauss, E., Begley, T. P., and Ealick, S. E. (2003) Structure of human phosphopantothenoylcysteine synthetase at 2.3 A resolution. *Structure 11*, 927-936.

23. Stanitzek, S., Augustin, M. A., Huber, R., Kupke, T., and Steinbacher, S. (2004) Structural basis of CTP-dependent peptide bond formation in coenzyme A biosynthesis catalyzed by *Escherichia coli* PPC synthetase. *Structure 12*, 1977-1988.

24. Beis, I., and Newsholme, E. A. (1975) The contents of adenine nucleotides, phosphagens and some glycolytic intermediates in resting muscles from vertebrates and invertebrates. *Biochem. J. 152*, 23-32.

25. Petersen, C., and Moller, L. B. (2000) Invariance of the nucleoside triphosphate pools of Escherichia coli with growth gate. *J. Biol. Chem. 275*, 3931-3935.

26. Miyatake, K., Nakano, Y., and Kitaoka, S. (1979) Pantothenate synthetase from *Escherichia coli* [D-pantoate: beta-alanine ligase (AMP-forming), EC 6.3.2.1]. *Methods Enzymol. 62*, 215–219.
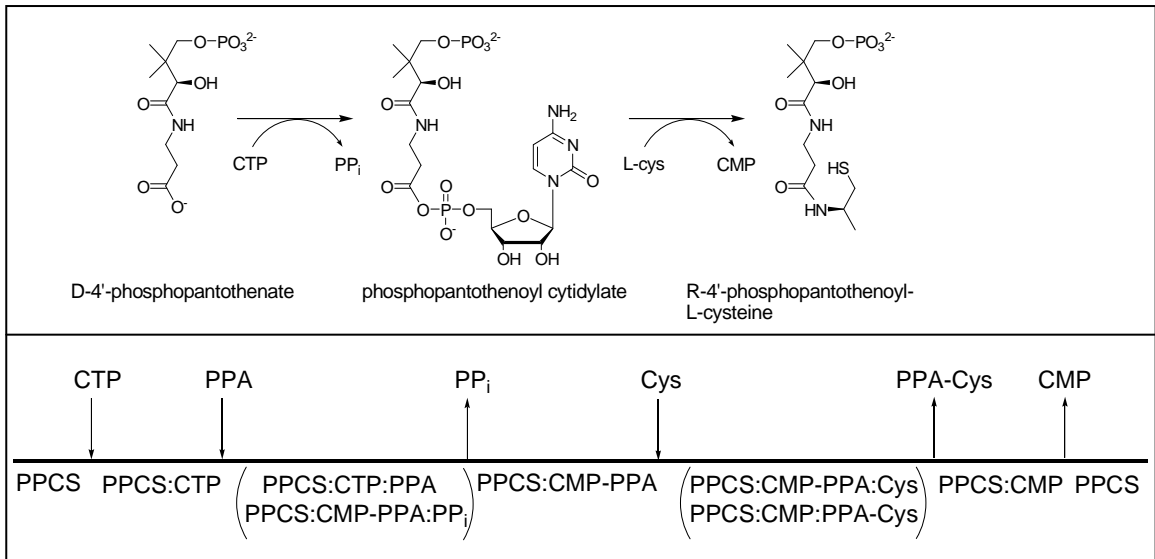
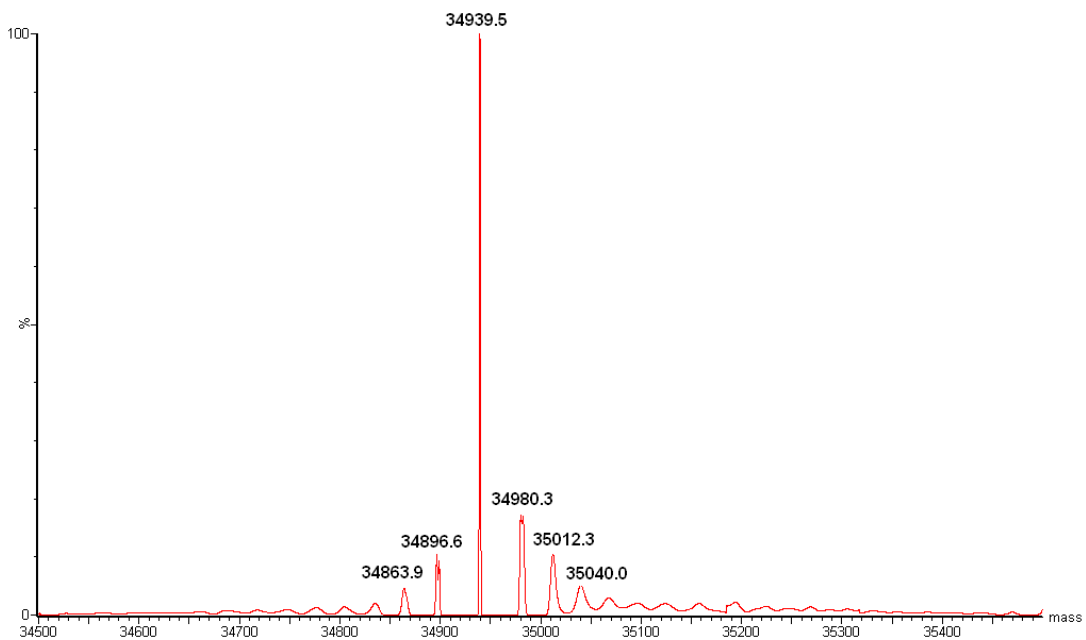Figure 3.1: Kinetic and chemical mechanism of *E. faecalis* PPCS.

Figure 3.2: Positive-ion ESI-MS of purified Human PPCS. The observed mass (34939.5 Da) corresponds to the calculated mass of the recombination PPCS (35072.7 Da) without the N-terminal methionine (133.2 Da).
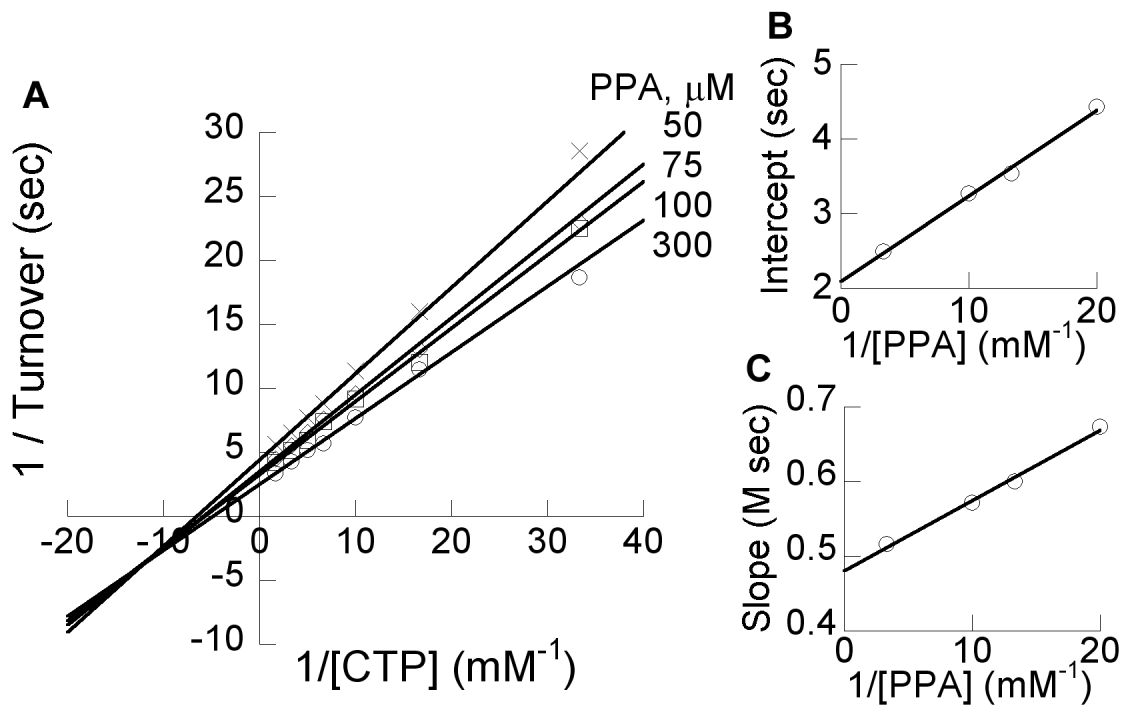
Figure 3.3: Pairwise analysis of CTP and PPA. Initial velocity of PPCS at various [CTP] and [PPA] and 1 mM cysteine. **A.** Double-reciprocal plot of initial velocity. **B.** Secondary plot of intercept versus reciprocal [PPA]. **C.** Secondary plot of slope versus reciprocal [PPA].
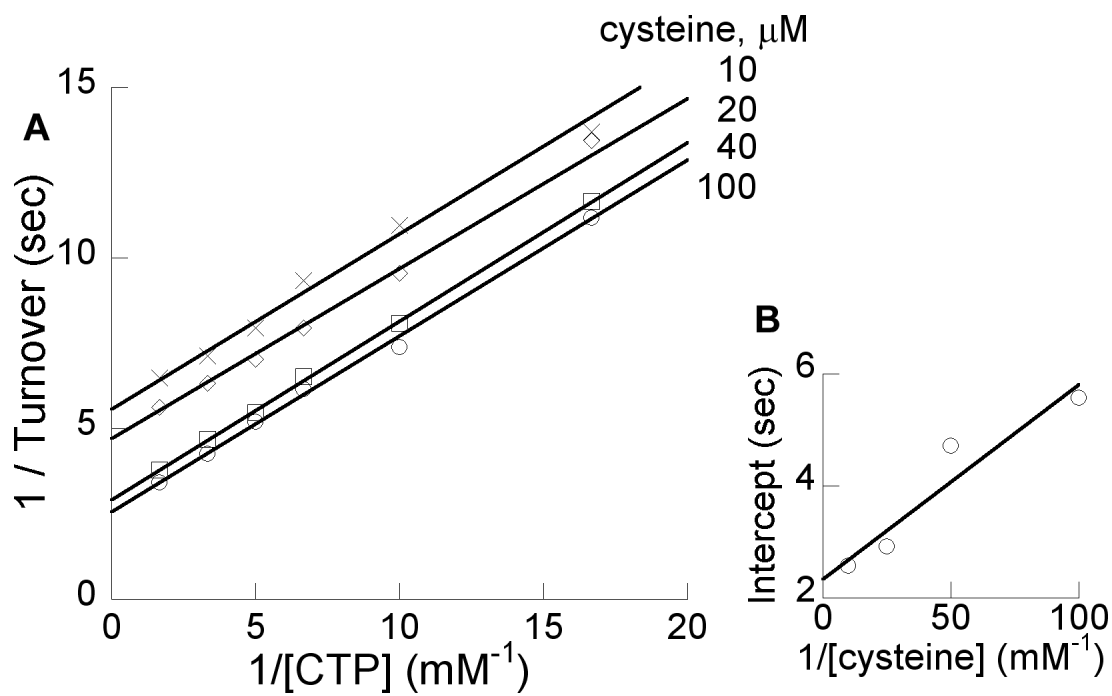
Figure 3.4: Pairwise analysis of CTP and cysteine. Initial velocity of PPCS at various [CTP] and [cysteine] and 0.3 mM PPA. **A.** Double-reciprocal plot of initial velocity. **B.** Secondary plot of intercepts versus reciprocal [cysteine].
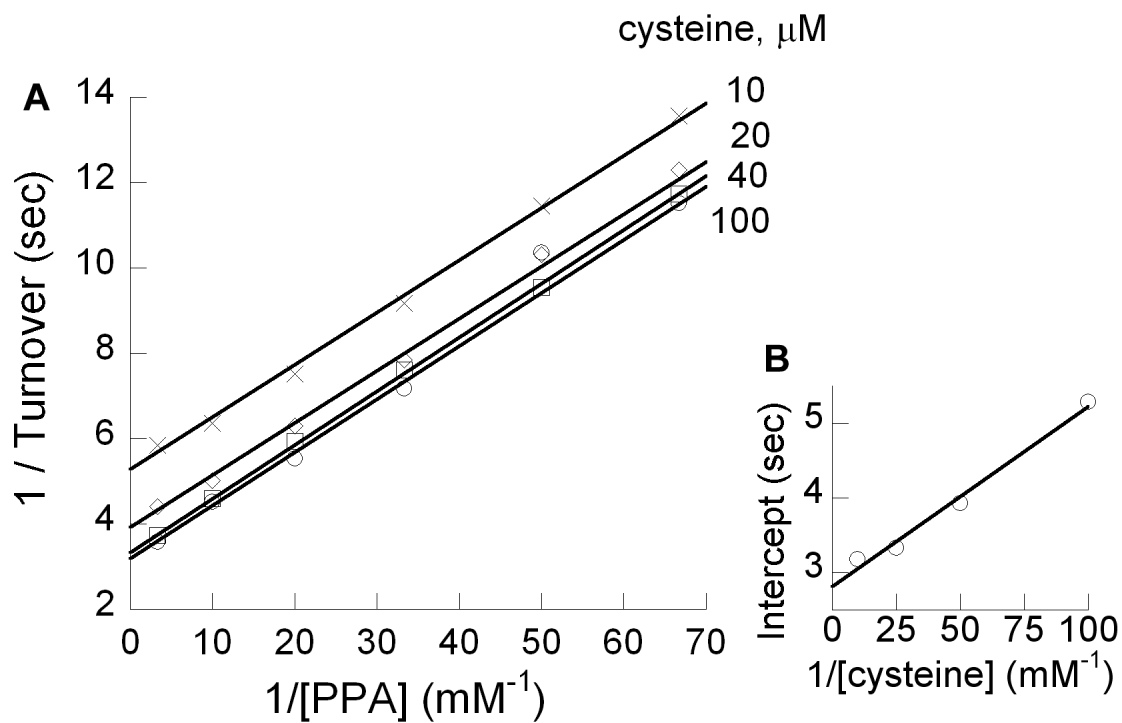
Figure 3.5: Pairwise analysis of PPA and cysteine. Initial velocity of PPCS at various [PPA] and [cysteine] and 0.6 mM CTP. **A.** Double-reciprocal plot of initial velocity. **B.** Secondary plot of intercepts versus reciprocal [cysteine].
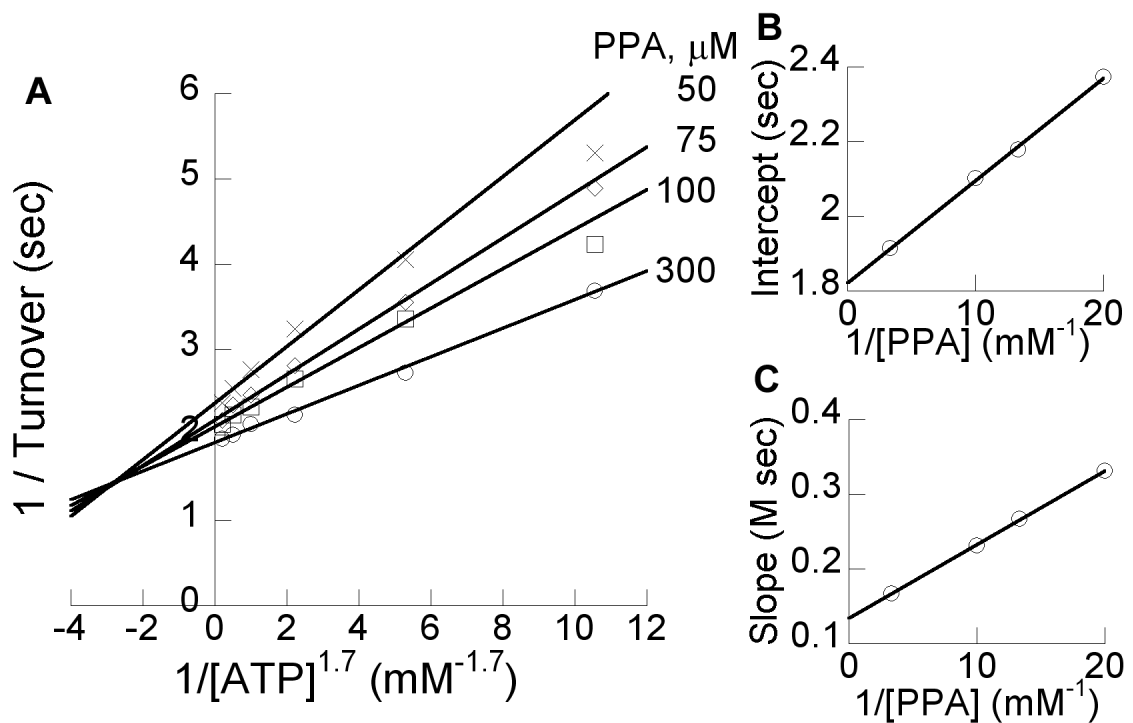
Figure 3.6: Pairwise analysis of ATP and PPA. Initial velocity of PPCS at various [ATP] and [PPA] and 1 mm cysteine. **A.** Double-reciprocal plot of initial velocity. **B.** Secondary plot of intercepts versus reciprocal [PPA]. **C.** Secondary plot of slope versus reciprocal [PPA].
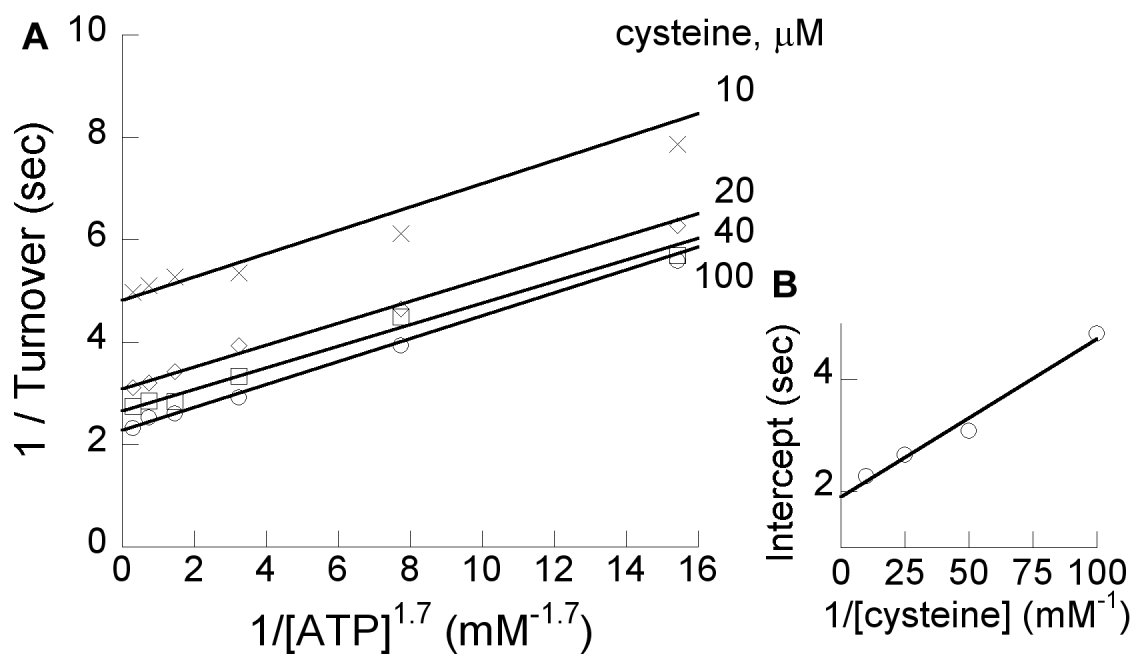
Figure 3.7: Pairwise analysis of ATP and cysteine. Initial velocity of PPCS at various [ATP] and [cysteine] and 0.3 mm PPA. **A.** Double-reciprocal plot of initial velocity. **B.** Secondary plot of intercepts versus reciprocal [cysteine].
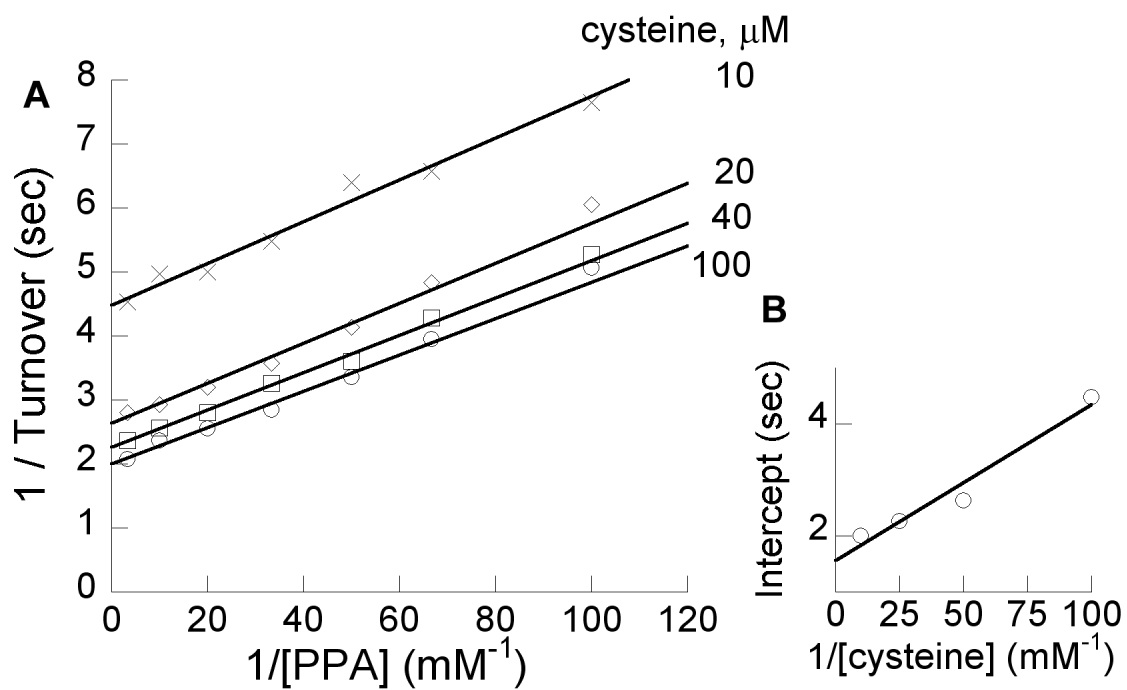
Figure 3.8: Pairwise analysis of PPA and cysteine. Initial velocity of PPCS at various [PPA] and [cysteine] and 2 mm ATP. **A.** Double-reciprocal plot of initial velocity. **B.** Secondary plot of intercepts versus reciprocal [cysteine].

Figure 3.9: Product inhibition analysis of human PPCS. Double reciprocal plot of velocity. **A.** Initial velocity of PPCS at various [CTP] and [CMP] with 0.1 mM cysteine and 0.1 mM PPA. **B.** Initial velocity of PPCS at various [CTP] and [AMP] with 0.1 mM cysteine and 0.1 mM PPA. Double reciprocal plot of velocity. **C.** Initial velocity of PPCS at various [ATP] and [CMP] with 0.1 mM cysteine and 0.1 mM PPA. Double reciprocal plot of velocity.

Figure 3.10: Hill plot of product inhibition analysis of AMP versus ATP. Initial velocity of PPCS at various [ATP] and [AMP] with 0.1 mM cysteine and 0.1 mM PPA. Hill plot.
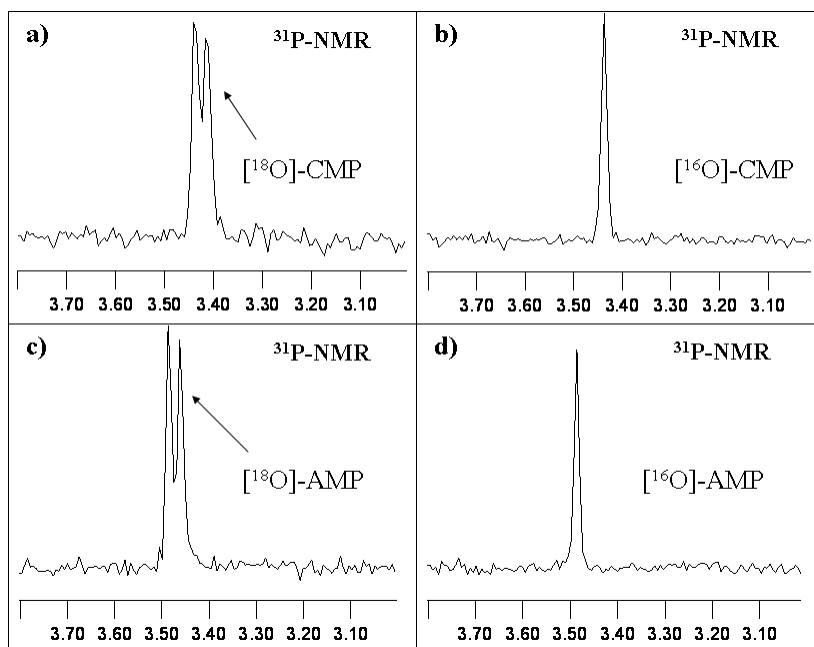
Figure 3.11: ^{31}P NMR spectra of PPCS [18]O transfer reaction. **A.** ^{31}P NMR (proton-decoupled) spectrum of CMP produced in the PPCS reaction using CTP and [*carboxyl-[18]O*] phosphopantothenate. **B.** ^{31}P NMR (proton-decoupled) spectrum of CMP produced in the PPCS reaction using CTP and unlabeled phosphopantothenate. **C.** ^{31}P NMR (proton-decoupled) spectrum of AMP produced in the PPCS reaction using ATP and [*carboxyl-[18]O*] phosphopantothenate. **D.** ^{31}P NMR (proton-decoupled) spectrum of AMP produced in the PPCS reaction using ATP and unlabeled phosphopantothenate.
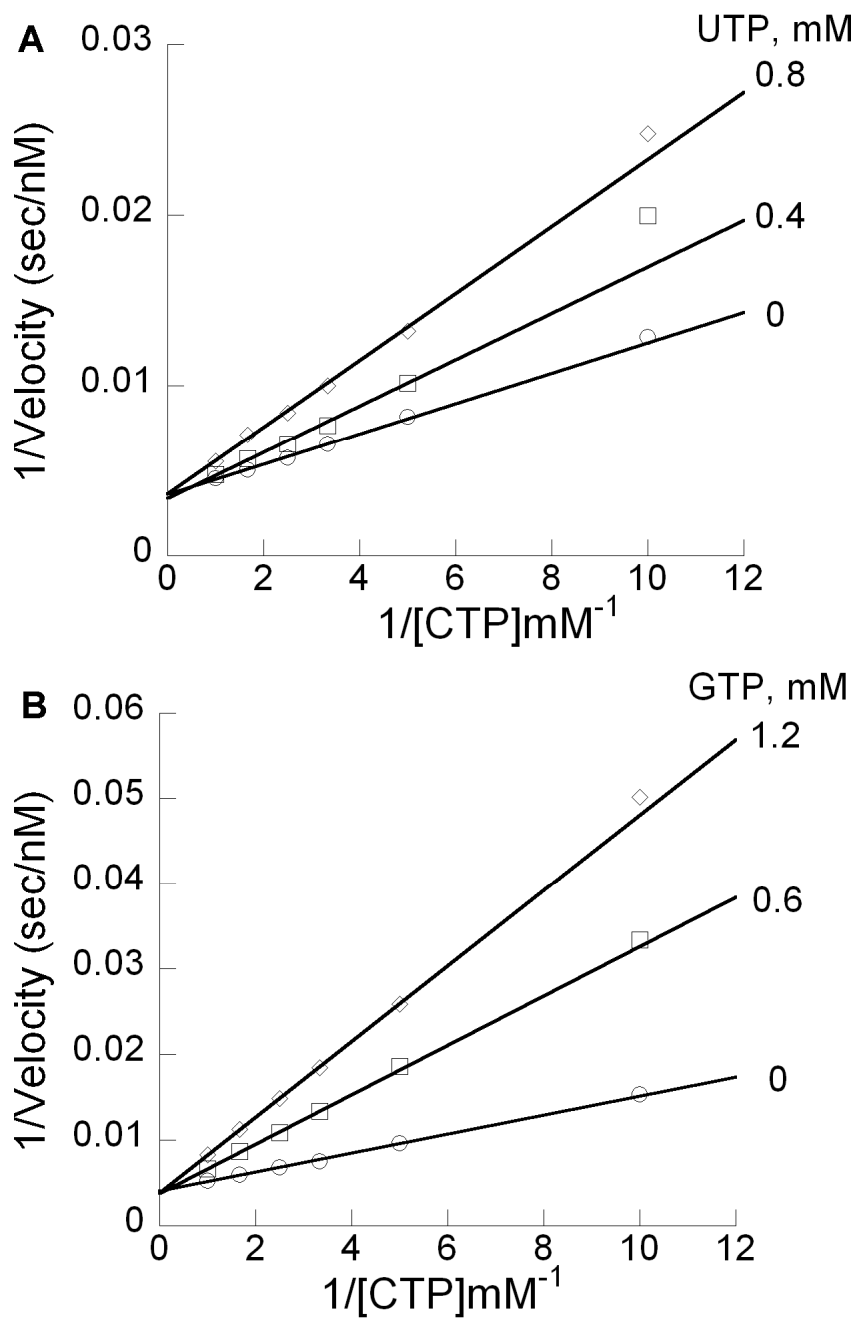
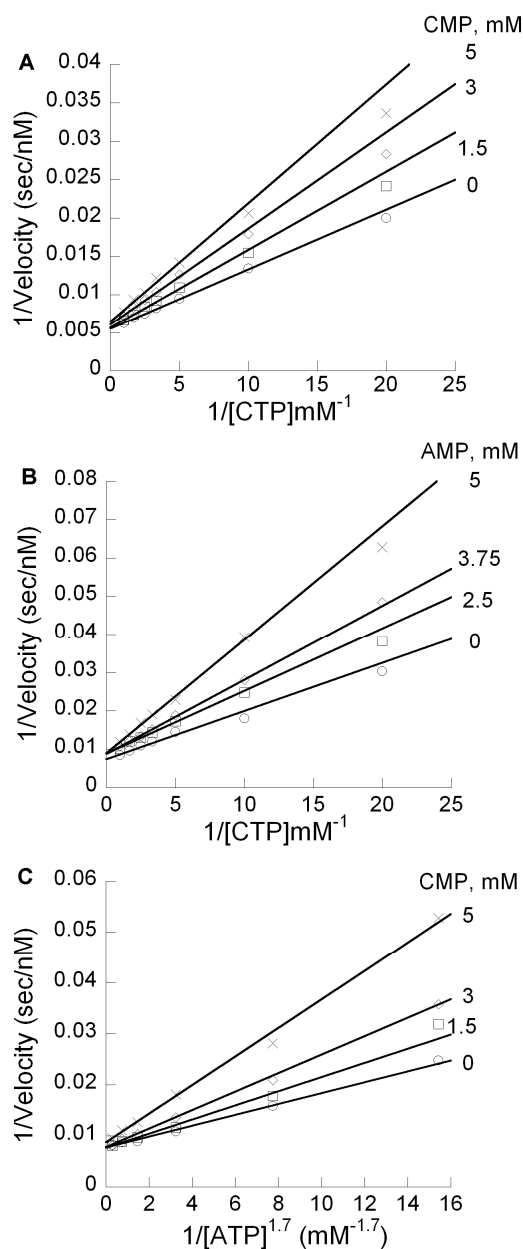Figure 3.12: Inhibition analysis of UTP and GTP. Double reciprocal plot of velocity. **A.** Initial velocity of PPCS at various [CTP] and [UTP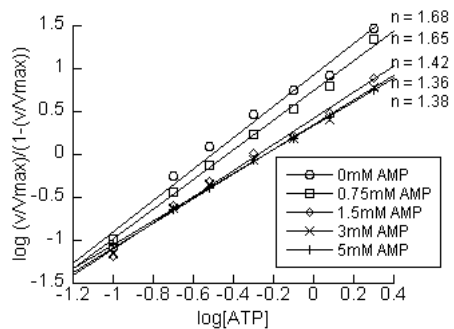] with 1 mM cysteine and 0.3 mM PPA. **B.** Initial velocity of PPCS at various [CTP] and [GTP] with 1 mM cysteine and 0.3 mM PPA.
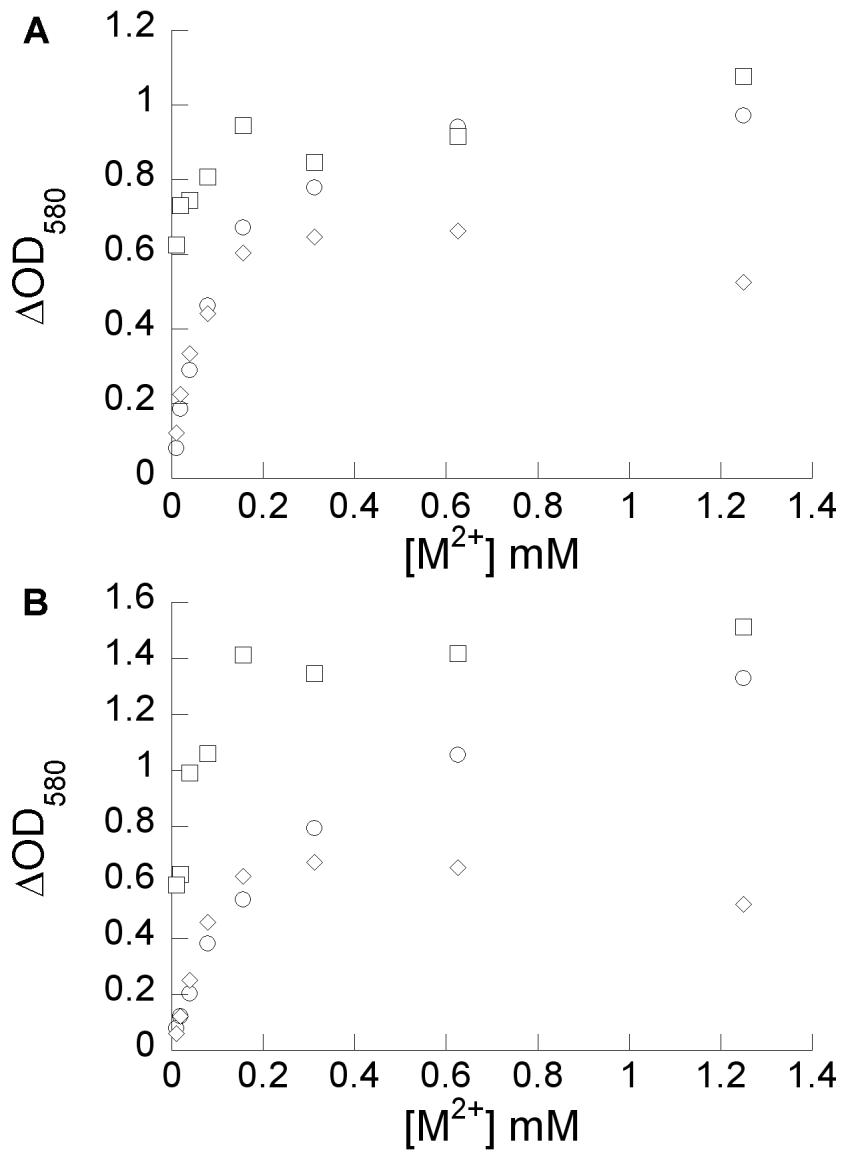
Figure 3.13: Metal dependency of human and *E. faecalis* PPCS. Velocity vs. concentration of Mg^{2+} (circle), Mn^{2+} (square), and Fe^{2+} (diamond). **A.** *E. faecalis* PPCS. **B.** Human PPCS.
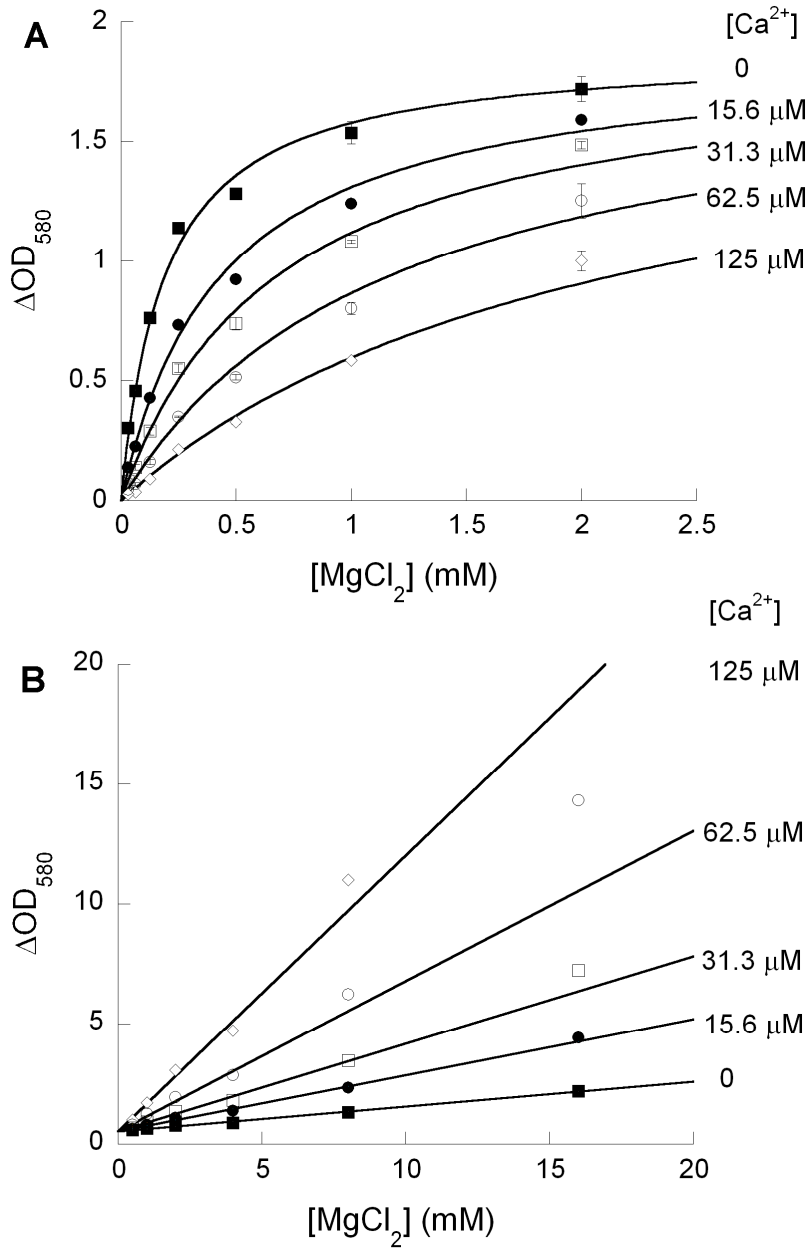
Figure 3.14: Mg^{2+} - Ca^{2+} competition experiment for *E. faecalis* PPCS. **A.** Initial velocity of PPCS against [Mg^{2+}] at fixed changing concentrations of [Ca^{2+}]. **B.** Double reciprocal replot of initial velocity.

Table 3.1: Kinetic Parameters of PPCS at pH 7.6 and 37ºC			
	Human (A = ATP)	Human (A = CTP)	E. faecalis (A = CTP)
K_{iA}	470 ± 90 μM	74 ± 30 μM	650 ± 350 μM
K_{mA}	270 ± 10 μM	270 ± 20 μM	160 ± 17 μM
K_{mPPA}	13 ± 1 μM	57 ± 5 μM	17 ± 6 μM
K_{mcys}	14 ± 0.7 μM	16 ± 1 μM	86 ± 7 μM
k_{cat}	0.56 ± 0.01 sec^{-1}	0.53 ± 0.02 sec^{-1}	2.9 ± 0.1 sec^{-1}

Table 3.2: Nucleotide affinity of human PPCS.
Calculated dissociation constants and Michaelis
constants of various nucleotides to human PPCS.

	K_i	K_m
CTP	74 ± 30 µM	270 ± 20 µM
ATP	470 ± 90 µM	270 ± 10 µM
GTP	370 ± 10 µM	-
UTP	660 ± 50 µM	-
CMP	4.7 ± 0.6 mM	-
AMP	3.70 ± 0.4 mM	-

Table 3.3: ICP-MS of purified PPCS enzymes

	Baseline	PPCS EF	Metal:PPCS EF	PPCS HS	Metal:PPCS HS
Mg^{2+} (μM)	29.6 ± 1.5	7.51 ± 0.38	0%	1.38 ± 0.13	0%
Ca^{2+} (μM)	6.23 ± 0.31	30.1 ± 1.5	27%	11.6 ± 0.1	5%
Mn^{2+} (μM)	0.028 ± 0.004	0.024 ± 0.004	0%	0.019 ± 0.004	0%
Fe^{2+} (μM)	0.08 ± 0.01	<0.04	0%	0.13 ± 0.01	0%
Co^{2+} (μM)	< 0.006	0.098 ± 0.005	0%	< 0.007	0%
Ni^{2+} (μM)	0.21 ± 0.03	< 0.10	0%	< 0.10	0%
Cu^{2+} (μM)	0.014 ± 0.001	0.184 ± 0.009	0%	0.350 ± 0.017	0%
Zn^{2+} (μM)	0.073 ± 0.004	0.202 ± 0.010	0%	0.230 ± 0.012	0%

Chapter 4

High-Throughput Screening for Inhibitors of Bacterial

Phosphopantothenoylcysteine Synthetase

INTRODUCTION

Antibiotic resistance is a major problem worldwide (*1-3*). Antibiotics have been effective treatments for bacterial infections since the 1930s, improving the quality of life for millions of people. However, the inevitable spread of antibiotic resistance in common bacterial pathogens coupled with the slow rate of antibiotic discovery recently have lead to the spread of pathogenic bacteria that are resistant to antibiotic treatments. For example, recent estimates have found that currently around 60% of *Staphylococcus aureus* infections in hospital intensive care units are resistant to penicillin and cephalosporin, the current frontline drugs against many bacterial infections, with high frequencies of additional resistance against tetracycline and erythromycin (*4, 5*). Around 30% of *Enterococci* infections, which are inherently resistant to penicillin and cephalosporin, are also resistant to vancomycin, one of the last-line drugs against bacterial infections (*2, 3*). The recent introductions of linezolid and daptomycin have alleviated some of the need for new antibiotics, but with resistance against linezolid and daptomycin already observed clinically, there is still a great need for new antibiotics and antibiotic targets (*6, 7*).

An antibiotic target should be essential for the survival of the pathogenic bacteria and allow selectivity between human and bacterial orthologs. One potential antibiotic target is coenzyme A biosynthesis, particularly phosphopantothenoylcysteine synthetase (PPCS), the second step of the biosynthetic pathway. Coenzyme A is an indispensible metabolite for all living organisms, involved in essential functions such as fatty acid metabolism (*8, 9*). Deprivation of CoA leads to cell stasis or improper cell development, while knockouts of CoA biosynthetic genes are lethal (*10, 11*).

PPCS, the second step of the five-step CoA biosynthesis, catalyzes the formation of an amide bond between phosphopantothenate and cysteine using the energy derived from hydrolyzing an ATP/CTP into AMP/CMP and pyrophosphate, Figure 4.1 (*12-14*). In the first half-reaction, the carboxylic acid group on phosphopantothenate (PPA) attacks the α-phosphate on ATP/CTP and displaces pyrophosphate to form an activated mixed anhydride intermediate. In the second step, cysteine attacks the activated anhydride and displaces AMP/CMP to make the amide bond. Kinetic characterizations of human and bacterial PPCS have found that while bacterial PPCS is CTP specific, human PPCS can use both ATP and CTP and binds all four NTPs (*12, 14-16*). The difference in nucleotide selectivity suggests that it should be possible to design bacterial selective inhibitors. This idea is validated by a series of intermediate-mimicking inhibitors. The intermediate-based inhibitors contained a cytidine moiety, and showed up to 1,000 fold selectivity for bacterial PPCS (*17*).

Here, we screen for novel inhibitors of bacterial PPCS against a library of 41,000 small molecules and 11,000 natural extracts. Hits from the primary screen were confirmed in triplicates and counterscreened to ensure that the hit does not interfere with

assay components. Top small-molecules hits remaining were tested in dose-response, with compounds obtained from commercial suppliers and retested. The organism producing the top natural product hits were regrown, and the natural products produced were retested. Here, we present the development and application of our screen as well as the hits identified from our screening efforts.

MATERIALS AND METHODS

Materials

Cytidine triphosphate, HEPES, cysteine, dithiothreitol (DTT), $MgCl_2$, bacterial inorganic pyrophosphatase, ammonium molybdate, concentrated HCl, and malachite green carbinol hydrochloride were reagent grade or higher and purchased from Sigma Aldrich. 384-well polystyrene nonbinding surface plates were purchased from Corning (cat. 3640). PPA was synthesized as previously reported (*14*). Synthesis of compound JDP03, a mimic of the 4'-phosphopantothenoyl cytidylate immediate with the carbonyl group of mixed anhydride removed, was described elsewhere (*17*).

The malachite green reagent used here consisted of a final concentration of 0.1125% w/v malachite green carbinol hydrochloride and 2.1% w/v ammonium molybdate in 3 M HCl. After mixing the components for 1 hour, the final mixture is filtered through a 0.22 µM filter and stored at 4°C until use.

Strep. pneumoniae PPCS was cloned, overexpressed, and purified as a 6x His-tagged protein as previously described (*17*). The concentration was determined using absorbance at 280 nm (12,150 $M^{-1}cm^{-1}$), while the purity was checked by SDS-PAGE

gel. The purified protein was >95% pure, and was stored in 20 mM HEPES, pH 8.0 and -80°C.

Inorganic Pyrophosphatase – Purine Nucleoside Phosphorylase Continuous Assay

The inorganic pyrophosphatase – purine nucleoside phosphorylase continuous assasy (PP$_i$ase - PNPase assay) was used for some inhibition kinetic studies. In this assay, the pyrophosphate produced from the PPCS reaction was cleaved into two inorganic phosphate molecules. Then, purine nucleoside phosphorylase catalyzes the phosphorolysis of a nucleoside with consumption of phosphate into ribose-1-phosphate and the nucleobase. The nucleoside used in our assay was 7-methyl-6-thioguanosine (MESG), which was cleaved into 7-methyl-6-thioguanine leading to an increase in absorbance at 355 nm ($\Delta\varepsilon_{355} = 12{,}000 \text{ M}^{-1} \text{ cm}^{-1}$). This assay was run on a 96-well, 100 μL format. The final concentration of the enzyme linked components was 1 U/mL *E. coli* inorganic pyrophosphatase, 3 U/mL *E. coli* purine nucleoside phosphorylase, 2 mM MgCl$_2$, and 200 μM MESG in 100 mM HEPES, pH 8.0 buffer along with the appropriate concentrations of PPCS, substrates, and inhibitors for the particular experiment.

Malachite Green Assay

For determining the steady state kinetic parameters of PPCS, the previously reported continuous pyrophosphate detection assay, where the production of pyrophosphate is linked to the oxidation of NADH, was used (*14*). The continuous assay is advantageous since it can detect pyrophosphate specifically without interference from phosphate contaminants. However, this assay is not suitable for high throughput screening. The NADH signal at 340 nm is prone to interference from compounds in small molecule libraries, while the multiple-read format of the assay is not convenient for high

102

throughput. Instead, a coupled inorganic pyrophosphatase and malachite green reagent assay was chosen. The pyrophosphate produced from the PPCS reaction is cleaved into two phosphates in the presence of inorganic pyrophosphatase. At predetermined time points, malachite green reagent is added to the enzymatic reaction to both quench the reaction and quantify the amount of phosphate produced. With the malachite green reagent, production of phosphate is determined by absorbance readings between 600 – 660 nm, a region that suffers from much less interference from small molecules. Since each PPCS turnover produces two phosphates, the assay is extremely sensitive, capable of detecting low micromolar concentrations of pyrophosphate produced by the enzymatic reaction.

High Throughput Assay Protocol

High throughput assays were performed in 384-well polystyrene NBS plates. Dispensing of the assay components were performed with a Thermo Scientific Multidrop dispenser. First, 30 µL of the enzyme mix, consisting of inorganic pyrophosphatase (PP$_i$ase), PPCS, and MgCl$_2$ buffered in 100 mM HEPES pH 8.0, was added to the plates. Then, compounds from the library (stored at 5 mM in DMSO solution) were added into the plates to a final concentration of ca. 15 µM with a BioMek FX automation working with high density replication pintool. The enzymatic reaction was started by adding 10 µL of substrate mix, consisting of CTP, cysteine, PPA, and DTT also buffered in 100 mM HEPES pH 8.0, to the plate. The reaction was stopped and the amount of phosphate produced (after 25 minutes for the actual screen) was determined by quenching the 40 µL reaction with 40 µL of malachite green. This mixture was incubated at room temperature for 5 min, and the absorbance at 600 nm was recorded on a PHERAstar microplate reader

103

(BMG Labtech). Different amounts of reaction components were used for the development of the assay, but the final concentration of the 40 µL enzyme reaction used in our high throughput screen was 12.5 nM PPCS, 0.1 U/mL PP_iase, 2 mM $MgCl_2$, 250 µM CTP, 250 µM DTT, 150 µM cysteine, and 150 µM PPA. Because phosphate contamination was a concern, the substrate mix was made up and kept on ice until used to minimize the hydrolysis of CTP and PPA. For every plate, the 32 wells of the left two columns were run as positive inhibition controls (no PPCS enzyme) while another 32 wells of the right two columns were run as negative inhibition controls (no compounds, 0.5% DMSO)

Confirmation and Counterscreen

Hits selected from the primary screen were confirmed by repeating the assay on those compounds in triplicates. Since compounds that inhibit inorganic pyrophosphatase would also show as positives in our screen, hits were evaluated for inorganic pyrophosphatase inhibition in a counterscreen. This was done in the same 40 µL, 384-well format where a final concentration of 250 µM PP_i was added to a solution of 10 µU/mL PP_iase, 1 mM $MgCl_2$, and the hit compound in 100 mM HEPES, pH 8.0 buffer. The reaction was incubated for 20 minutes, and then quenched with malachite green reagent and absorbance was determined at 600 nm. A hit that showed inhibition against PP_iase or did not confirm in the confirmation screen was not pursued further.

HTS Dose Response and Determination of pAC$_{50}$

Hit compounds were tested in dose response using similar protocols as the primary assay, except performed as duplicates with serial dilutions of the hit compound ranging from 80 nM to 100 µM final concentration. The activity versus inhibitor

concentrations was plotted and fit to a four variable sigmoidal dose response model, equation 1, where pAC_{50} is defined as $-\log [IC_{50}]$, n is the Hill slope, max is the activity observed under no inhibition, and min is defined as the activity observed under full inhibition of a particular compound (which is usually set to no enzyme activity except for a few partial inhibitors).

$$\text{activity} = \min + \frac{(\max - \min)}{(1 + 10^{(pAC_{50} - \log[I]) \times n})} \quad \text{Equation 1}$$

Continuous Assay Dose Response

Compounds that showed activity in the dose response were obtained from the manufacturer and retested using the previously described continuous pyrophosphate detection assay. This assay, which has different coupling components, allows independent verification of inhibitor activity. Assays were run in 100 μL, 96 well-format with 80 nM *Strep.* PPCS, 250 μM CTP, 250 μM PPA, 250 μM cysteine, and 10 mM DTT against varying concentrations of compounds. IC_{50} was determined by fitting the initial velocity data to a standard four parameter IC_{50} equation.

RESULTS AND DISCUSSION

Kinetic Determination of Streptococcus pneumoniae PPCS

PPCS from *Streptococcus pneumoniae* was selected over other characterized bacterial PPCS. *Strep. pneumoniae* PPCS was more stable and exhibited better linearity than *E. coli* PPCS, as well as less non-productive CTP hydrolysis in our assay than the *E. faecalis* PPCS. The apparent K_m and k_{cat} at conditions similar to those used for the primary assay were determined, Figure 4.2. For the CTP dimension, K_m^{app} of CTP is 55 μM with a strong positive cooperativity, measured as a Hill constant of 2 and k_{cat}^{app} is

2.65 sec^{-1} at 150 µM PPA and 200 µM cysteine. For the PPA dimension, K_m^{app} of PPA is 22 µM and k_{cat}^{app} is 1.98 sec^{-1} at 400 µM CTP and 200 µM cysteine. For the cysteine dimension, K_m^{app} of cysteine is 282 µM and k_{cat}^{app} is 3.55 sec^{-1} at 150 µM PPA and 400 µM ATP.

Assay Development

      To ensure that enzyme activity is linear over the course of the reaction, reactions were run with different concentrations of enzymes and quenched at different times (n = 4), Figure 4.3. We found that activity was linear until the amount of pyrophosphate produced saturates the limit of optical detection ($OD_{600} > 2.5$). We also observed a linear relationship between PPCS concentration and velocity of the reaction. The concentration of PPCS was selected as 12.5 nM and reaction time was selected as 25 min for the primary assay to maximize our assay sensitivity and throughput. Reactions were also evaluated in presence of up to 7.5% DMSO to ensure that DMSO world not interfere, and no statistical difference was observed when reactions with DMSO were compared with reactions without DMSO. The Z'-factor (*18*) for the screen was determined by running the primary assay, as described, in 384 well plate format, using reactions with PPCS enzyme as positive signal control and without PPCS enzyme as negative signal control. With 192 samples (half the plate) each for the positive and negative controls and using equation Z'-factor = $1 - [3 \times (\sigma_p + \sigma_n)/|\mu_p + \mu_n|]$, Z'-factor = 0.83, Figure 4.4.

      Finally, the assay was used to determine the IC_{50} of a previously characterized inhibitor, JDP03, to verify the robustness and fidelity of the assay, Figure 4.5. Because JDP03 was previously determined to have a low nanomolar affinity, the assay was run with 8.75 nM of PPCS and fit to the Morrison equation for tight-binding inhibitors (*19*).

The calculated IC_{50} from the assay was 1.3 nM, a close match with the previously

reported value (<10 nM).

HTS for small molecule inhibitors of bacterial PPCS

Bacterial PPCS was screened against approximately 41,000 small molecules from

a number of commercially available libraries (Maybridge McMaster and HitFinder,

Chembridge 3028, ChemDiv 20K, MicroSource 2000, and BioFocus NCC). Z'-factor

was calculated from the positive and negative controls on every plate, and values varied

from 0.55 to 0.8 with median of 0.65 over the course of the screen. Compounds that

exhibited more than 25% inhibition of PPCS activity or greater than 4 standard deviations

over the negative control were selected as hits. Hits with reactive structural alerts were

eliminated. There were 1,470 hits, or 3.6% of the library, using these criteria.

The 1,470 hits were counter-screened for pyrophosphatase activity and confirmed

in triplicates. A total of 908 of the hits were confirmed to have greater than 25%

inhibition of PPCS activity or greater than 4 standard deviations over the negative

control. Of these remaining hits, 14 showed greater than 20% inhibition of

pyrophosphatase activity, and were eliminated. Compounds that violated the promiscuity

index where they showed activity in greater than 30% of the over 60 screens previously

performed at the Center for Chemical Genomics at the University of Michigan were

eliminated as well. Compounds with SlogP of greater than 6 or contained 5 or more rings

were also eliminated. A total of 510 compounds were left at this point. For these 510

compounds, the percent activity observed in the primary screen was plotted against the

median percent activity (n = 3) observed in the confirmation screen. The correlation

coefficient, r^2, is determined to be 0.375, Figure 4.6.

The 240 of the 510 hits with the highest activity in the confirmation screen were measured for dose response inhibition. Of these, 160 hits showed concentration-dependent inhibition, but many had exhibited poor inhibition – 35 compounds have $pAC_{50} < 4$ and 86 compounds have pAC_{50} between 4 and 5, with distribution of hits based on pAC_{50} given in Table 4.1. The IC_{50} of 30 compounds with pAC_{50} of 5 to 8, corresponding to micromolar or lower IC_{50} values, are presented in Table 4.2. Compounds from similar structural families (similarity of 70% or more based on Tanimoto algorithm) are denoted by having the same symbol in the structure class column. Representative dose response of 6 compounds from the dose response are plotted, Figure 4.7.

Our primary screen hit rate of 3.6% is significantly higher than most published primary assays, which tend to be 1% or less (*20, 21*). Originally, we hypothesized that the hit rate might be because inhibition of inorganic pyrophosphatase would also show up as hits, so the assay is effectively screening for inhibitors of two enzymes and thus would have twice the hit rate. However, very few compounds (14 of 908 that confirmed) showed pyrophosphatase inhibition in the counter-screen, while confirmation rates were as expected with 908 confirmed out of 1470 primary hits for 62% reconfirmation rate. During the dose-response measurements, the reason for the high-hit rate became apparent. Because of the high assay sensitivity, we were able to detect many marginal inhibitors, with $pAC_{50} < 5$ ($IC_{50} > 100$ µM), when screening at 15 µM of compound.

Preliminary Properties of Hit Compounds

The 160 compounds with $IC_{50} < 100$ µM in the screen exhibited overall diverse structural and physiochemical properties. Of the top 30 compounds, however, half of the

identified compounds are structurally related with each other with 70% or more similarity. Of this class of structurally similar compounds, the compound with the best potency has IC_{50} of 10.2 nM ($pAC_{50} = 7.99$). More structurally similar compounds were identified outside of the top 30 as well. Two other compounds showed structural similarity in the top 30, and a few more related structures appeared in the dose response as well. These two compounds were less potent, with the most potent member having IC_{50} of 1 µM ($pAC_{50} = 6.01$). From the dose response titrations, the lowest IC_{50} identified for hit compounds is 8.9 nM ($pAC_{50} = 8.05$), with several more in the tens of nanomolar range. This is near the limit of detection of the assay – it is impossible to get IC_{50} values less than half of the 12.5 nM of PPCS enzyme used in the assay.

Retest of Hit Compounds – First Set

Due to the large number of hits we obtained, we compared our hit list to the results of anti-bacterial screens that have been performed at the CCG. We were able to identify 20 compounds that showed inhibition in our screen and in antibacterial screens. Of these compounds, 11 were ordered and retested. The inhibition of four compounds was reconfirmed using the protocol for the HTS. Out of the four, only two showed inhibition in the continuous assay, and the two that did not reconfirm were presumed to be pyrophosphatase inhibitors. CCG-17201 had an IC_{50} of 196 µM and a Hill slope of 0.71, while compound 18864 had an IC_{50} of 90 µM and a Hill slope of 3.23, Figure 4.8. Upon further examination, CCG-18864 formed aggregates in the assay solution and the aggregates were responsible for the observed inhibition. CCG-17201 was tested against *E. facaelis* PPCS, and exhibited IC_{50} of approximately 175 µM and a Hill slope of 0.9.

Due to the poor inhibition of CCG-17201 and the aggregate formation of CCG-18864, neither was followed up.

Compounds were retested after soaking in DMSO at room temperature for a week. This time, compounds 25131 and 22784, which are members of a group of approximately 20 structurally similar compounds showed inhibition. However, these compounds were clear initially, but become a dark green color when retested a week later. The two compounds had IC_{50} values in the 100 µM range, but more detailed characterization was difficult due to the dark color of the compound interfering with the assay signal.

Second Pyrophosphatase Counterscreen

The counterscreen did not remove all the inhibitors of inorganic pyrophosphatase, as evidenced by inorganic pyrophosphatase inhibitors that were found in the retest of hit compounds. The likely explanation is that in the counterscreen, pyrophosphate is added at a large dose initially, while pyrophosphate is produced in small doses over time in the PPCS screen. Thus, competitive inhibitors of inorganic pyrophosphatase would appear as hits in the primary screen, but missed in the counterscreen. A counterscreen that could simulate the slow production of pyrophosphate would be more efficient at identifying pyrophosphatase inhibitors. Since the malachite green – inorganic pyrophosphatase assay has been optimized for finding inhibitors of PPAT (see Chapter 5), which also produces pyrophosphate, the PPAT – Malachite Green – inorganic pyrophosphatase assay was used as the counterscreen.

The family of compounds that showed activity only after an extensive DMSO soak as well as compounds already tested was removed from the set of 160 compounds

showing a dose-response. The dose-response inhibitions of the remaining 120 hits were tested against the PPAT screen (described in Chapter 5). Compounds that demonstrated inhibition against both PPCS and PPAT were assumed to be nonspecific inhibitors or inhibitors of pyrophosphatase and eliminated. Only 80 compounds remained on the hit-list after this counterscreen.

Retest of Hit Compounds – Second Set

Of the 80 compounds, 48 were available and purchased from ChemDiv or Maybridge. These compounds were brought up in DMSO at 5 mM concentration, and the dose response inhibition of these compounds were measured (with final compound concentration ranging from 1 µM to 125 µM) via the malachite green HTS assay. Nine compounds were found to have IC_{50} less than 50 µM, Table 4.3. Of these compounds, four looked promising - with Hill Slopes between 0.7 and 1.3 and IC_{50} values ranging from 1 µM to 20 µM, Figure 4.9. Of these four, CCG-48365 (IC_{50} = 3.8 µM, Hill slope = 0.7) had solubility problems in aqueous solution at up to 125 µM, which might account for the observed Hill slope of less than 1. The other three compounds - CCG-20295 (IC_{50} = 10.1 µM, Hill slope = 1.1), CCG-43108 (IC_{50} = 18 µM, Hill slope = 1), and CCG-44564 (IC_{50} = 0.9 µM, Hill slope = 1.2) – were soluble up to 0.5 mM and had a weak yellow or pink color. Efforts are currently underway to determine the mechanism of inhibition of these compounds.

Natural Product Screening

The PPCS screen was also run against a collection of 11,000 natural product extracts collected by Dr. David Sherman. The natural product extracts were stored in DMSO at 10 mg/mL, and screened at a final concentration of 0.1 mg/mL using the same

protocol as described above for small molecules. Natural extracts showing greater than 50% inhibition were retested in triplicates and counter-screened to remove inorganic pyrophosphatase inhibitors. Extracts demonstrating greater than 80% PPCS inhibition in the retest and less than 10% pyrophosphatase inhibition in the counterscreen were selected as hits. A total of 68 hits were obtained. Because some extracts came from different solvent extractions of the same organism strain, the natural products produced from 22 strains were pursued.

Natural product extracts from the 22 strains were obtained from Dr. Fengan Yu in Dr. Sherman's group. These natural product extracts were dissolved in 10% methanol/ 90% water to a final concentration of 1 mg/mL and the dose response inhibitions of these compounds (from 2 µg/mL to 200 µg/mL final concentration) were measured via the HTS malachite green assay. Extracts from seven strains showed dose response inhibition, with IC_{50} values lower than 62.5 µg/mL. Of these extracts, SID-21269 showed an IC_{50} of 0.03 mg/mL and a Hill Slope of 2.6, Figure 4.10, and was chosen for further analysis. SID-21269 was fractionated via reverse phase HPLC into 65 fractions by Dr. Yu, and the fractions were retested. After fractionation, there was not enough material to get an accurate mass. Fractions were dissolved such that the stock concentration would be approximately 0.25 mg/mL if the original mass was equally distributed across the fractions. However, since the exact mass was unknown, the IC_{50} values for the fractions were reported as the percent of the stock solution of the fraction in the final assay volume rather than a concentration in further experiments.

The dose response inhibitions of the 65 fractions from SID-21269 were measured using the HTS Malachite Green assay. Inhibition of PPCS activity was observed in

fractions 37 – 45, with the greatest inhibition found in fractions 41 – 42, Figure 4.11. The observed IC_{50} for the most potent fraction (fraction 42) was approximately 1% of the stock solution in the final assay volume, and the Hill slopes were approximately 1 for these fractions. Assuming that the inhibition found in the set of fractions was from one inhibitor, the relative concentration of the inhibitor in each fraction must be inversely related to the observed IC_{50}. Therefore, the inverse of IC_{50} for each fraction was plotted against the fraction number to get a sense of how the inhibitor eluted from the column, Figure 4.12. From this plot, the inhibitor appeared to elute as one peak centered on fractions 41 – 42.

Fraction 41 was chosen for further analysis. The inhibition against PPCS was reconfirmed. Enzymatic reactions with 80 nM PPCS, 2 mM $MgCl_2$, 250 μM CTP, 250 μM PPA, and 250 μM cysteine in 100 mM HEPES, pH 8.0 with and without 15% final solution of fraction 41 were run for 25 minutes, and then quench with the Eikonogen assay (Chapter 3) to determine the amount of pyrophosphate produced. With 15% final solution of fraction 41, no pyrophosphate production was observed, compared to approximately 100 μM pyrophosphate production without inhibitor.

Inhibition kinetic study of fraction 41 against CTP was conducted for the *E. faecalis* PPCS enzyme via the PP_iase - PNPase assay at 30°C. Velocity versus [CTP] was measured at 0%, 2%, 4%, and 6% final concentration of fraction 41 at 300 μM PPA, 300 μM cysteine, and 35 nM PPCS. Increasing concentrations of fraction 41 increased the apparent K_m of CTP with minimal effects on the apparent V_{max}. As a result, the replot of the data as a Lineweaver-Burk plot, Figure 4.13, showed that the fitted lines intersected on the y-axis, consistent with a mechanism where SID-21269 fraction 41 acts as a

competitive inhibitor of CTP. Kinetic experiments were run with and without

preincubating fraction 41 with PPCS for 15 minutes, and no significant change in

inhibition effects was observed, suggesting that the inhibitor is not a slow binding or

covalent inhibitor.

Based on the available kinetic data, the natural product inhibitor contained in

SID-21269 fraction 41 inhibits PPCS by binding to the free enzyme form of PPCS in a

manner that prevents CTP binding (and thus PPCS turnover), Figure 4.14. The inhibitor

binding is also rapid and reversible. This proposed inhibition mechanism is the only

simple kinetic mechanism that is consistent with the observed kinetic data. If the inhibitor

bound to other enzyme forms over the PPCS enzymatic reaction, the observed inhibition

pattern against CTP would be uncompetitive or noncompetitive. Furthermore, a clear

competitive inhibition pattern suggests strongly that a single inhibitor (or a class of

inhibitors with very similar affinities) from the fraction is responsible for the observed

inhibition. Efforts are currently underway to identify the structure of the natural product

responsible for the PPCS inhibition activity.

REFERENCES

1. Finch, R. G. (2004) Antibiotic resistance: a view from the prescriber. *Nat Rev Micro 2*, 989-994.
2. Fridkin, S. K., Steward, C. D., Edwards, J. R., Pryor, E. R., McGowan, J. E., Archibald, L. K., Gaynes, R. P., and Tenover, F. C. (1999) Surveillance of Antimicrobial Use and Antimicrobial Resistance in United States Hospitals: Project ICARE Phase 2. *Clin Infect Dis 29*, 245-252.
3. Hidron, A. I., Edwards, J. R., Patel, J., Horan, T. C., Sievert, D. M., Pollock, D. A., and Fridkin, S. K. (2008) NHSN Annual Update: Antimicrobial-Resistant Pathogens Associated With Healthcare-Associated Infections: Annual Summary of Data Reported to the National Healthcare Safety Network at the Centers for Disease Control and Prevention, 2006-2007. *Infection Control and Hospital Epidemiology 29*, 996-1011.
4. Crum, N. F., Lee, R. U., Thornton, S. A., Stine, O. C., Wallace, M. R., Barrozo, C., Keefer-Norris, A., Judd, S., and Russell, K. L. (2006) Fifteen-Year Study of the Changing Epidemiology of Methicillin-Resistant Staphylococcus aureus. *Am J Med 119*, 943-951.
5. Hiramatsu, K., Hanaki, H., Ino, T., Yabuta, K., Oguri, T., and Tenover, F. C. (1997) Methicillin-resistant Staphylococcus aureus clinical strain with reduced vancomycin susceptibility. *J. Antimicrob. Chemother. 40*, 135-136.
6. Herrero, I. A., Issa, N. C., and Patel, R. (2002) Nosocomial Spread of Linezolid-Resistant, Vancomycin-Resistant Enterococcus faecium. *N Engl J Med 346*, 867-869.
7. Hidron, A. I., Schuetz, A. N., Nolte, F. S., Gould, C. V., and Osborn, M. K. (2008) Daptomycin resistance in Enterococcus faecalis prosthetic valve endocarditis. *J. Antimicrob. Chemother.*, dkn105.
8. Spry, C., Kirk, K., and Saliba, K. J. (2008) Coenzyme A biosynthesis: an antimicrobial drug target. *FEMS Microbiol. Rev. 32*, 56-106.
9. Leonardi, R., Zhang, Y.-M., Rock, C. O., and Jackowski, S. (2005) Coenzyme A: Back in action. *Progress in Lipid Research 44*, 125-153.
10. Spitzer, E. D., and Weiss, B. (1985) *dfp* gene of *Escherichia coli* K-12, a locus affecting DNA synthesis, codes for a flavoprotein. *J. Bacteriol. 164*, 994-1003.
11. Jackowski, S., and Rock, C. O. (1986) Consequences of reduced intracellular coenzyme A content in Escherichia coli. *J. Bacteriol. 166*, 866-871.
12. Kupke, T. (2002) Molecular characterization of the 4'-phosphopantothenoylcysteine synthetase domain of bacterial Dfp flavoproteins. *J. Biol. Chem. 277*, 36137-36145.
13. Strauss, E., Kinsland, C., Ge, Y., McLafferty, F. W., and Begley, T. P. (2001) Phosphopantothenoylcysteine synthetase from *Escherichia coli*. Identification and characterization of the last unidentified coenzyme A biosynthetic enzyme in bacteria. *J. Biol. Chem. 276*, 13513-13516.
14. Yao, J., Patrone, J. D., and Dotson, G. D. (2009) Characterization and kinetics of phosphopantothenoylcysteine synthetase from *Enterococcus faecalis*. *Biochemistry 48*, 2799-2806.
15. Daugherty, M., Polanuyer, B., Farrell, M., Scholle, M., Lykidis, A., de Crecy-Lagard, V., and Osterman, A. (2002) Complete reconstitution of the human

coenzyme A biosynthetic pathway via comparative genomics. *J. Biol. Chem. 277*, 21431-21439.

16. Yao, J., and Dotson, G. D. (2009) Kinetic characterization of human phosphopantothenoylcysteine synthetase. *Biochim. Biophys. Acta, Proteins Proteomics 1794*, 1743-1750.

17. Patrone, J. D., Yao, J., Scott, N. E., and Dotson, G. D. (2009) Selective Inhibitors of Bacterial Phosphopantothenoylcysteine Synthetase. *J. Am. Chem. Soc. 131*, 16340-16341.

18. Zhang, J.-H., Chung, T. D. Y., and Oldenburg, K. R. (1999) A Simple Statistical Parameter for Use in Evaluation and Validation of High Throughput Screening Assays. *J Biomol Screen 4*, 67-73.

19. Morrison, J. F. (1969) Kinetics of the reversible inhibition of enzyme-catalysed reactions by tight-binding inhibitors. *Biochim Biophys Acta. 185*, 269-286.

20. Doman, T. N., McGovern, S. L., Witherbee, B. J., Kasten, T. P., Kurumbail, R., Stallings, W. C., Connolly, D. T., and Shoichet, B. K. (2002) Molecular Docking and High-Throughput Screening for Novel Inhibitors of Protein Tyrosine Phosphatase-1B. *J Med Chem 45*, 2213-2221.

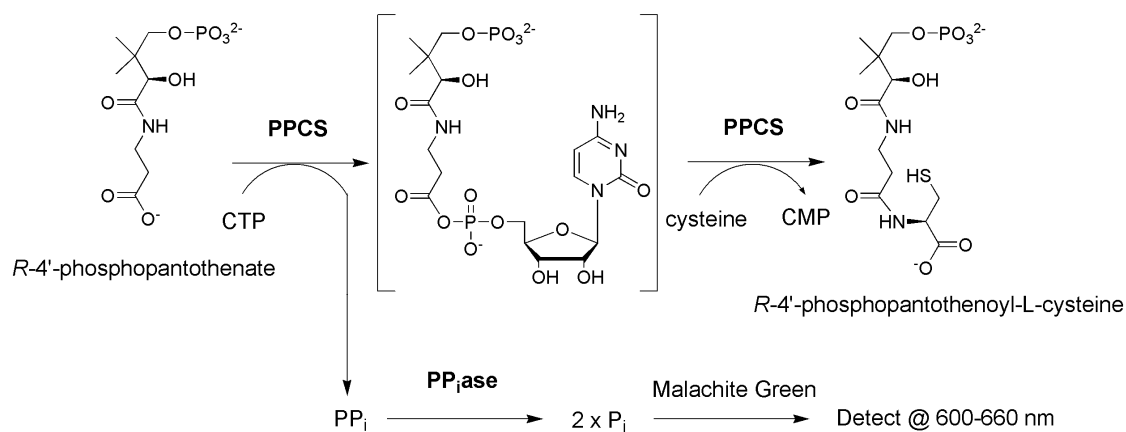21. Shoichet, B. K. (2004) Virtual screening of chemical libraries. *Nature 432*, 862-865.

Figure 4.1: PPCS HTS assay. PPCS catalyzes the amide bond formation between phosphopantothenate and cysteine, proceeding through a phosphopantothenoyl cytidylate intermediate. The pyrophosphate formed from the PPCS reaction is cleaved by inorganic pyrophosphatase and then detected via malachite green to monitor PPCS activity in our HTS assay.
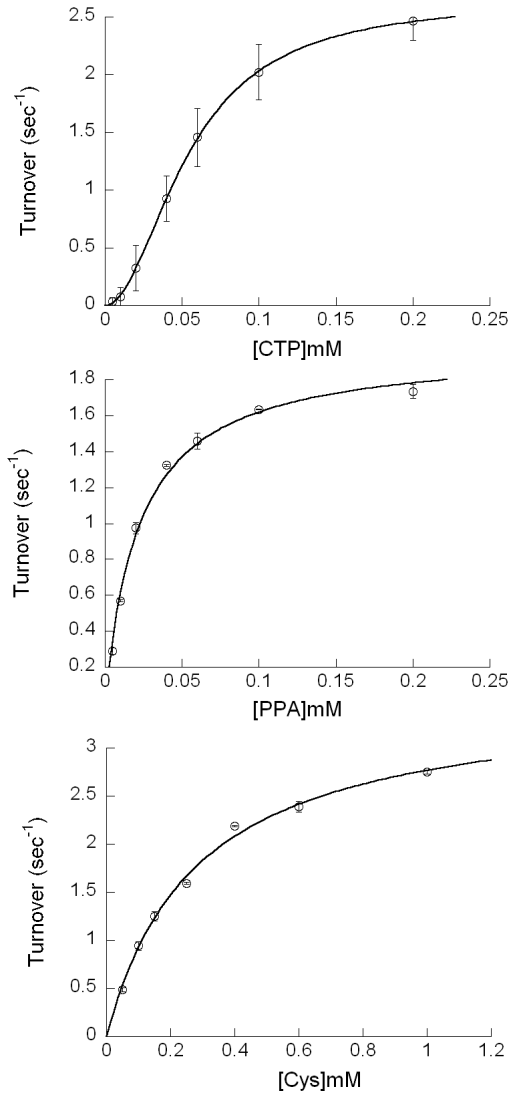
Figure 4.2: Kinetic determination of *Strep. pneumoniae* PPCS. The K_m^{app} and k_{cat}^{app} for each substrate is determined at fixed levels of the other two substrates. CTP binding showed strong positive cooperativity.
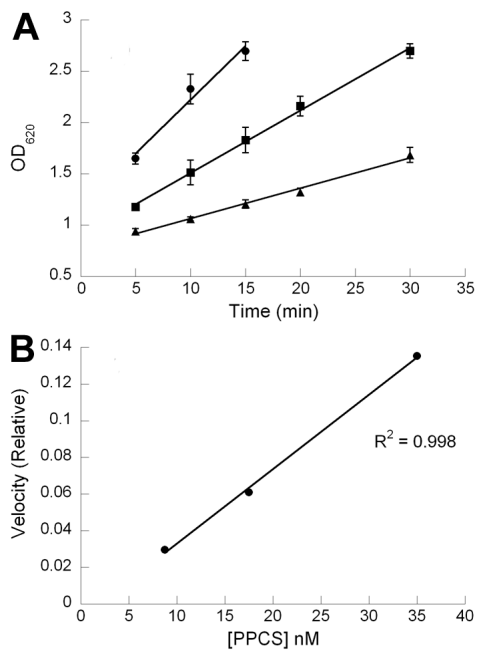
Figure 4.3: HTS Assay development. A. Absorbance at 620 nm as a function of time for the reaction with 35 nM (circle), 17.5 nM (square), and 8.75 nM (triangle) of PPCS. B. Plot of velocity vs. enzyme concentration.
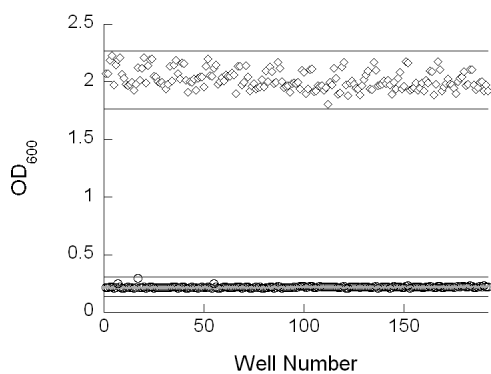
Figure 4.4: Z'-factor determination for HTS assay. The PPCS reaction (circle) was run in 192 wells of a 384-well plate, while blank control without PPCS (diamond) was run in another 192 wells. Mean and standard deviation of PPCS reaction and blank control were calculated, with mean ± 3 SD plotted around the data point. Z'-factor is 0.83.
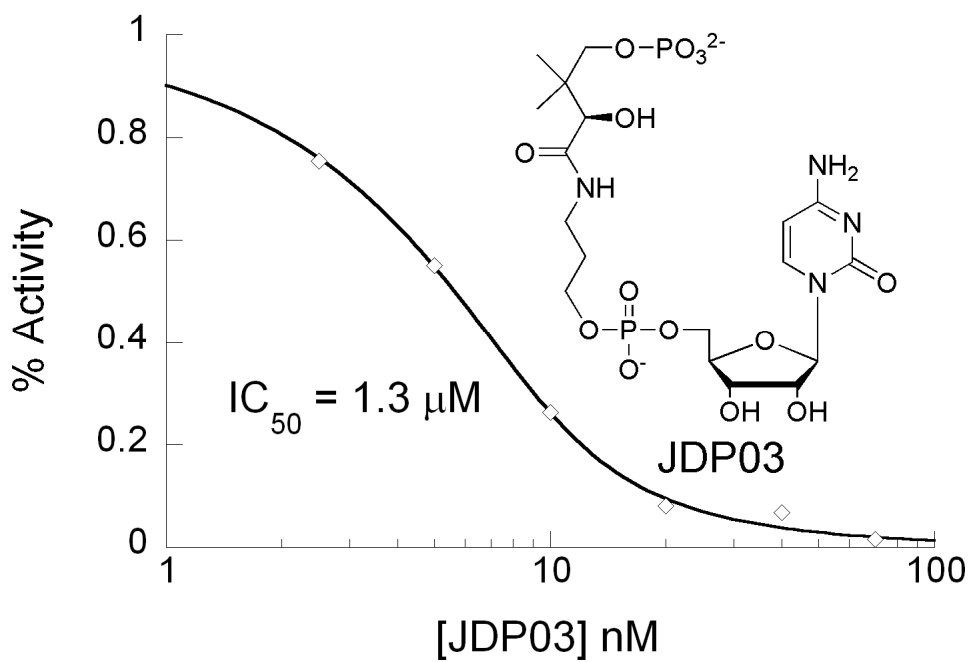
Figure 4.5: Dose response curve for previously characterized inhibitor JDP03 using our malachite green HTS assay. The calculated IC_{50} is consistent with the previously determined IC_{50}.
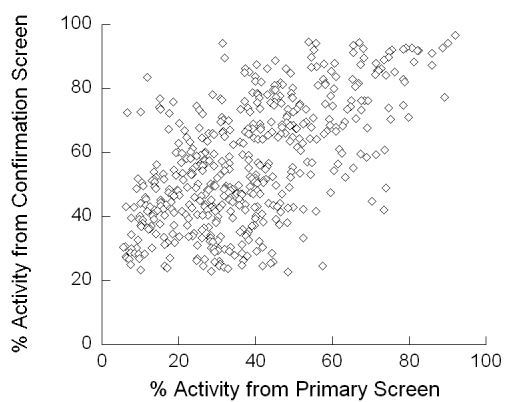
Figure 4.6: Primary versus confirmation screen. The percent activities observed in the primary screen for the top 510 compounds were plotted against the median (n = 3) percent activities of the corresponding compounds observed in the confirmation screen.
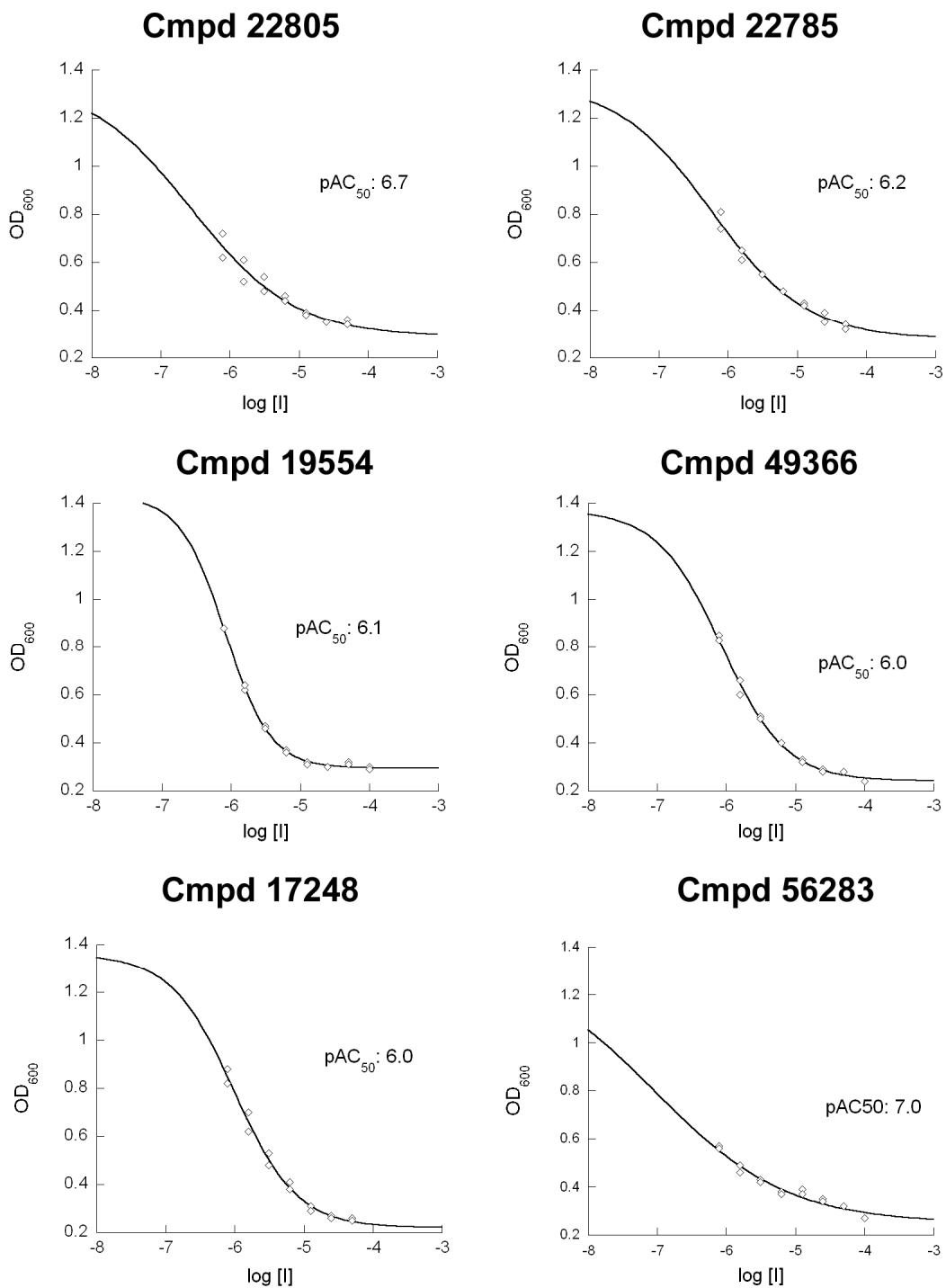
Figure 4.7: Determination of pAC$_{50}$ and Hill slope for select compounds. Data were collected in duplicates (both points shown). Fit via a standard sigmoidal dose response curve.
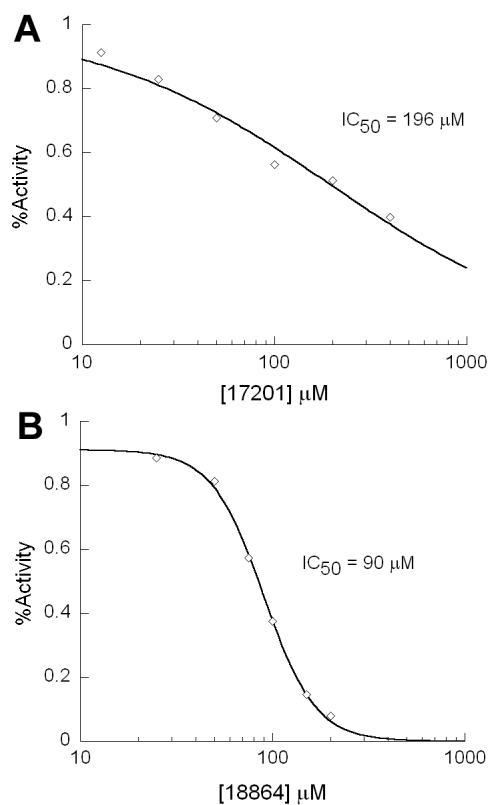
Figure 4.8: Reconfirmation of top hits – first set. Determination of IC_{50} for fresh compound samples using the continuous pyrophosphate assay. A. Dose response of compound CCG-17201. B. Dose response of compound CCG-18864.
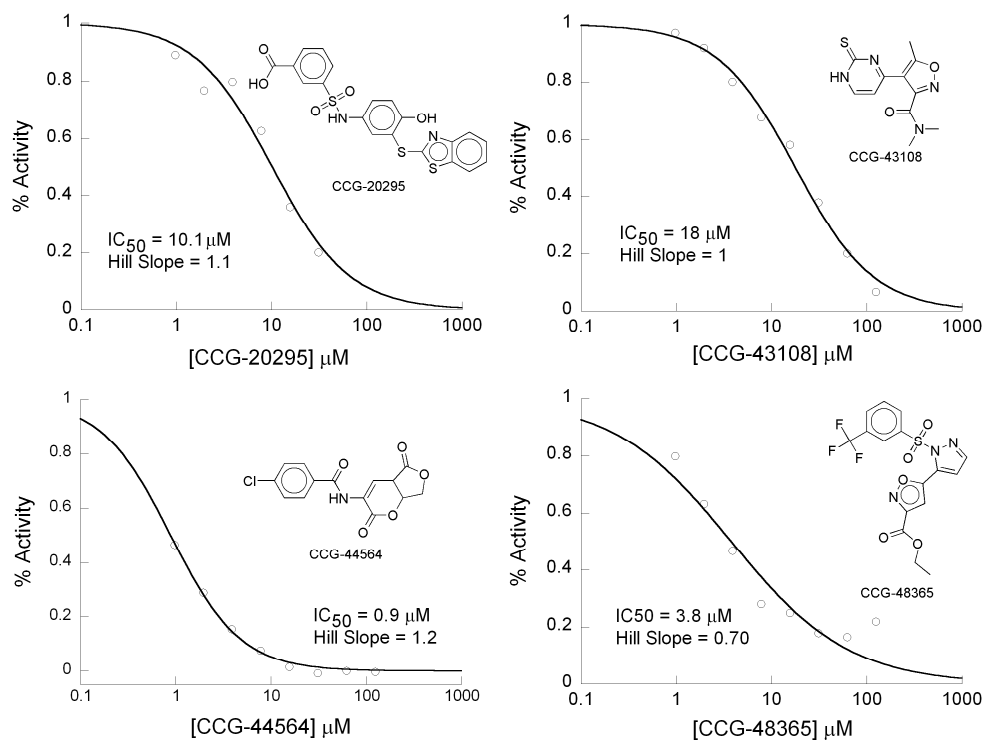
Figure 4.9: Reconfirmation of top hits – second set. Determination of IC_{50} and Hill slope for fresh compound samples using the malachite green assay. IC_{50}, Hill slope, and structure of hits are reported.

Activity vs [SID-21269]

IC$_{50}$ = 0.03 mg/mL

Hill Slope of 2.6

% Activity

[SID-21269] mg/mL
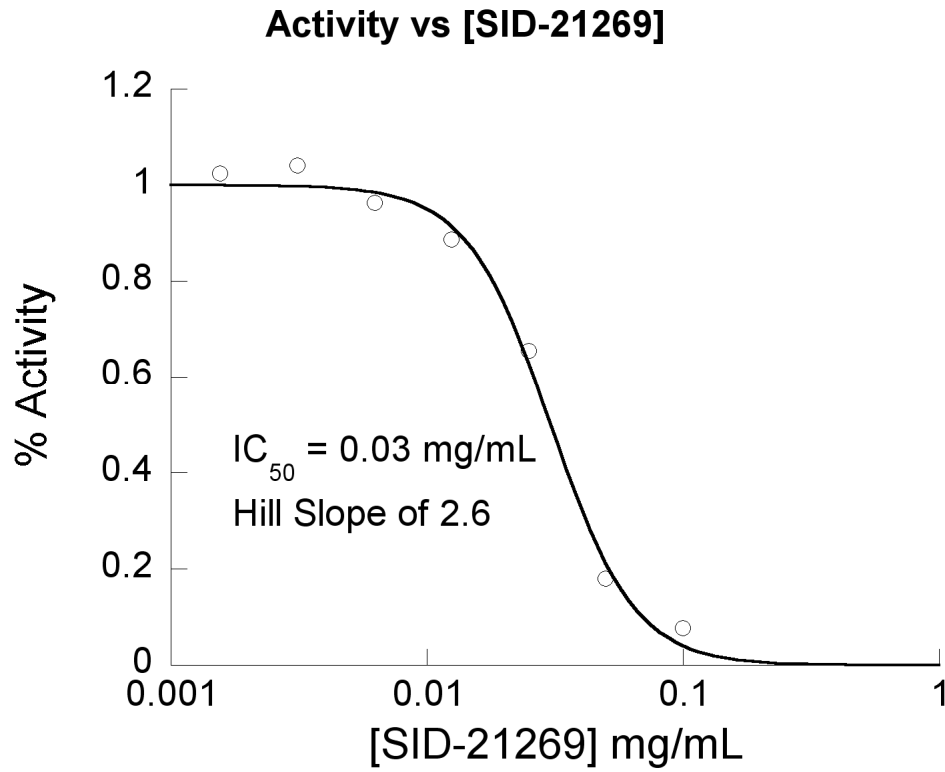
Figure 4.10: Determination of IC$_{50}$ and Hill slope of SID-21269. Data were fit via a standard sigmoidal dose response curve.
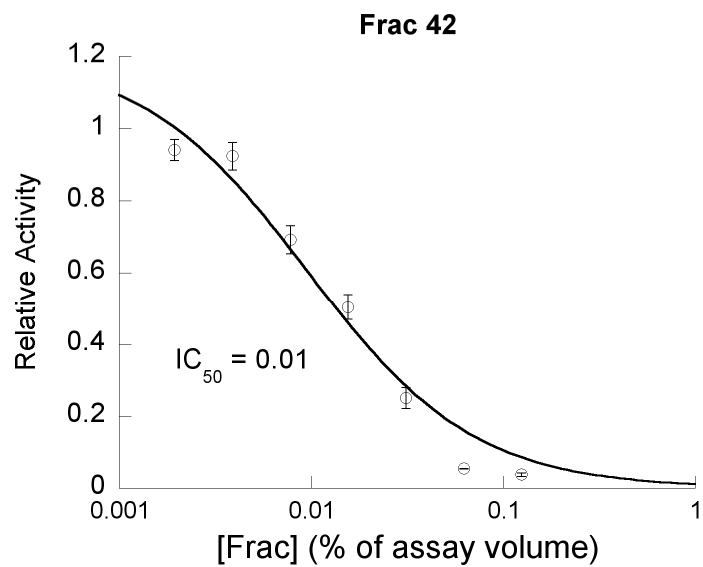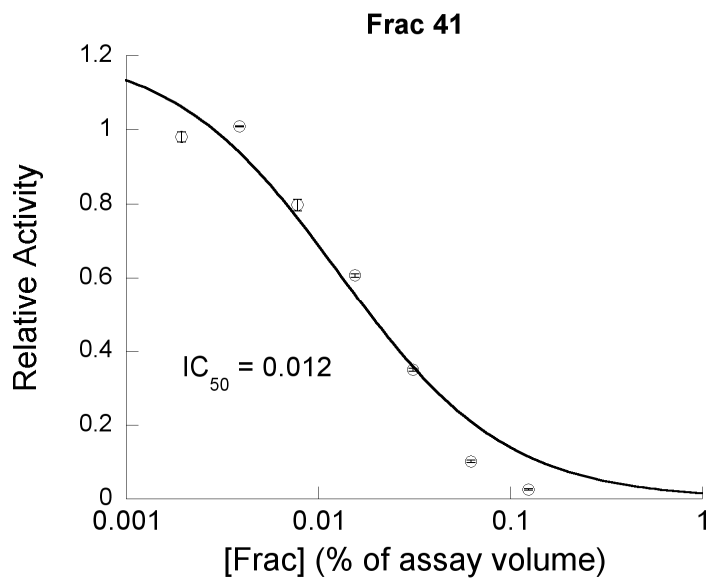
Figure 4.11: Determination of IC$_{50}$ and Hill slope of SID-21269 fractions. The most potent activity was found in fractions 41 and 42, data shown above. Data were fit via a standard sigmoidal dose response curve with Hill slope set at 1.
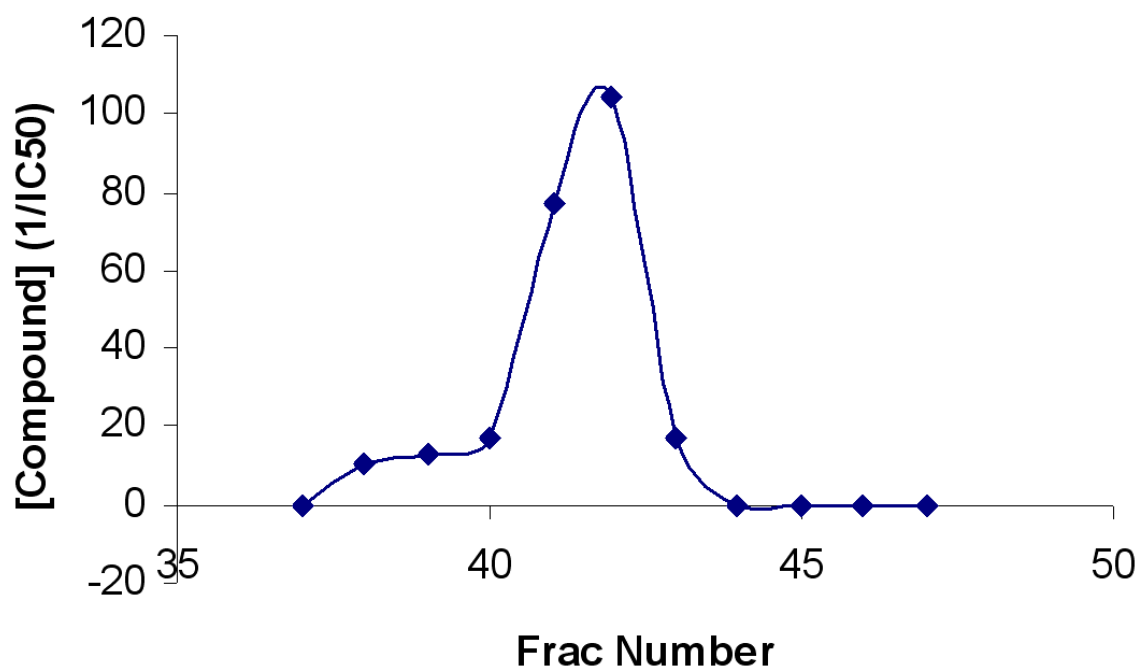
Figure 4.12: Reconstructed elution curve of SID-21269. The elution curve of the active component of SID-21269 is reconstructed based on the assumptions that observed inhibition activity is from one compound and that observed IC_{50} is inversely related to the concentration of the compound.
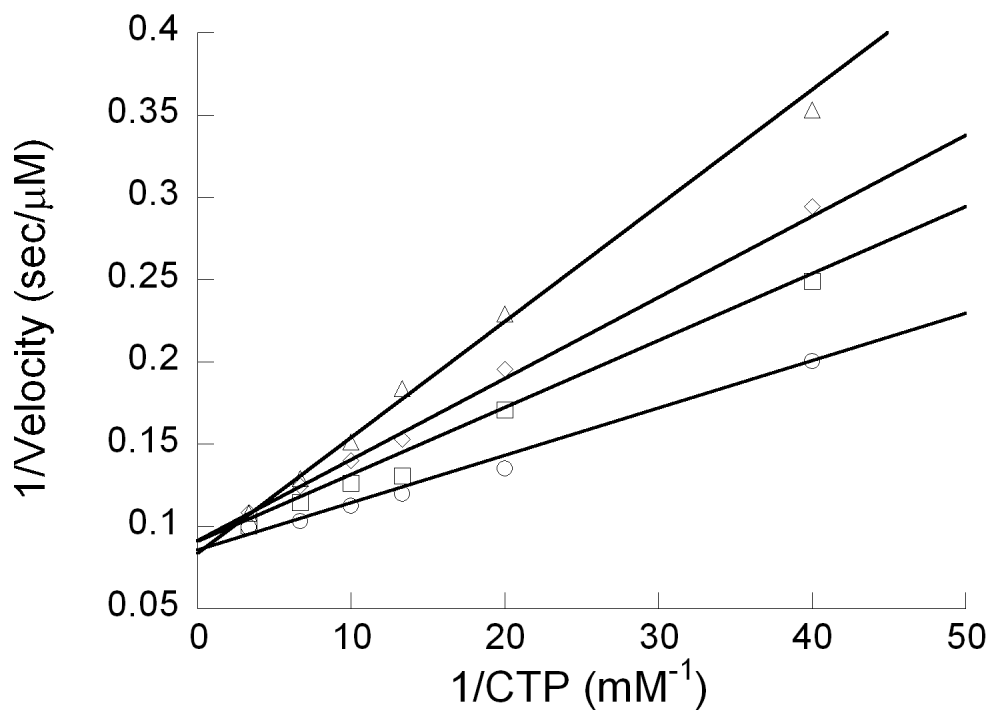
Figure 4.13: Inhibition of *E. facaelis* PPCS by SID-21269, Frac 41. Initial velocity of PPCS vs. [CTP] at 0% (circle), 2% (square), 4% (diamond), and 6% (triangle) solution of Frac 41 at 0.3 mM PPA and 0.3 mM cysteine. Double-reciprocalplot of initial velocity.

CTP PPA PP$_i$ Cys PPA-Cys CMP

PPCS PPCS:CTP ⟮ PPCS:CTP:PPA ⟯ PPCS:CMP-PPA ⟮ PPCS:CMP-PPA:Cys ⟯ PPCS:CMP PPCS
PPCS:CMP-PPA:PP$_i$ PPCS:CMP:PPA-Cys

K$_i$

PPCS:I
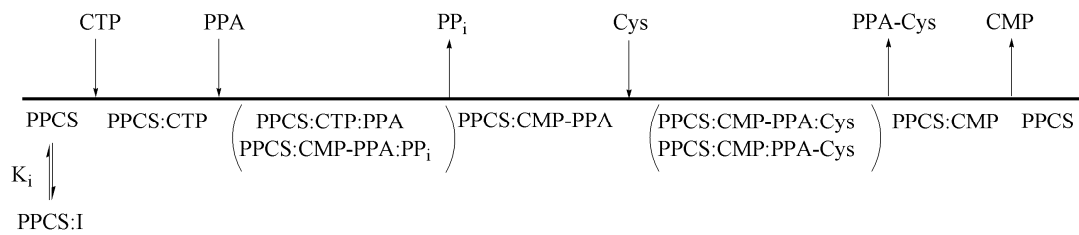
Figure 4.14: Proposed kinetic mechanism of SID-21269 inhibition.

	$4 < pAC_{50} \leq 5$	$5 < pAC_{50} \leq 6$	$6 < pAC_{50} \leq 7$	$7 < pAC_{50}$
Number of Hits	86	53	16	5

Table 4.1: Distribution of hits from the HTS dose response based on pAC_{50}.

Compound	IC_{50}	MW	structure class
CCG-3624	9 nM	228.27	
CCG-22766	10 nM	324.79	α
CCG-25131	56 nM	318.4	α
CCG-56283	60 nM	260.29	
CCG-16474	98 nM	230.24	α
CCG-22779	0.2 μM	318.4	α
CCG-24714	0.2 μM	304.37	α
CCG-22805	0.2 μM	372.37	α
CCG-4848	0.2 μM	391.36	
CCG-15821	0.3 μM	308.33	α
CCG-4653	0.3 μM	399.43	
CCG-22780	0.4 μM	320.37	α
CCG-47490	0.4 μM	399.4	
CCG-22801	0.7 μM	291.33	α
CCG-22785	0.7 μM	338.81	α
CCG-19554	0.8 μM	328.35	
CCG-25908	0.9 μM	302.31	
CCG-49366	0.9 μM	262.27	
CCG-17248	1 μM	354.36	β
CCG-22783	1 μM	354.81	α
CCG-19743	1 μM	314.36	
CCG-22800	1 μM	286.31	α
CCG-22804	1.1 uM	358.34	α
CCG-17201	1.2 μM	340.33	β
CCG-22782	1.2 μM	308.33	α
CCG-22768	1.3 μM	362.41	α
CCG-52408	1.3 μM	307.8	
CCG-2587	1.4 μM	226.28	
CCG-45886	1.4 μM	262.26	
CCG-44564	1.5 μM	307.69	

Table 4.2: Top hits identified from the screen. Calculated IC_{50} from the HTS dose response and molecular weight of the hits are reported. Compounds with similar structures have the same symbol under structure class column.

Compound	IC_{50}	Hill Slope	MW
CCG-49183	6.6 uM	0.49	347.4
CCG-48365	3.8 uM	0.7	415.4
CCG-45252	14.5 uM	0.61	274.3
CCG-44564	0.9 uM	1.2	307.7
CCG-43108	18 uM	1	264.3
CCG-24518	10.9 uM	0.53	412.2
CCG-20295	10.2 uM	1.1	457.5
CCG-18227	14.3 uM	0.41	420.4
CCG-17074	37.5 uM	0.85	320.3

Table 4.3: Reconfirmed top hits. Fresh compounds were obtained and went dose response. Calculated IC_{50} and Hill from dose response and molecular weight of the hits are reported.

Chapter 5

Characterization, Kinetics, and Screening of Phosphopantetheine

Adenylyltransferase from *Enterococcus faecalis*

BACKGROUND

PPAT catalyzes the adenylylation of 4'-phosphopantetheine using an ATP to form dephospho-coenzyme A (dPCoA) and pyrophosphate in the penultimate step of CoA biosynthesis. PPAT from several species have been identified and characterized (*1, 4-6*). In the first published kinetic study of the *E. coli* PPAT, the PPAT enzymatic reaction was measured in the reverse (ATP formation) to determine the kinetic mechanism of PPAT (*5*). It was found that pyrophosphate and dPCoA exhibited a sequential binding mechanism consistent with the formation of a ternary complex, so the kinetic mechanism was either an ordered Bi Bi mechanism or a random Bi Bi mechanism. Another kinetic study found that ATP, PPan, pyrophosphate, and dPCoA can all bind to the free PPAT, and that the products are competitive inhibitors of the substrates, supporting that *E. coli* PPAT follows a random Bi Bi kinetic mechanism, Figure 5.2 (*7*). In the same study, the thermodynamic equilibrium (K_{eq}) of the PPAT reaction was determined to be between 1 and 2, suggesting that the phosphorylation of dephospho-CoA (dPCoA) by DPCK is necessary to drive the overall equilibrium towards the formation of CoA. CoA was also found to be a competitive inhibitor to ATP and PPan.

Crystal structure studies where the *E. coli* PPAT is cocrystallized with substrates and products suggest that PPAT exhibits half site reactivity, because ATP is found in all subunits of the hexamer but only with partial density, but phosphopantetheine was found only in the active site of one trimer (*8, 9*). CoA was found to bind in a distinctly different mode than dPCoA and suggested to act as an allosteric inhibitor of PPAT, although the nature of the proposed allosteric inhibition as well as whether allosteric inhibition is observed in PPAT orthologs is not well explored.

In contrast, human PPAT and DPCK are expressed as a bifunctional fusion protein, called CoA synthase (*6*). CoA synthase is expressed as a monomer that localizes to the outer mitochondrial membrane via insertion of its N-terminus (*2*). PPAT from different bacteria genus exhibits medium to high homology (40% or higher) when compared, but bacterial PPAT has essentially no homology when compared to human CoA synthase. Due to differences between human and bacterial homologues, PPAT could be a possible antibacterial target, which warrants investigation on PPAT from other species. Furthermore, type II pantothenate kinase is refractory to CoA feedback, suggesting that CoA inhibition on PPAT could be the only regulatory step in CoA biosynthesis for some organisms. A better understanding of the nature of CoA inhibition on PPAT would help elucidate how CoA biosynthesis is regulated. Here, we clone, overexpress, and purify PPAT from *Enterococcus faecalis*, an organism whose upstream CoA biosynthesis enzymes exhibit differences from the *E. coli* homologues (*10*). We present the characterization of the enzyme mechanism and the mode of CoA inhibition for *E. faecalis* PPAT, the metal dependency of *E. faecalis* PPAT, as well as optimize a

high throughput assay and conduct a pilot screen to attempt to identify inhibitors of *E. faecalis* PPAT.

MATERIALS AND METHODS

Materials. The chemicals used were of reagent grade or the highest grade available and not further purified. Source 15Q, Source 15S, and Superdex 200 resin and columns were from GE Healthcare. AG MP-1M and Bio-Gel P2 resin were from Bio-Rad. D-Pantethine, L-arabinose, HEPES, ATP, Pyrophosphate Reagent, ampicillin, sodium chloride, sodium pyrophosphate, bacterial inorganic pyrophosphatase, ammonium molybdate, concentrated HCl, malachite green carbinol hydrochloride, and dithiothreitol were from Sigma-Aldrich. 384-well polystyrene nonbinding surface plates were purchased from Corning (cat. 3640).

Biosynthesis of 4'-phosphopantetheine. 4'-Phosphopantetheine (PPan) was biosynthesized via the phosphorylation of pantetheine by pantothenate kinase (PanK). In a 15 mL reaction, 7.5 mM pantethine, 20 mM ATP, 20 mM $MgCl_2$, 20 mM DTT, and 0.5 μM *E. faecalis* PanK were incubated in 100 mM HEPES, pH 8.0 at room temperature for 72 hours. The reaction was chromatographed via a 15 mL AG MP-1M column, pre-equilibrated with 100 mL deionized water, over a 15 column-volume linear gradient of 0 to 1 M NaCl at 1 mL/min flow rate. Eluted fractions were tested with Ellman's reagent, which detects thiol groups, such as on phosphopantetheine. DTT eluted first from the column, and was reactive with Ellman's reagent. The second set of fractions (approximately 40 mL volume) that were reactive with Ellman's reagent was assumed to be phosphopantetheine, and was freeze-dried. Then, the fractions were run over a 250 mL

136

Bio-Gel P2 column at 1 mL/min to desalt the phosphopantetheine, which was again

detected with Ellman's reagent. Fractions with phosphopantetheine (approximately 100

mM) were freeze-dried, and purified phosphopantetheine was stored at -80°C until used.

NMR spectra were taken on approximately 2 mg of the resulting phosphopantetheine

dissolved in deuterated DMSO to confirm the identity of the purified compound.

Cloning, Overexpression, and Purification of E. faecalis PPAT. The *coaD* gene

was amplified from *E. faecalis* genomic DNA (strain ATCC 700802), via PCR using pfu

DNA polymerase with the forward primer CGTAAAATTGCTCTATTTCC and the

reverse primer TGCA<u>CTCGAG</u>TTAGCTCCAGTCATTCTTC to generate the insert

starting at the second codon of the *coaD* gene and with a *Xho*I site after the stop codon of

the gene. Plasmid pET23d(+) (Novagen) was sequentially digested with *Nco*I, treated

with T4 DNA polymerase to fill in sticky ends, and then digested with *Xho*I. The

resulting plasmid with a blunt end and a *Xho*I sticky end was ligated with the *Xho*I

digested insert to generate the desired plasmid, designated as pUMJY130. *E. coli* strain

BL21 AI transformed with pUMJY130 was grown in LB media with 100 mg ampicillin

per liter media at 37ºC with 250 rpm shaking until the optical density at 600 nm reached

0.6-0.8. Then, the culture was cooled to 17ºC, induced with a final concentration of

0.065% w/v L-arabinose, and shaken at 250 rpm overnight at 17ºC. The cell culture was

harvested via centrifugation at 5,000 x g, washed with 20 mM HEPES pH 8.0, and

suspended in 20 mM HEPES pH 8.0 (80 mL per liter culture). The cells were lysed via

French press, the lysate was centrifuged at 20,000 x g for 30 minutes to separate the

cytosol (supernatant) from cellular debris (pellet). The cytosol was chromatographed on a

Source 15Q column (8 mL of resin per 250 mL of cell culture), preequilibrated with 20

mM HEPES pH 8.0, over a 10 column-volume linear gradient of 0 - 0.5 M NaCl in 20

mM HEPES pH 8.0. Fractions were analyzed by SDS-PAGE gel and fractions containing

PPAT were pooled, and further purified through a 320 mL HiLoad 26/60 Superdex 200

prep grade column in 20 mM HEPES pH 8.0 containing 150 mM NaCl. The purified

fractions were stored at -80°C.

Enzyme Assay. The previously optimized enzyme-linked continuous assay, where

production of pyrophosphate is linked to the oxidation of NADH, was used to study the

kinetics and inhibition of PPAT. The assays were performed in 96-well format in a final

volume of 150 µL, using the SpectraMax M5 microplate reader from Molecular Devices.

The assay components were preincubated at 37°C for 15 min and the enzymatic reaction

was started by adding PPAT (75 nM final concentration) to the assay mix, consisting of

the enzyme linked assay components, 10 mM DTT, and various concentrations of

substrates and product/inhibitor. The activity of PPAT was calculated by observing the

oxidation of NADH at 340 nm ($\varepsilon_{340} = 6.22$ mM^{-1}cm^{-1} for NADH) and taking into account

that each mole of pyrophosphate produced leads to the oxidation of 2 moles of NADH in

the assay. The average activity of duplicate assay runs is reported.

To determine the kinetic mechanism and the steady state kinetic parameters of

PPAT, initial velocity was measured against varying concentrations of ATP (0.075 mM,

0.1 mM, 0.15 mM, 0.2 mM, 0.25 mM, 0.5 mM, and 1 mM) at fixed, changing

concentrations of phosphopantetheine (5 µM, 7.5 µM, 10 µM, 20 µM, and 80 µM). To

determine the order of substrate binding and product release, the inhibition by dPCoA

with respect to the substrates was determined. The inhibition by CoA, previously reported

to be a feedback inhibitor of PPAT, with respect to the substrates was also determined.

Initial velocity was measured against varying concentrations of one substrate (ATP or PPan) at fixed, changing concentrations of the inhibitor (dPCoA or CoA) and a fixed concentration of the other substrate (PPan or ATP).

Data analysis. Initial velocity was first graphically analyzed as Lineweaver-Burke double-reciprocal plots using Kaleidagraph 4.0. Velocity versus [substrate] data were fit to equation 1 to determine the K_m^{app} and k_{cat}^{app}, which were in turn used to derive the fitting lines in the Lineweaver-Burke plots. The different patterns in the Lineweaver-Burke plots arising from the pairwise and product inhibition experiments were used to determine which Bi Bi kinetic mechanism properly describes PPAT (*11*). ATP displayed apparent positive cooperativity, so the data were fit to a modified Michaelis-Menten equation (equation 2) and plotted to a modified double reciprocal plot where the x-axis has dimension $1/[\text{ATP}]^n$, where n is the Hill constant for cooperativity. The initial velocity data were fit to the initial velocity equation (equation 3) describing the appropriate mechanism to determine the relevant kinetic parameters using PSI-Plot 8.81. Likewise, inhibition data were fit to the appropriate product inhibition equations (equations 4-5) to determine the relevant kinetic parameters.

$$v = \frac{V_{max}^{app}[\text{A}]}{K_m^{app} + [\text{A}]} \quad (1)$$

$$v = \frac{V_{max}^{app}[\text{A}]^n}{K_m^{app\,n} + [\text{A}]^n} \quad (2)$$

$$v = \frac{V_{max}[\text{A}]^n[\text{B}]}{K_{ia}{}^n K_{mB} + K_{mB}[\text{A}]^n + K_{mA}{}^n[\text{B}] + [\text{A}]^n[\text{B}]} \quad (3)$$

$$v = \frac{V_{max}[\text{A}]^n}{K_{mA}{}^n\left(1 + \dfrac{[\text{Q}]}{K_{iq}}\right)\left(1 + \dfrac{K_{ia}{}^n K_{mB}}{K_{mA}{}^n[\text{B}]}\right) + [\text{A}]^n\left(1 + \dfrac{K_{mB}}{[\text{B}]}\right)} \quad (4)$$

$$v = \frac{V_{max}[B]}{K_{mB}\left[1 + \frac{K_{ia}^{\ n}}{[A]^n}\left(1 + \frac{[Q]}{K_{iq}}\right)\right] + [B]\left[1 + \frac{K_{mA}^{\ n}}{[A]^n}\left(1 + \frac{[Q]}{K_{iq}}\right)\right]} \quad (5)$$

In these equations, v is initial velocity and V_{max} is maximum velocity. K_{mA} and

K_{mB} are the Michaelis constants for substrates A and B. Cooperativity is modeled via the

Hill model, with the Hill constant, n, used as a measure of cooperativity. K_{iA} is the

dissociation constant of substrate A and K_{iq} is the dissociation constant of the product Q.

Inductively Coupled Plasma Mass Spectrometry of PPAT. Inductively coupled

plasma mass spectrometry (ICP-MS) were performed on purified *E. faecalis* PPAT to

determine the amount of various divalent metals associated with the purified enzymes.

ICP-MS was performed by the W. M. Keck Elemental Geochemistry Laboratory at the

University of Michigan. Samples containing approximately 250 µM of PPAT, along with

the blank purification buffer, were submitted.

Metal Dependence Assays. The activity of PPAT in the presence of Mg^{2+}, Mn^{2+},

Zn^{2+}, Fe^{2+}, and Cd^{2+} as well as no divalent metal was measured via the previously

described Eikonogen assay (*12*). A 40 µL enzymatic reaction containing 150 nM of

PPAT, 600 µM ATP, 600 µM PPan, 5 mM DTT, and one of the above divalent metals

(over a concentration range of 78 µM – 1 mM) in 25 mM HEPES, pH 8.0 was run at

room temperature. The reaction was quenched with the Eikonogen assay after 10 min,

and the activity was determined. The results were compared to a control with no divalent

metals and a control with no enzyme. The enzyme turnover was calculated using $\varepsilon_{580} =$

25,000 M^{-1} cm^{-1} for the detection of pyrophosphate by the Eikonogen assay and

accounting for the dilution of the original enzymatic reaction by the assay quench. Assays

were run in duplicates with averages reported.

High throughput screen for inhibitors of E. faecalis PPAT. E. faecalis PPAT was screened against the MicroSource 2000 collection of biologically active compounds to identify novel inhibitors via the previously described inorganic pyrophosphatase – malachite green assay (Chapter 4), where the pyrophosphate produced in the PPAT reaction is cleaved into 2 inorganic phosphates and detected via the malachite green reagent. The assays were run in 384 well plates, with 20 µL enzymatic reaction quenched with 20 µL of malachite green reagent. The reaction was started by adding 5 µL of substrate mix (composed of ATP, phosphopantotheine, and DTT) to 15 µL of enzyme mix (composed of PP$_i$ase, PPAT, and MgCl$_2$). The reaction was incubated for 25 minutes, and then quenched with malachite green reagent. The final concentration of the enzymatic reaction is 300 µM ATP, 100 µM phosphopantotheine, 0.5 mM DTT, 0.1 U/mL PP$_i$ase, and 30 nM PPAT buffered in 100 mM HEPES, pH 8.0. In the primary screen, compounds were dispensed into the plates with a BioMek FX automation workstation to a final concentration of 25 µM and incubated with the enzyme mix for 15 minutes prior to starting the reaction. Positive (no enzyme) and negative (no inhibitor) inhibition controls were included in each plate, and compounds showing greater than 25% inhibition of activity were considered hits, and underwent further dose response.

Hits underwent dose response using a similar protocol as the primary assay, but performed in duplicates with serial dilutions of the hit compounds ranging from 100 µM to 80 nM final concentration. The activity versus inhibitor concentration data was fit to a four variable sigmoidal dose response model, equation 6, where pAC$_{50}$ is defined as –log [IC$_{50}$], n as the Hill slope, max as the activity observed under no inhibition, and min as the activity observed under full inhibition.

$$activity = min + \frac{(max - min)}{(1 + 10^{(pAC_{50} - \log[I]) \times n})} \quad (6)$$

RESULTS

Expression and Purification of Recombinant E. faecalis PPAT. Recombinant *E. faecalis PPAT* overexpressed well in our system, with PPAT composing of approximately 50% of expressed proteins. A majority of the PPAT protein was soluble, with only a small fraction found in the crude pellet. PPAT is eluted off the Source 15Q anion exchange column centered around 200 mM NaCl. After anion exchange and gel filtration chromatography, PPAT was >98% pure as determined by SDS-PAGE, Figure 5.3. Approximately 45 mg of purified PPAT was obtained per liter of cell culture. The native oligomerization state of PPAT was determined via gel filtration. The elution volume of PPAT on a Superdex 200 HR column was compared to the elution volumes of a known protein standard (Bio-Rad gel filtration standard) in order to determine its apparent molecular weight. PPAT eluted as a 105 kDa molecule based on comparison with the protein standard, suggesting a homohexamer since monomers are 18.5 kDa each for a theoretical homohexamer mass of 111 kDa.

Kinetic Mechanism. When plotting the initial velocity against [ATP] , the data were not found to fit to standard Michaelis-Menten equation (equation 1). Rather, the curve was sigmoidal, typical of a ligand with positive cooperativity. When fit to a Michaelis-Menten equation modified to a simple Hill cooperativity model, we found that the Hill constant, n, is approximately 2.2 for ATP over the different fixed concentrations of PPan, Figure 5.4A. In contrast, initial velocity against [PPan] fit to a standard Michaelis-Menten equation, suggesting that PPan binding is not cooperative. Initial

velocity against [ATP] at different [PPan] was replotted as a double reciprocal plot (modified for n = 2.2), and the fitted lines intersect to the left of the y-axis, Figure 5.4B, suggesting that ATP and PPan bind sequentially to form a ternary complex. To determine whether the mechanism is ordered or random, competition experiments between the product, dPCoA, and the substrates ATP and PPan were conducted. In the double-reciprocal replot of initial velocity vs. [ATP] at different [dPCoA], the fitted lines intersect at the y-axis, signifying competitive inhibition of dPCoA with respect to ATP, Figure 5.5A. In the double-reciprocal replot of velocity vs. [PPan] at different [dPCoA], the fitted lines intersect left of the y-axis, signifying mixed inhibition of dPCoA with respect to PPan, Figure 5.5B. The resultant inhibition patterns are consistent with an ordered mechanism. The steady-state kinetic constants were calculated by fitting to the equation (equation 3) of an ordered Bi Bi mechanism, and collected in Table 5.1. The dissociation constant of dPCoA, from the two competition experiments, were determined via fit to the equations (equations 4 and 5) consistent with the mechanism, and collected in Table 5.2.

 Inhibition by CoA. It has been shown that CoA inhibits *E. coli* PPAT with low micromolar affinity. Here, the dissociation constant and the mechanism of CoA inhibition on *E. faecalis* PPAT was determined. Inhibition experiment of initial velocity vs. [ATP] at different [CoA] gave double-reciprocal plots where the fitted lines intersect on the y-axis, signifying that CoA is a competitive inhibitor ATP, Figure 5.6A. Inhibition experiment of initial velocity vs. [PPan] at different [CoA] gave double-reciprocal plots where the fitted lines intersect left of the y-axis, suggesting mixed inhibition of CoA on PPan, Figure 5.6B. Together, the inhibition patterns suggest that CoA binds to only the

143

free enzyme, similar to how dPCoA inhibits the enzyme. The dissociation constant of

CoA was determined via fit to the relevant equations (equations 4 and 5), and collected in

Table 5.2.

Metal Dependency. ICP-MS analysis found that no more than the base level of

magnesium, manganese, cobalt, and cadmium were associated with the purified *E.*

faecalis PPAT. Low levels of iron (0.479 µM) and zinc (3.74 µM) were found with the

purified PPAT (250 µM), suggesting that none of these divalent metals associated

strongly with the enzyme. The metal dependency of PPAT was determined. Minimal

pyrophosphate production was detected in the control reaction with no PPAT, but a low

level of activity was observed in the control reaction with no divalent metal (~ 0.1 sec^{-1}).

The reactions with Fe^{2+}, Cd^{2+}, and Zn^{2+} did not show any additional activity than the no

divalent metal control. The reactions with Mg^{2+} and Mn^{2+} showed good activity (from 0.2

sec^{-1} to 1 sec^{-1}) depending on the concentration of the metal, Figure 5.7. Interestingly, the

PPAT activity was the highest at around 0.25 mM of Mg^{2+} or Mn^{2+}. Increasing

concentrations of Mg^{2+} did not affect the observed velocity significantly, while increasing

concentrations of Mn^{2+} caused a noticeable drop in the observed activity. The activity at

1 mM Mn^{2+} is approximately 75% of the activity at 0.25 mM of Mn^{2+}.

High throughput screen. Prior to conducting the screen, the Z'-factor and [PPAT]

versus signal of the assay was determined to assess the sensitivity of the HTS assay. For

[PPAT] vs. velocity, the assays were run as described, but with 7.5 nM, 15 nM, 30 nM,

and 45 nM of PPAT and quenched after 5, 10, 15, 20, 25, and 30 minutes of reaction with

n = 16. The resulting signal versus time for different concentrations of PPAT, as well as

the replot of rate of change in signal versus [PPAT] is presented in Figure 5.8. The Z'-

factor of the assay was determined by running half of the 384-well plate with PPAT, and half without PPAT. Z'-factor of the assay was found to equal 0.81 (*13*).

E. faecalis PPAT was screened against the MicroSource 2000 collection. From the primary screen, 67 compounds showed greater than 25% inhibition of activity, and were classified as hits. These compounds underwent dose response, and only seven hits had pAC_{50} greater than 4 (corresponding to IC_{50} of 100 µM or less). All seven hits also appeared in the previously conducted PPCS screen, suggesting that the hits are either promiscuous inhibitors or inhibitors of assay components.

DISCUSSION

PPAT from *E. faecalis* was cloned, overexpressed, and purified. The kinetic mechanism of PPAT was studied via steady state kinetics. Pairwise kinetic study with the two substrates, ATP and PPan, found that ATP and PPan bind sequentially to form a ternary complex. Inhibition studies with one of the products of the enzymatic reaction – dPCoA, found that dPCoA is a competitive inhibitor of ATP and a mixed inhibitor of PPan. The observed kinetic patterns – the formation of a ternary complex, competitive inhibition of dPCoA with ATP, and mixed inhibition of dPCoA and PPan are consistent with an ordered Bi Bi mechanism and eliminate most possibilities of a random binding mechanism, Figure 5.9. From a purely theoretical standpoint, mixed inhibition patterns of a product with respect to a substrate can be observed in a random binding mechanism if the particular product and substrate do not overlap in their binding. However, since dPCoA contains both the AMP portion of the ATP molecule as well as the entirety of the PPan molecule, it must overlap in binding with ATP and PPan, and thus should demonstrate competitive inhibition to both ATP and PPan if substrate binding is truly

random (as was reported for the *E. coli* PPAT). Overall, an ordered Bi Bi mechanism is the only minimal mechanism that is consistent with all the experimental data. We also found that CoA was a competitive inhibitor of ATP, with a mode of inhibition and dissociation constant similar to that of dPCoA.

Interestingly, the previously characterized *E. coli* PPAT was found to have a random Bi Bi mechanism (*7*). We found that *E. faecalis* PPAT demonstrated an ordered binding mechanism, where dPCoA was competitive with respect to ATP and noncompetitive with respect to PPan. Given the different mechanisms exhibited by different amino-acyl tRNA synthetases, the observed mechanistic differences between *E. coli* and *E. faecalis* PPAT homologues is possible, although rather unusual since *E. coli* and *E. faecalis* PPAT have 70% amino acid sequence similarity, with 44% sequence identity (*14-16*).

Looking at the paper by Miller et al, we found some discrepancies between the reported data and their proposed random binding mechanism (*7*). All substrate-product pairs exhibited competitive inhibition relationships, except PPan (and CoA) was found to be a noncompetitive inhibitor of pyrophosphate in reverse kinetics, which suggests that the enzyme mechanism is more complicated than a straight forward random Bi Bi mechanism. Also, no plots of the competition experiments, except ATP versus CoA, were provided in the paper, making it impossible to independently verify their conclusions. Furthermore, many of the calculated dissociation constants do not match in the paper. For instance, PPan was determined to have a K_d of 8.4 µM from competition experiment against dPCoA, and K_d of 131 µM from competition experiment against pyrophosphate, which is over one order of magnitude apart. Then, from ITC experiments at similar

temperatures, PPan was found to have a K_d of 0.27 µM, a difference of over another order of magnitude. Similarly, the K_d of CoA ranges from 11 µM to 117 µM in competition experiments and 0.06 µM or less from ITC experiments. While ITC experiments showed binding, establishing that a substrate binds to an enzyme does not prove that the binding event is catalytically relevant, particularly when the dissociation constants differ so significantly between kinetic and binding experiments. It's impossible to explain the discrepancies without access to their data and fits, but one possibility is that they are fitting their kinetic data to the incorrect mechanism.

Our metal dependency experiments found that while purified *E. faecalis* PPAT showed a low level of activity without additional divalent metals, Mg^{2+} or Mn^{2+} are required to achieve full activity. However, high levels of Mn^{2+} seem to decrease the enzyme turnover. Other biologically relevant divalent metals, such as Zn^{2+} or Fe^{2+}, did not increase the observed activity.

A high throughput screen was conducted to find inhibitors of *E. faecalis* PPAT. The developed assay showed good sensitivity, but no leads were found from the pilot screen against the MS2000 collection. Screens against bigger collections might lead to suitable leads.

Here, we cloned, overexpressed, and purified *E. faecalis* PPAT. Kinetic studies found that *E. faecalis* PPAT follows an ordered Bi Bi mechanism, in contrast to the random Bi Bi mechanism reported for the *E. coli* PPAT. Metal dependency studies found that *E. faecalis* PPAT requires Mg^{2+} or Mn^{2+} to achieve maximal activity. A high throughput screen was optimized to identify inhibitors of PPAT, but no PPAT inhibitors were found in the pilot screen against the MS2000 collection.

REFERENCES

1.   Martin, D. P., and Drueckhammer, D. G. (1993) Separate Enzymes Catalyze the Final Two Steps of Coenzyme A Biosynthesis in Brevibacterium ammoniagenes: Purification of Pantetheine Phosphate Adenylyltransferase. *Biochem. Biophys. Res. Commun. 192*, 1155-1161.

2.   Zhyvoloup, A., Nemazanyy, I., Babich, A., Panasyuk, G., Pobigailo, N., Vudmaska, M., Naidenov, V., Kukharenko, O., Palchevskii, S., Savinska, L., Ovcharenko, G., Verdier, F., Valovka, T., Fenton, T., Rebholz, H., Wang, M.-L., Shepherd, P., Matsuka, G., Filonenko, V., and Gout, I. T. (2002) Molecular Cloning of CoA Synthase. *J. Biol. Chem. 277*, 22107-22110.

3.   Leonardi, R., Zhang, Y.-M., Rock, C. O., and Jackowski, S. (2005) Coenzyme A: Back in action. *Progress in Lipid Research 44*, 125-153.

4.   Worrall, D. M., and Tubbs, P. K. (1983) A bifunctional enzyme complex in coenzyme A biosynthesis: purification of pantetheine phosphate adenylyltransferase and dephospho-CoA kinase. *Biochem. J. 215*, 153-157.

5.   Geerlof, A., Lewendon, A., and Shaw, W. V. (1999) Purification and Characterization of Phosphopantetheine Adenylyltransferase from Escherichia coli. *J. Biol. Chem. 274*, 27105-27111.

6.   Aghajanian, S., and Worrall, D. M. (2002) Identification and characterization of the gene encoding the human phosphopantetheine adenylyltransferase and dephospho-CoA kinase bifunctional enzyme (CoA synthase). *Biochem. J. 365*, 13-18.

7.   Miller, J. R., Ohren, J., Sarver, R. W., Mueller, W. T., Dreu, P. d., Case, H., and Thanabal, V. (2007) Phosphopantetheine Adenylyltransferase from Escherichia coli: Investigation of the Kinetic Mechanism and Role in Regulation of Coenzyme A Biosynthesis. *J. Bacteriol. 189*, 8196-8205.

8.   Izard, T. (2002) The crystal structures of phosphopantetheine adenylyltransferase with bound substrates reveal the enzyme's catalytic mechanism. *J. Mol. Biol. 315*, 487-495.

9.   Izard, T. (2003) A Novel Adenylate Binding Site Confers Phosphopantetheine Adenylyltransferase Interactions with Coenzyme A. *J. Bacteriol. 185*, 4074-4080.

10.   Yao, J., Patrone, J. D., and Dotson, G. D. (2009) Characterization and kinetics of phosphopantothenoylcysteine synthetase from *Enterococcus faecalis*. *Biochemistry 48*, 2799-2806.

11.   Segel, I. H. (1993) in *Enzyme Kinetics: Behavior and Analysis of Rapid Equilibrium and Steady-State Enzyme Systems*, p 711, Wiley-Interscience.

12.   Putnins, R. F., and Yamada, E. W. (1975) Colorimetric determination of inorganic pyrophosphate by a manual or automated method. *Anal. Biochem. 68*, 185-195.

13.   Zhang, J.-H., Chung, T. D. Y., and Oldenburg, K. R. (1999) A Simple Statistical Parameter for Use in Evaluation and Validation of High Throughput Screening Assays. *J Biomol Screen 4*, 67-73.

14.   Allende, C. C., Chaimovich, H., Gatica, M., and Allende, J. E. (1970) The aminoacyl transfer ribonucleic acid synthetases. II. Properties of an adenosine triphosphate-threonyl transfer ribonucleic acid synthetase complex. *J. Biol. Chem. 245*, 93-101.

15.   Papas, T. S., and Mehler, A. H. (1971) Kinetic studies of the prolyl transfer ribonucleic acid synthetase of Escherichia coli. Order of addition of substrates and release of products. *J. Biol. Chem. 246*, 5924-5928.

16.   Freist, W., Sternbach, H., and Cramer, F. (1981) Arginyl-tRNA synthetase from Baker's Yeast. *Eur. J. Biochem. 119*, 477-482.
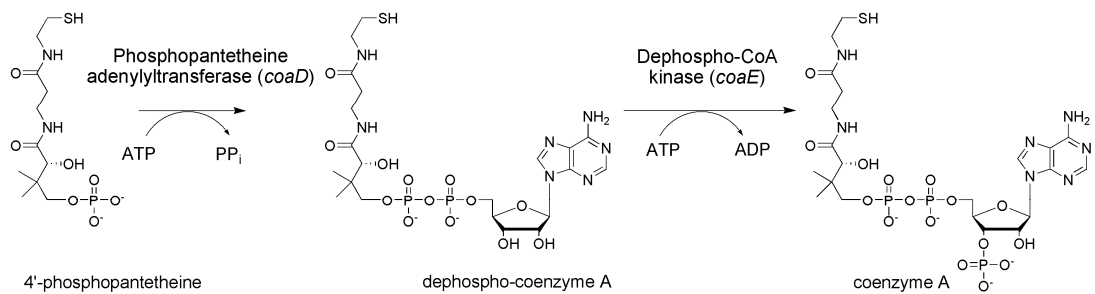
Figure 5.1: Final two steps of Coenzyme A biosythesis. Coenzyme A is biosynthesized from 4'-phosphopantheine by phosphopantetheine adenylyltransferase (PPAT) and dephospho-CoA kinase.
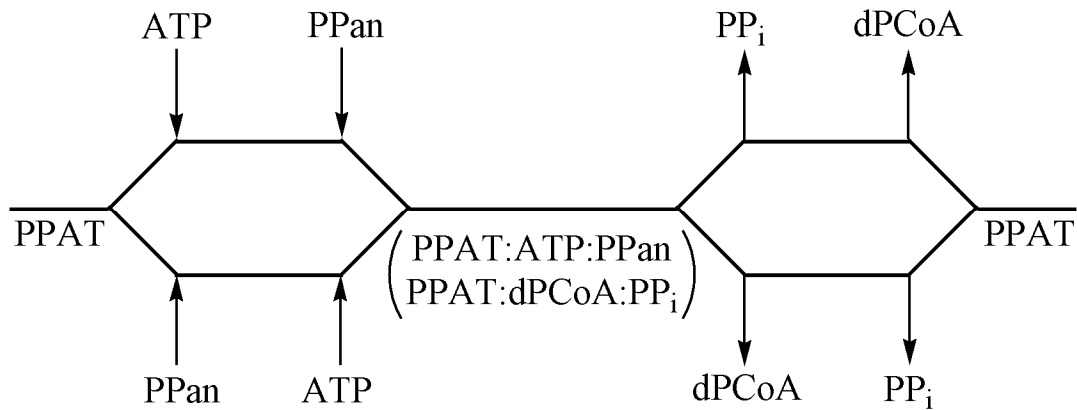
Figure 5.2: The *E. coli* PPAT was proposed to follow a random Bi Bi Mechanism.
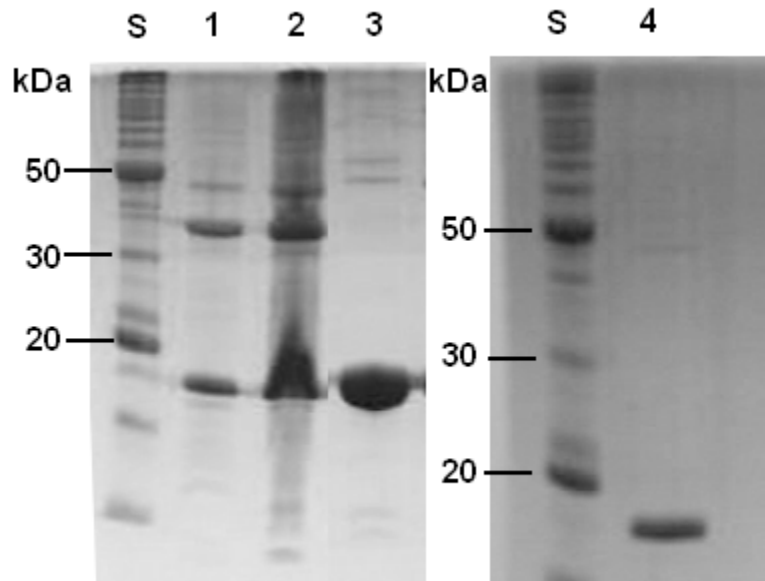
Figure 5.3: PPAT SDS-PAGE. *Lanes S*: Protein weight standards. *Lane 1*: *E. coli* BL21 AI/ pUMJY130 crude pellet expressing recombinant *E. faecalis* PPAT. *Lane 2*: *E. coli* BL21 AI/ pUMJY130 crude extract expressing recombinant *E. faecalis* PPAT. *Lane 3*: *E. faecalis* PPAT extract after purification through source 15Q anion exchange. *Lane 4*: *E. faecalis* PPAT extract after both source 15Q and Superdex 200 gel filtration.
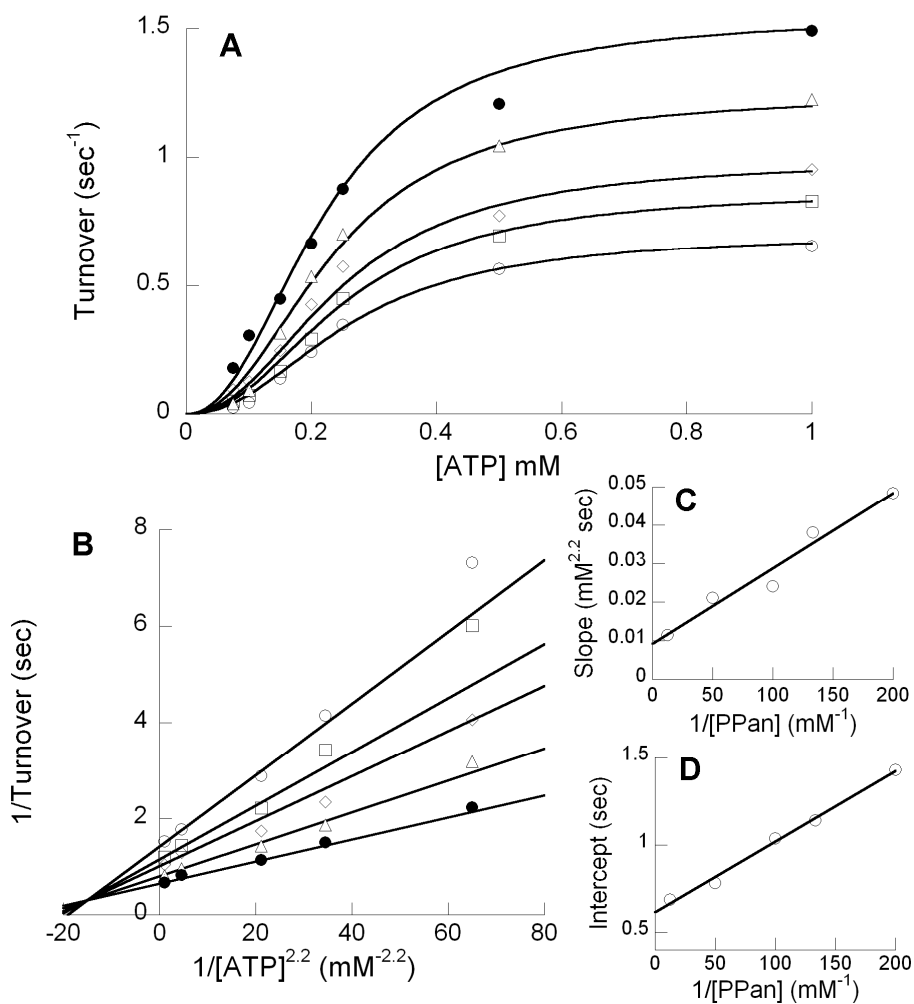
Figure 5.4: Forward kinetics of PPAT. **A.** Initial velocity of PPAT vs. [ATP] at 5 µM (open circle), 7.5 µM (square), 10 µM (diamond), 20 µM (triangle), and 80 µM (closed circle) of PPan. **B.** Double-reciprocal plot of velocity data. **C.** Secondary plot of slopes versus reciprocal [PPan]. **D.** Secondary plot of intercepts versus reciprocal [PPan].
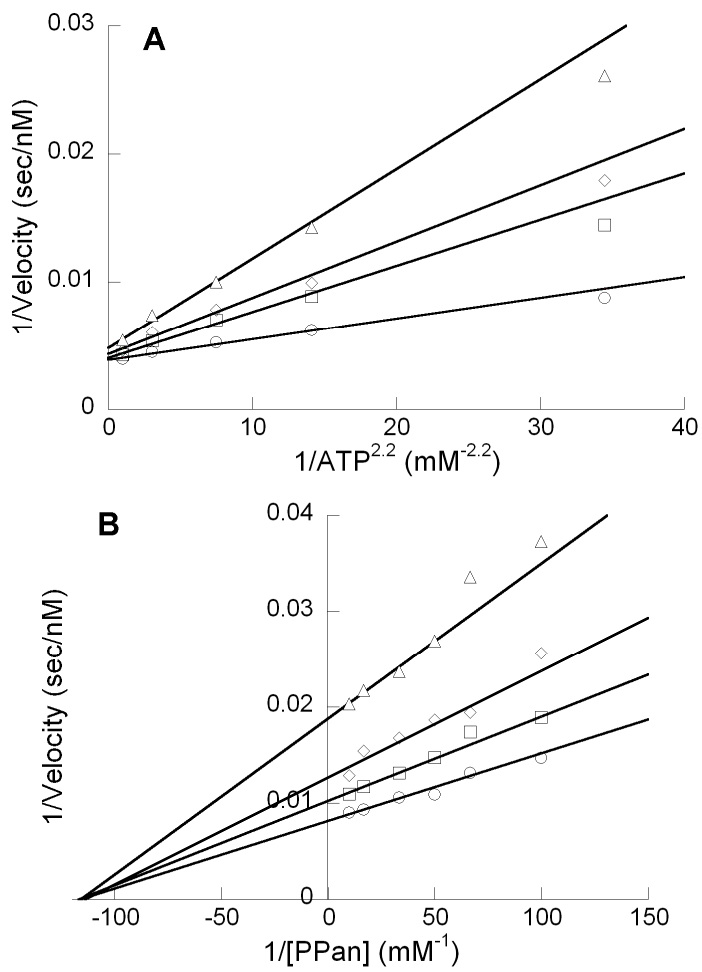
Figure 5.5: Product inhibition of PPAT by dPCoA. **A.** Initial velocity of PPAT vs. [ATP] at 0 µM (circle), 20 µM (square), 40 µM (diamond), and 80 µM (triangle) of dPCoA with 0.05 mM PPan. Double-reciprocal plot of initial velocity. **B.** Initial velocity of PPAT vs. [PPan] at 0 µM (circle), 20 µM (square), 40 µM (diamond), and 80 µM (triangle) of dPCoA with 0.33 mM ATP. Double-reciprocal plot of initial velocity.

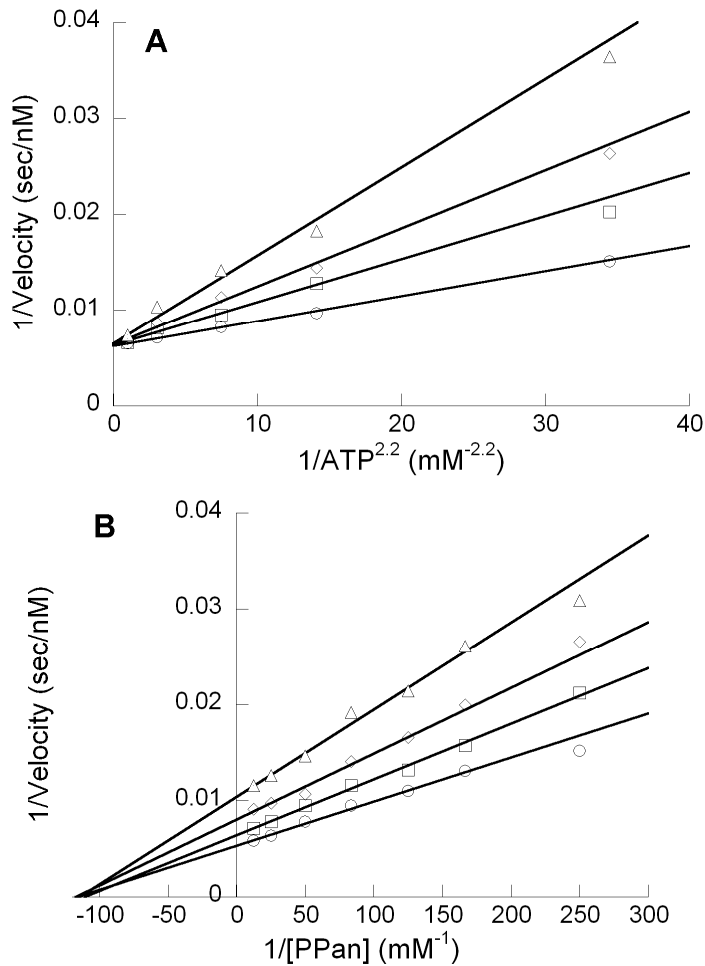Figure 5.6: Inhibition of PPAT by CoA. **A.** Initial velocity of PPAT vs. [ATP] at 0 µM (circle), 20 µM (square), 40 µM (diamond), and 80 µM (triangle) of CoA with 0.05 mM PPan. Double-reciprocal plot of initial velocity. **B.** Initial velocity of PPAT vs. [PPan] at 0 µM (circle), 20 µM (square), 40 µM (diamond), and 80 µM (triangle) of CoA with 0.33 mM ATP. Double-reciprocal plot of initial velocity.
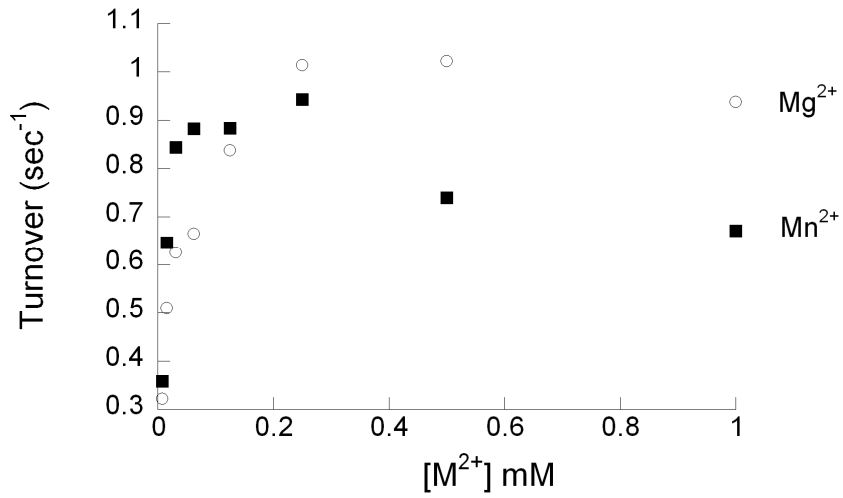
Figure 5.7: PPAT metal dependency. Velocity of the PPAT enzymatic reaction at various concentrations of Mg^{2+} and Mn^{2+}.
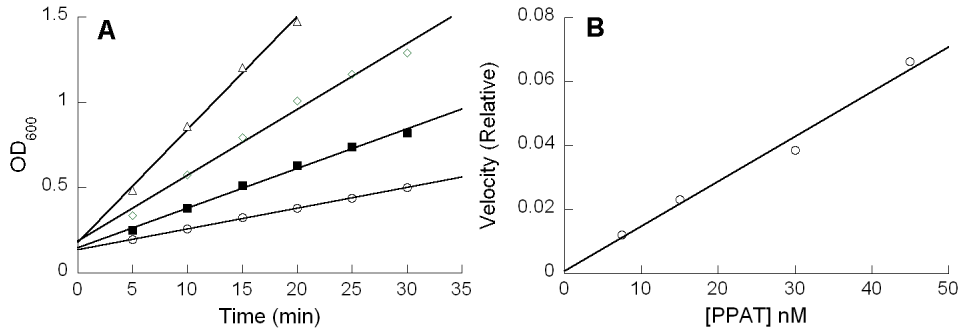
Figure 5.8: PPAT HTS assay development. **A.** Absorbance at 600 nm as a function of time for the reaction with 45 nM (triangle), 30 nM (diamond), 15 nM (square), and 7.5 nM (circle) of PPAT. **B.** Plot of velocity vs. PPAT concentration.
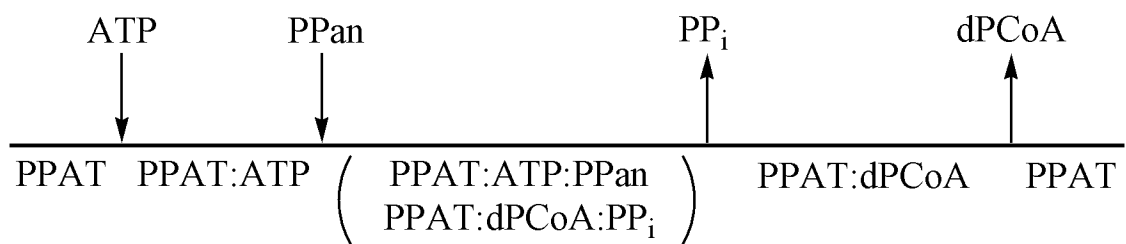
Figure 5.9: The *E. faecalis* PPAT follows an ordered Bi Bi Mechanism.

Table 5.1: Steady state kinetic constants of *E. faecalis* PPAT.

K_{iATP}	290 ± 20 μM
K_{mATP}	212 ± 9 μM
K_{mPPan}	7 ± 1 μM
k_{cat}	1.69 ± 0.05 sec^{-1}

Table 5.2: Inhibition patterns and dissociation constants of dPCoA and CoA.

Inhibitor	Variable Substrate	Fixed Substrate	Inhibition Pattern	K_i (μM)
dPCoA	ATP	PPan	C	16.4 ± 1.4
dPCoA	PPan	ATP	NC	20.1 ± 1.1
CoA	ATP	PPan	C	24.4 ± 1.6
CoA	PPan	ATP	NC	26.1 ± 1.1

Virtual Screen for Inhibitors of Bacterial PPCS

BACKGROUND

Previous works on human and *E. faecalis* PPCS suggest that human and bacterial PPCS have some differences in substrate selectivity that could allow the design of a selective inhibitor of bacterial PPCS (*1, 2*). Here, we virtual screened the *E. coli* PPCS structure against the NCI Diversity Library, FDA approved compounds, and Asinex Platinum library to find potential inhibitors of PPCS.

MATERIALS AND METHODS

Computational Screen. A model of the *E. coli* PPCS enzyme was built based on the published 4'-phosphopantothenoyl cytidylate intermediate bound *E. coli* crystal structure (PDBID: 1U7Z) (*3*). Coordinates of residues missing from the structure were built in two ways. If the residues are resolved in other *E. coli* crystal structures, the coordinates of the residues in that structure were used after that structure was aligned against the intermediate-bound structure. Coordinates unresolved in any of the *E. coli* PPCS structures were built in SYBYL 7.2 by searching against local similar sequences with known coordinates in the Protein Database.

The PPCS enzyme model was virtual screened against the Asinex Platinum library, FDA approved compounds, and NCI Diversity Library using Gold 3.11 with the GS_3 protocol (automatic GA parameter settings, 20% efficiency, 10 runs per compound) (*4*). In order to validate the docking method, the 4'-phosphopantothenoyl cytidylate intermediate was docked against the enzyme model to see if the crystallographic pose can be reproduced. The top docking pose for each compound was further scored with X-score, M-score, and DrugScore in addition to the Gold Score generated from the docking (*5, 6*). The compounds were ranked relative to each other for each scoring function, and the rankings for the different functions were averaged for each compound. The top 50 compounds for each collection were further examined visually, and the top compounds that were available were obtained and tested *in vitro*.

Compound Testing. A modified protocol of the enzyme-linked pyrophosphate detection assay previously described (Chapter 2) was used to measure the activity of the PPCS enzymes in presence of the inhibitors. For initial screening, activity of the *E. coli* enzyme at 0.6 mM CTP, 0.6 mM PPA, 1 mM cysteine, and 100 μg/mL of the test compound was measured and compared to the activity with no inhibitor. PPCS was preincubated with the test compound for 15 minutes before the mixture was added to the rest of the assay components to start the assay. To insure that the test compound was not inhibiting the enzyme-linked assay components, the test compound or a blank control was preincubated with the assay mix for 15 minutes. Pyrophosphate solution at a final concentration of 25 μM was added to the assay mix to start the assay, and the activity with the test compound was compared to the activity with a blank control.

Compounds that showed inhibition with $IC_{50} < 100$ µM against the *E. coli* PPCS were further characterized. First, PPCS was incubated with the inhibitor for varying lengths of time before starting the reaction to determine if there was time-dependent inhibition. Then, the IC_{50} of the compound against the *E. coli* and the *E. faecalis* PPCS enzyme at 0.6 mM CTP, 0.6 mM PPA, and 1 mM cysteine as well as the human PPCS enzyme at 1.2 mM ATP, 0.6 mM PPA, and 1 mM cysteine was determined by measuring velocity at varying concentrations of the compound. Last, if the compound showed selective inhibition for the bacterial PPCS, the kinetic mechanism of inhibition of the compound against the *E. faecalis* PPCS enzyme was studied.

Inhibition Studies. Initial velocity of the *E. faecalis* PPCS enzyme against varying concentrations of one substrate with different fixed concentrations of the inhibitor and fixed concentrations of the other two substrates was measured. The data were plotted in double-reciprocal Lineweaver-Burk form, and the different patterns of the Lineweaver-Burk plots for each substrate and inhibitor combination were used to deduce the mechanism of the inhibitor.

RESULTS AND DISCUSSION

The phosphopantothenoyl cytidylate intermediate was docked against the *E. coli* PPCS model to validate that GOLD could reproduce the crystallographic pose. In 10 docking runs, 3 runs reproduced poses for the cytidylate intermediate that were within 2.0 RMSD of crystallographic pose. One of these 3 poses also had the most favorable docking score of the 10 runs, showing that GOLD can reproduce the crystallographic pose using the GS_3 protocol.

163

NCI Diversity Set. From the NCI Diversity Set, 38 of the top 40 ranked

compounds were tested *in vitro*. Only one compound, 211736, showed in vitro activity

against *E. faecalis* and *E. coli* PPCS. The IC_{50} of 211736 was estimated to be around 50

µM, but the full range of inhibition was not explored because the compound was not

soluble at above 100 µM. Because of the poor solubility, 211736 was not followed up.

Asinex Platinum Library. From the Asinex Platinum Library, 13 of the top 20

ranked compounds were tested. Five compounds (ASN 03962135, 03970073, 08914269,

07029331, 155364903) showed low levels of inhibition, with IC_{50} values between 100

µM to 1 mM. These compounds also had poor solubility at higher concentration ranges,

and were not followed up. A list of these weak inhibitors is collected in Table A.1.

FDA Approved Compound Set. Seven of the top 20 compounds from the FDA

Approved Compound set was tested. Only one compound, folinic acid was found to

inhibit *E. coli* PPCS activity. Further characterization found that folinic acid was a fast

on/off inhibitor with an IC_{50} of approximately 50 µM against the *E. coli* PPCS, an IC_{50} of

approximately 75 µM against the *E. faecalis* PPCS, and less than 5% inhibition at 2 mM

folinic acid against the human PPCS. Competition experiments of folinic acid against the

three substrates were carried out to determine the mechanism of inhibition.

Inhibition experiments where the initial velocity was measured against changing

concentration of one substrate with fixed changing concentration of inhibitor were carried

out and plotted in Lineweaver-Burk plot form. In the double-reciprocal plot of initial

velocity against [CTP] with fixed, changing concentrations of folinic acid and saturating

fixed concentrations of PPA and cysteine, the fitted lines showed a parallel pattern,

Figure A.1, consistent with a mechanism where folinic acid is an uncompetitive inhibitor
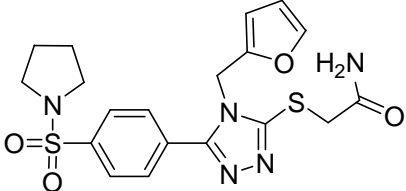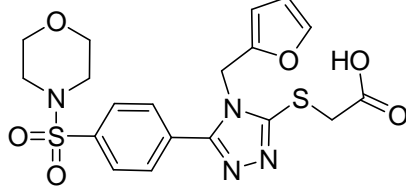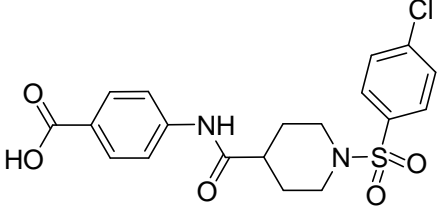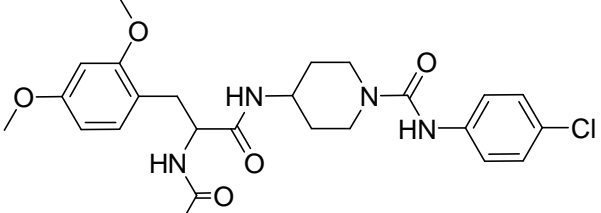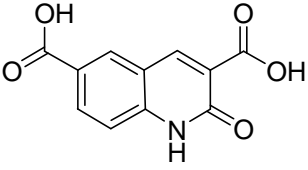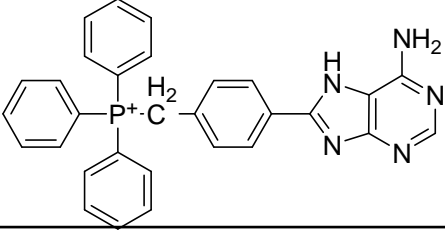
with respect to CTP. In the double-reciprocal plot of initial velocity against [PPA] with fixed, changing concentrations of folinic acid and saturating CTP and cysteine, the fitted lines intersect to the left of the y-axis, Figure A.2, indicative of a mechanism where folinic acid is a mixed inhibitor with respect to PPA. Likewise, the double-reciprocal plot of initial velocity against [cysteine] with fixed changing concentrations of folinic acid and saturating CTP and cysteine also intersected to the left of the y-axis, Figure A.3, suggesting a mechanism where folinic acid is a mixed inhibitor with respect to cysteine as well. The observed inhibition patterns are complicated and the inhibition mechanism of folinic acid is unclear.

Several folinic acid analogues, including aminopterin, folic acid, and methotrexate, were tested for inhibition activity against PPCS. None of them showed any inhibition activity. Upon further examination, folinic acid is a calcium salt, while all other analogues were sodium salts. Calcium was tested, and reproduced the observed inhibitory activity of folinic acid. Further studies (as described in Chapter 3) found that calcium inhibited *E. faecalis* PPCS by acting as a competitive inhibitor to magnesium. However, calcium did not inhibit human PPCS noticeably at up to 2 mM concentration, raising another interesting difference between human and bacterial PPCS.

REFERENCE

1. Yao, J., and Dotson, G. D. (2009) Kinetic characterization of human phosphopantothenoylcysteine synthetase. *Biochim. Biophys. Acta, Proteins Proteomics 1794*, 1743-1750.
2. Yao, J., Patrone, J. D., and Dotson, G. D. (2009) Characterization and kinetics of phosphopantothenoylcysteine synthetase from *Enterococcus faecalis*. *Biochemistry 48*, 2799-2806.
3. Stanitzek, S., Augustin, M. A., Huber, R., Kupke, T., and Steinbacher, S. (2004) Structural basis of CTP-dependent peptide bond formation in coenzyme A biosynthesis catalyzed by *Escherichia coli* PPC synthetase. *Structure 12*, 1977-1988.
4. Chen, H., Lyne, P. D., Giordanetto, F., Lovell, T., and Li, J. (2005) On Evaluating Molecular-Docking Methods for Pose Prediction and Enrichment Factors. *Journal of Chemical Information and Modeling 46*, 401-415.
5. Wang, R., Lu, Y., and Wang, S. (2003) Comparative Evaluation of 11 Scoring Functions for Molecular Docking. *Journal of Medicinal Chemistry 46*, 2287-2303.
6. Yang, C.-Y., Wang, R., and Wang, S. (2005) M-Score: A Knowledge-Based Potential Scoring Function Accounting for Protein Atom Mobility. *Journal of Medicinal Chemistry 49*, 5903-5911.

Table A.1: Identified PPCS hits. Observed inhibition of hit compounds at 600 µM CTP, 300 µM PPA, 1 mM cysteine, and 100 µg/mL of compound against the *E. coli* PPCS.

	ASN 03962135 24% Inhibition
	ASN 03970073 20% Inhibition
	ASN 08914269 25% Inhibition
	ASN 07029331 18% Inhibition
	ASN 15364903 23.3% Inhibition
	NCI 211736 42% Inhibition

Figure A.1: Product inhibition analysis of folinic acid versus CTP. Initial velocity analysis of PPCS versus varying [CTP] at 0 µM (circle), 25 µM (square), 50 µM (diamond), and 100 µM (triangle) of folinic acid with 0.3 mM PPA and 1mM cysteine. Double-reciprocal plot of velocity data.

Figure A.2: Product inhibition analysis of folinic acid versus PPA. Initial velocity analysis of PPCS versus varying [PPA] at 0 µM (circle), 25 µM (square), 50 µM (diamond), and 100 µM (triangle) of folinic acid with 0.3 mM CTP and 1mM cysteine. Double-reciprocal plot of velocity data.
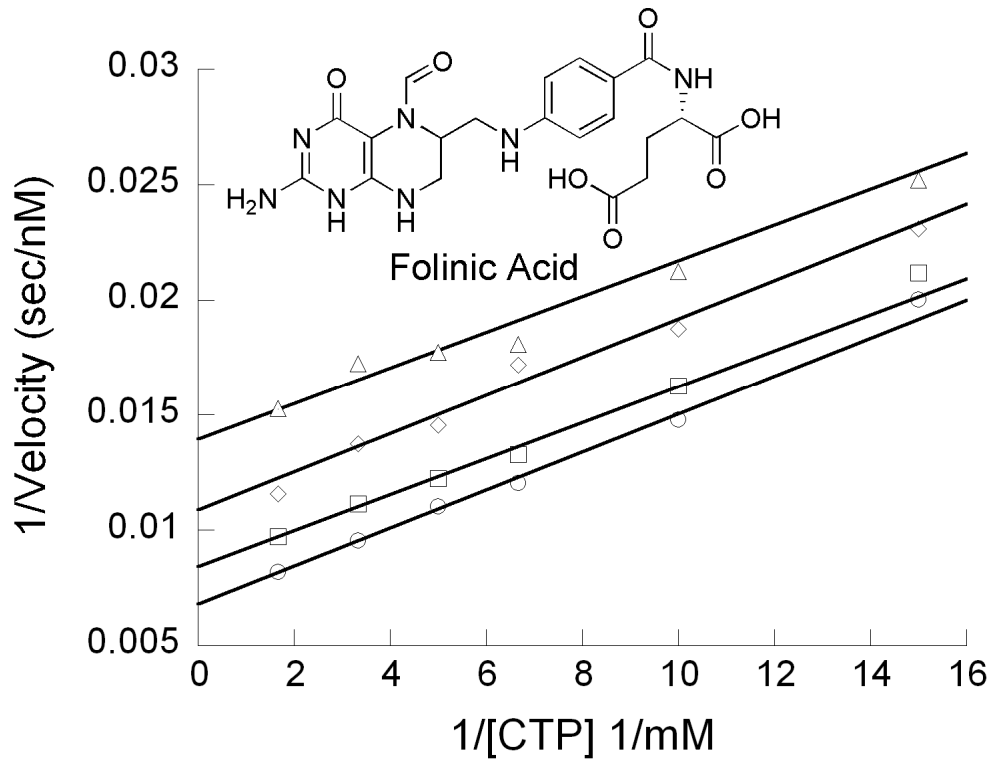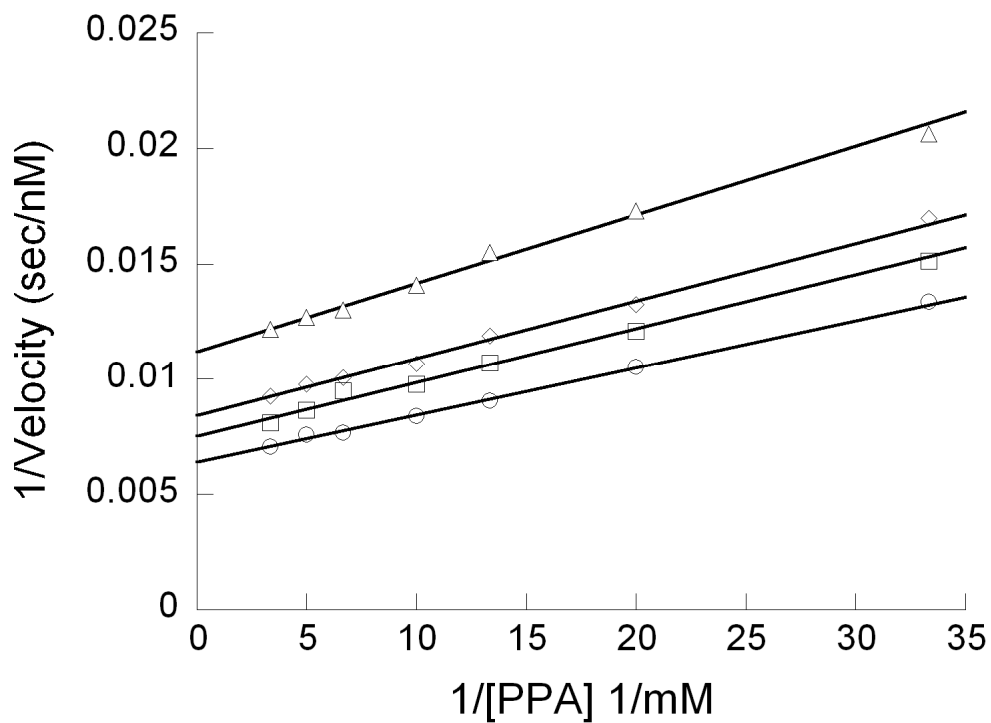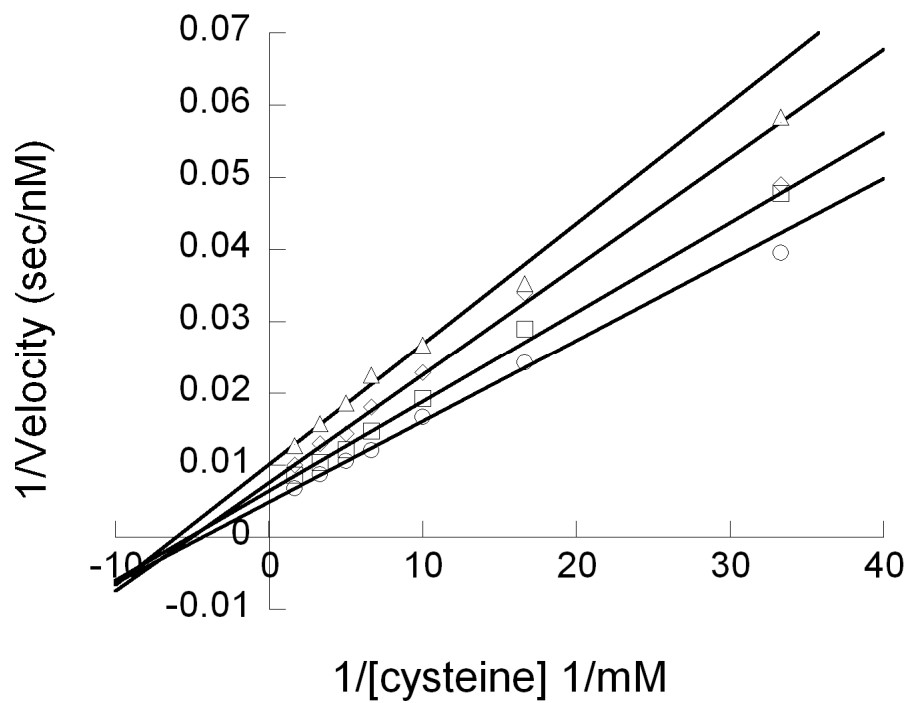
Figure A.3: Product inhibition analysis of folinic acid versus cysteine. Initial velocity analysis of PPCS versus varying [cysteine] at 0 µM (circle), 25 µM (square), 50 µM (diamond), and 100 µM (triangle) of folinic acid with 0.3 mM CTP and 0.3 mM PPA. Double-reciprocal plot of velocity data.

dfp Gene Knockout

BACKGROUND

In *E. coli*, PPCS is expressed as a bifunctional fusion protein with PPCDC (*1*). The gene encoding the fusion protein is named *dfp* (*2*). Normally, coenzyme A is biosynthesized from pantothenate via 5 enzymatic steps, and the PPCS/PPCDC fusion protein is essential in this pathway. However, there is literature precedent that CoA could be biosynthesized from pantetheine via three enzymatic steps that bypasses the PPCS/PPCDC enzymatic reactions, Figure B.1 (*3, 4*). In this alternative pathway, pantetheine is phosphorylated by PanK to form phosphopantethine, which skips the need for PPCS/PPCDC to generate the natural substrate for PPAT. With pantetheine as a supplement, we were able to knockout the otherwise essential *dfp* gene in *E. coli* strain MG1655 using the lambda red recombinase system (*5*). By controlling the amount of pantetheine supplement, we could control the amount of CoA the *E. coli* cell could produce, which allowed us to observe how the levels of CoA affect the growth and antibiotic resistance of *E. coli*.

MATERIALS AND METHODS

The *E. coli* MG1655 *dfp* gene knockout was generated using the lambda red recombinase system using a similar protocol as described in literature (*5*). To knockout

the desired gene, the parent strain was first transformed with the pKD46 plasmid, which encodes for proteins Gam, Bet, and Exo (all under the araC promoter) that carries out recombination of homologous DNA. Next, the transformed *E. coli* strain was induced with L-arabinose to express the Gam, Bet, and Exo proteins, and then electroporated with a PCR insert containing a selection marker and flanked with 40 base pair nucleotides that are homologous to the nucleotides flanking the desired gene in order to excise the desired gene from the chromosome via DNA recombination. The plasmids, pKD46 (described above) and pKD4 (the DNA template to generate a PCR insert with kanamycin resistance marker), were obtained from the *E. coli* Genetic Stock Center.

Generating Homologous PCR Insert. The 3' end of the *dfp* gene overlaps with the 5' end of the *dut* gene. Therefore, the 5' homologous region is the 40 base pairs sequence directly before the start codon of the *dfp* gene, while the 3' homologous region ended at 20 base pairs before the start of the *dut* gene. A PCR insert containing the kanamycin resistance marker and flanked by the homologous regions described above was generated via PCR using *pfu* polymerase with the primers AATCGCCAACTTCTGGTGTCACCCTACAGGAAAAATCATCGTGTAGGCTGGAGCTGCTTC and TTTCATCATAACGGGTCACGATCTCGTCGAGTAATAATTGATGGGAATTAGCCATGGTCC off the pK4 template. The products of the PCR reaction was gel-purified, quantified by measuring absorbance at 260 nm, and stored at -20°C until use.

Transformation Protocol. E. coli MG1655 (*ATCC* 47076) was grown in 100 mL of LB media culture at 37°C until OD_{600} reached 0.4. The culture was cooled on ice, and then centrifuged at 5,000 g for 10 minutes to pellet the cells. The cell pellet was further washed with 25 mL of ice cold water twice and brought up in 200 µL of ice cold water.

An aliquot of 50 µL of the resuspended cell was electroporated with 50 ng of pKD46 (0.2 cm cuvette and 2.5 kV, ~ 5 ms single pulse), recovered in 1 mL SOC for 2 hours at 37°C, and plated on LB-AMP plates overnight at 30°C. Cells harboring the pKD46 plasmid were grown in 100 mL of LB-AMP media culture at 30°C until OD_{600} reached 0.1. The culture was induced with a final concentration of 10 mM arabinose, and grown at 30°C until OD_{600} reached 0.4. The culture was made electrocompetent as described above, and transformed with 200 ng of the PCR insert. Cells were recovered in 1 mL SOC for 3 hours, and plated on LB-Kan plates with 10 mM pantethine (the oxidized dimer of pantetheine) supplement at 37°C overnight. Colonies growing on LB-Kan plate was checked for proper recombination via colony PCR using the primers CTCGGGAAGACGTTGCAGAG (sequence of the nucleotides immediately before the *dfp* gene) and GAAGAACTCGTCAAGAAGGC (sequence of the reverse complement of portion of the *kan* resistance marker) using HotStar Taq. Single colonies with the *dfp* gene knockout were grown in 1 mL LB-Kan, 10 mM pantethine media at 42°C overnight, and then replated to check for the loss of the pK46 plasmid (reversion to AMP sensitivity) as well as for pantethine auxotrophy.

Minimal Inhibitory Concentration. The antibiotic susceptibility of our *dfp* knockout with 1 mM and 10 µM pantethine supplements was compared to the antibiotic susceptibility of the parent MG1655 strain. The minimal inhibitory concentration (MIC) against a panel of various antibiotics for the *E. coli* strains was determined in a 384 well-format. Each well was filled with 50 µL of LB media, the appropriate concentration of antibiotic and pantethine supplement, and *E. coli* (either the parent or knockout strain) at a final concentration of OD_{600} of 0.004. Antibiotic concentration started from 1 to 1000

μg/mL, and the dilutions were made via a series of 14 serial dilutions where the antibiotic concentration was halved. The outer edge of the plate is filled with media, but not used for the experiment due to observed heating differences between the edge and interior wells. Plates were incubated overnight at 37°C, and positive bacterial growth was defined as an OD_{600} of higher than 0.05. Experiments were run in duplicates, and the lowest concentration of an antibiotic with no bacterial growth is defined as the MIC.

RESULTS AND DISCUSSION

A *dfp* gene knockout strain of *E. coli* MG1655 was generated. The *dfp* knockout strain was unable to grow on M9, Luria-Bertani, or Mueller Hinton cation adjusted media without pantethine supplement. The concentration of pantethine supplement affected the growth rate of the knockout strain, Table B.1. With 10 mM pantethine supplement, the doubling rate and saturating concentration of the *dfp* knockout strain was similar to the parent MG1655. Decreasing concentrations of the pantethine supplement decreased the growth rate, with the doubling rate and saturating concentration at less than 10% of the parent MG1655 when supplemented with 10 µM pantethine. No growth was observed at lower pantethine levels. Pantethine deprivation was not lethal for the *dfp* knockout strain. Cultures without pantethine grown for up to 2 days at 37°C with rigorous shaking (250 rpm) could be recovered by addition of 1 mM pantethine.

Using our gene knockout strain with a pantethine supplement, we were able to examine how decreased levels of CoA biosynthesis affect the antibiotic susceptibility of *E. coli*. The MIC of the *dfp* knockout strain with 10 µM and 1 mM pantethine supplement against a panel of antibiotics was compared to the MIC of the parent MG1655 strain,

174

Table B.2. Significant increases in antibiotic sensitivity were observed for a number of antibiotics, such as novobiocin (256-fold increase, gyrase inhibitor), erythromycin (64-fold increase, protein synthesis inhibitor), triclosan (32-fold increase, fatty acid inhibitor), tetracycline (32-fold increase, protein synthesis inhibitor), and cefaxin (32-fold increase, cell wall synthesis inhibitor). However, very little increase in sensitivity was observed for some other antibiotics, such as rifampin (2-fold increase, RNA polymerase inhibitor), gentamycin (2-fold increase, aminoglycoside), lincomycin (2-fold increase, protein synthesis inhibitors), polymyxin (2-fold increase, membrane depolarization), and spectinomycin (2-fold increase, protein synthesis inhibitor). No correlation between mode of action of the antibiotic and increase in sensitivity was observed. For instance, erythromycin and tetracycline both had significant increase in sensitivity, but lincomycin and spectinomyin has little increase in sensitivity, even though all four inhibit protein synthesis. Likewise, antibiotic size also did not correlate with increased sensitivity. For example, novobiocin had a 256-fold increase in sensitivity, while rifampin only had a 2-fold increase. Increased sensitivity also did not show correlation with other common chemical descriptors, such as LogP or polar surface area. Because coenzyme A availability effects a variety of biochemical pathways both directly and indirectly, the complicated effects on antibiotic susceptibility observed is somewhat expected.

Inhibitors of PPCS/PPCDC (the proteins coded by the *dfp* gene) are expected to be bacteriostatic rather than bactericidal based on our knockout study. Even if such an inhibitor is not potent enough to be used alone as an antibiotic, increased antibiotic susceptibility from partial inhibition of coenzyme A biosynthesis means that it could be valuable when used in conjunction with other antibiotics. Inhibition of coenzyme A

biosynthesis might also have other unexpected, but desirable therapeutic effects. For example, *Mycobacterium tuberculosis* that are auxotrophic for pantothenate have decreased virulence and actually serve as vaccines in mice models (*6*). The essential function of the *dfp* gene, along with the observed increase in antibiotic susceptibility when CoA levels are decreased, make CoA biosynthesis a promising target for antibacterial therapy.

REFERENCES

1. Strauss, E., Kinsland, C., Ge, Y., McLafferty, F. W., and Begley, T. P. (2001) Phosphopantothenoylcysteine synthetase from *Escherichia coli*. Identification and characterization of the last unidentified coenzyme A biosynthetic enzyme in bacteria. *J. Biol. Chem. 276*, 13513-13516.
2. Spitzer, E. D., and Weiss, B. (1985) *dfp* gene of *Escherichia coli* K-12, a locus affecting DNA synthesis, codes for a flavoprotein. *J. Bacteriol. 164*, 994-1003.
3. Leonardi, R., Zhang, Y., Rock, C. O., and Jackowski, S. (2005) Coenzyme A: Back in action. *Prog Lip Res 44*, 125-153.
4. Spry, C., Kirk, K., and Saliba, K. J. (2008) Coenzyme A biosynthesis: an antimicrobial drug target. *FEMS Microbiology Reviews 32*, 56-106.
5. Datsenko, K. A., and Wanner, B. L. (2000) One-step inactivation of chromosomal genes in Escherichia coli K-12 using PCR products. *Proceedings of the National Academy of Sciences of the United States of America 97*, 6640-6645.
6. Sambandamurthy, V. K., Wang, X., Chen, B., Russell, R. G., Derrick, S., Collins, F. M., Morris, S. L., and Jacobs, W. R. (2002) A pantothenate auxotroph of Mycobacterium tuberculosis is highly attenuated and protects mice against tuberculosis. *Nat Med 8*, 1171-1174.
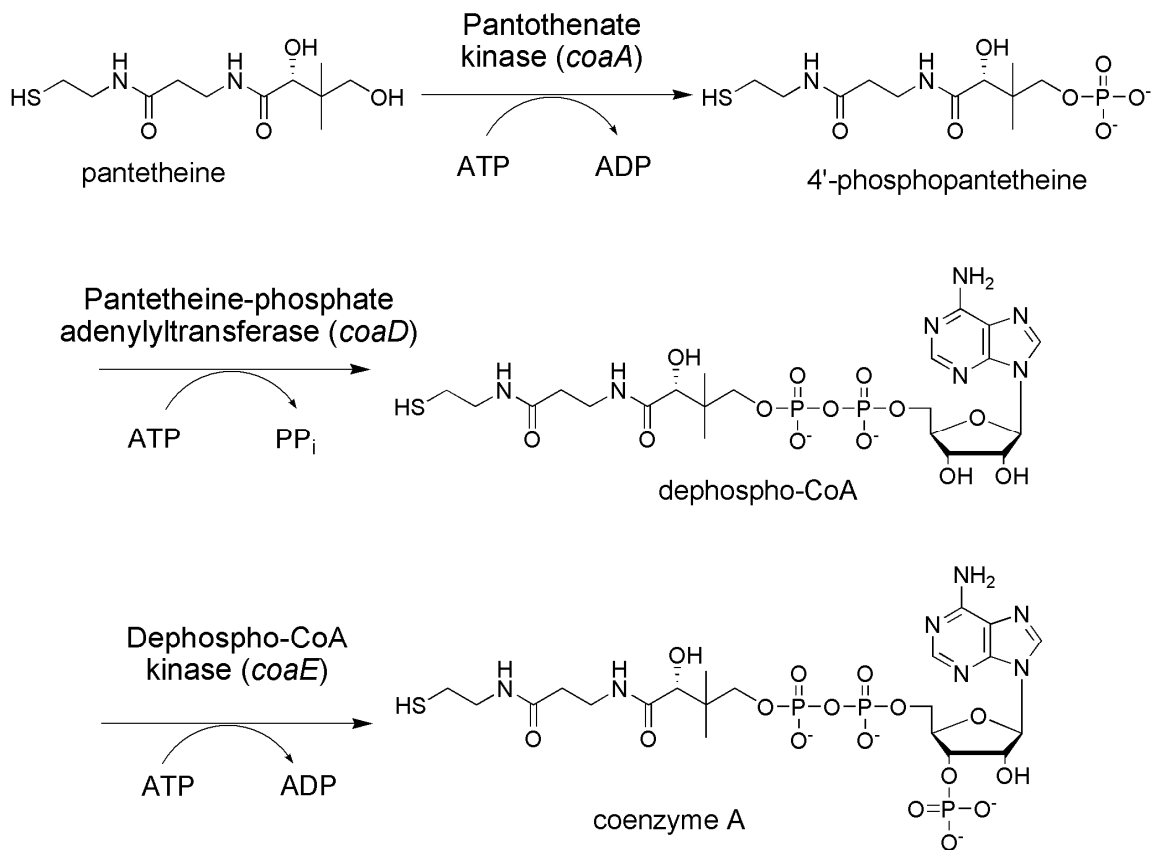
Figure B.1: Alternative CoA biosynthetic pathway. CoA can be biosynthesized from pantetheine using only three enzymes of the normal CoA biosynthetic pathway.

Table B.1: Doubling times in LB media.

	doubling time (min)	Overnight OD_{600}
MG1655	35	5
dfp KO with		
10 mM pantethine	36	5
1 mM pantethine	44	3
100 uM pantethine	77	1.2
10 uM pantethine	>210	0.4

Table B.2: Antibiotic resistance of the *dfp* KO strain.

	MG1655 (ug/mL)	dfpKO 1mM Pan (ug/mL)	dfpKO 10 uM (ug/mL)	1 mM Fold difference	10 uM Fold difference
Vancomycin	500	250	62.5	2	8
Rifampin	15.625	15.625	7.8125	1	2
Bacitracin	5000	5000	625	1	8
Novobiocin	125	0.488	0.488	256	256
Erythromycin	250	3.9	3.9	64	64
Gentamycin	1.95	1.95	0.976	1	2
Bile Salts	>10000	5000	1250	>2	>8
Amp	12.5	3.125	0.78125	4	16
Lincomycin	500	250	250	2	2
Triclosan	1	0.03125	0.03125	32	32
Polymyxin	1	1	0.5	1	2
Ciproflaxicin	0.125	0.015625	0.03125	8	4
Spectinomyin	50	25	25	2	2
Tetracycline	6.25	0.1953125	0.1953125	32	32
Chloramphenicol	6.25	0.78125	0.78125	8	8
Streptomycin	7.8125	3.90625	0.97656	2	8
Cefaxin	15.625	7.8125	0.48828125	2	32